論文 / 著書情報
Article / Book Information

題目(和文)	PWRタービンプラントにおける二相流挙動に関する設計手法の開発と実機ユニットへの適用研究
Title(English)	A study on design method for two-phase flow behaviors and its application to actual units in PWR turbine plant
著者(和文)	真鍋純
Author(English)	Jun Manabe
出典(和文)	学位:博士(工学), 学位授与機関:東京工業大学, 報告番号:乙第4022号, 授与年月日:2010年3月31日, 学位の種別:論文博士, 審査員:
Citation(English)	Degree:Doctor (Engineering), Conferring organization: Tokyo Institute of Technology, Report number:乙第4022号, Conferred date:2010/3/31, Degree Type:Thesis doctor, Examiner:
学位種別(和文)	博士論文
Type(English)	Doctoral Thesis

A study on design method for two-phase flow behaviors and its application to actual units in PWR turbine plant

Jun Manabe

Content

Abbreviation p.5

Chapter 1 Introduction p. 8

1.1 Nuclear steam turbine system

1.1.1 Steam condition and reheat cycle

1.1.2 System construction

1.2 Surveillance of issues of the system

1.2.1 Performance of the unit

1.2.2 Turbine load variation

1.2.3 Flow accelerated corrosion and succeeding scale adhesion

1.2.4 Remained items

1.3 Issues studied in this thesis

1.3.1 Moisture separator reheater in the reheat system

1.3.2 High all volatile water treatment

1.3.3 High temperature NPSH

1.4 Composition of the thesis

Chapter 2 Reheat System and Moisture Separator Reheater p. 34

2.1 Introduction

2.1.1 Reheat cycle

2.1.2 Reheat pressure

2.1.3 Current model MSR for PWR in Japan

2.1.4 Comparison of MSRs overseas and in Japan

2.1.5 Mist separator

2.1.6 Tube drainage and ventilation steam

2.1.7 Vessel diameter of 1,500 MW class units

2.1.8 Core design issues

2.2 Mist separator performance prediction

2.2.1 Air-water two-phase flow test

2.2.2 Prediction formula for critical velocity

2.2.3 Steam test

2.2.4 Prediction for the critical velocity under actual steam condition based on air-water condition

2.2.5 Evaluation of the prediction

2.3 Tube drainage suppression method

2.3.1 Measurement on an existing unit

2.3.2 Results of the measurement

2.3.3 Distribution of heat transfer resistance
2.3.4 Mechanism of the drainage instability
2.3.5 Results in application to newly constructed units
2.4 Design concept for 1,500 to 1,700 MW class units
2.4.1 Cycle steam flow pattern
2.4.2 Mass velocity and optimum economy
2.5 Conclusion

Chapter 3. High All Volatile Water Treatment p. 87
3.1 Introduction
3.2 Requirement for water treatment
3.2.1 Requirement from FAC and scale adhesion
3.2.2 Reliability for steam generator
3.3 Concept of high all volatile water treatment
3.3.1 Alkalizing agent
3.3.2 Purification method
3.3.3 System design
3.4 Numerical value of pH for HAVT
3.4.1 Distribution of ammonia and numerical value of pH in the system
3.4.2 Estimated iron concentration in feedwater
3.5 HAVT application results and evaluation of the effect
3.5.1 Ammonia and pH distribution in the system
3.5.2 Iron concentration in feedwater and in the system
3.5.3 Scale adhesion
3.5.4 Evaluation for reliability for steam generator
3.6 Conclusion

Chapter 4. High Temperature NPSH and Its Application to A Feedwater System p. 97
4.1 Introduction
4.1.1 System behavior at load rejection
4.1.2 Experience in actual unit
4.1.3 History
4.2 Available NPSH ($NPSH_{av}$)
4.2.1 Simulation method for $NPSH_{av}$
4.2.2 $NPSH_{av}$ in actual unit
4.2.3 Problem to be solved
4.3 Required NPSH ($NPSH_{req}$)
4.3.1 Planning of the study procedure
4.3.2 Experiment of high temperature $NPSH_{req}$

4.3.3 Test results and error assessment
4.3.4 Prediction for high temperature $NPSH_{req}$
4.4 Configuration of high temperature NPSH
4.4.1 Extension of Ruggeri-Moore method to negative area
4.4.2 Integrated configuration of high temperature NPSH
4.4.3 Overview of the system on the condition of insufficient NPSH for FWBP
4.5 A design theory of high temperature NPSH
4.5.1 NPSH
4.5.2 NPSH controller
4.5.3 Effect of high temperature NPSH design
4.6 Conclusion

Chapter 5. Conclusions of the Study p. 135

Acknowledgment p.136

Abbreviation

Admission steam:	Turbine inlet main steam rate controlled by GV but limited by first stage nozzle of turbine when GV fully opens
Alloy 600 MA:	Inconel alloy contains nickel, chrome and others
600TT:	Inconel alloy with thermal treatment for alloy 600 MA
690TT:	Inconel alloy contains nickel, chrome and others with thermal treatment, endurable for SCC.
Anion-exchange:	Anion exchange resin which capture anion ion
AVT:	All volatile water treatment
Cation-exchange:	Cation exchange resin which capture cation ion
CBP:	Condensate booster pump
Chevron vane:	Mist separator in a shape of chevron
Condensate:	Condensed LP-turbine exhaust steam in condenser
Condensate demineralizer:	Purification facility by ion exchanger for demineralizing condensate water
Condensate demineralizing:	purification method by demineralizing condensate
Condensate water:	Water condensed in the condenser and supplied for deaerator via LP FWHs
Condenser:	Heat exchanger to get vacuum for LP-turbine exhaust, cooled by sea water in Japan
CP:	Condensate pump
Cycle steam:	High pressure turbine exhausting steam entering into MSR
Cross under piping:	Piping from high pressure turbine exhausting to MSR inlet
Deaerator:	Direct contact type heat exchanger of regenerative cycle associated with a function to deaeratiton
$Dea._{in}$:	Condensate water flowing in to deaerator
DO:	Dissolved oxygen
Double stage reheat:	Reheat system with two stages, heating by HP-turbine extraction and main steam
Drain:	Water condensed from heating steam in heat exchangers
DTR-tank:	Feedwater storage tank combined with deaerator
$\Delta\omega$:	The deviation of actual rotation speed from the rated.
ETA:	Ethanol ammine;An ammine which does not form complex with copper material
FAC:	Flow accelerated corrosion
FCB:	First cut back; Fuel cut back at load rejection in fossil unit
Feedwater:	Water supplied for SG from DTR-tank via HP HTR driven by FWBP and FWP
Fouling factor:	Decreased ratio or value of heat transfer coefficient by fouling
FWBP:	Feedwater booster pump
FWH:	Feedwater heater of regenerative cycle
FWP:	Feedwater pump
FWP&T:	FWP and FWPT
FWP_{in}:	Feedwater inlet of the FWP
FWPT:	Turbine for driving FWP

GV: Governing valve; control valve located in front of the HP turbine controlling the main steam

HAVT: High all volatile water treatment

Heat consumption rate: The ratio of heat supplied to the cycle divided by the power output.

House load: Load necessary for operating power station as condenser cooling sea water pump, reactor coolant pump, feedwater pump and others, which corresponds to about 5% of rated generating power of the station.

HP-: Prefix of high pressure

HP drain: Condensed turbine extraction steam drain water at high pressure feedwater heater

LC: Level controller

IGA: Inter granular attack

ICV: Intercepter valve; control valve located in front of the LP turbine controlling the reheat steam

Ion chromatography: Ion analyzer with high degree of accuracy

LP-: Prefix of low pressure

Last stage blade: Low pressure turbine last stage blade

Leak tight condenser: Condenser adopted with titanium heat transfer tubes with seal welded to tube sheet prohibiting for sea water in-leakage

Load follow up operation: An operation altering the generation power according to the grid request

Load rejection: Sudden load rejection caused by outer grid trouble, generally from full load to house load of 5%

LP drain: Condensed turbine extraction steam drain water at low pressure feedwater heater

Main steam: Steam generated in SG being supplied for HP turbine

Make up water: Purified supply water for the miscellaneous loss in the turbine plant system

MSR: Moisture separator reheater

Minimum flow: Minimum flow requested form pump prohibiting from temperature rise and cavitation

Mist separator performance: Wetness fraction out of the separator or critical velocity where the carryover starts

MSV: Main stop valve; stop valve located in front of GV

Morphorine: An amine; distribution factor of which is 1.0.

MS drain: Separated drain water at mist separator of MSR

NPSH: Net Positive Suction Head

$NPSH_{av}$: Available NPSH

$NPSH_{req}$: Required NPSH

NSSS: Nuclear steam supply system, System of primary cycle

OPC: Turbine over speed protection controller

P_{1st}: Turbine first stage pressure used as indication of turbine generating capability

ppb: Parts per billion

Primary system: Nuclear steam supply system

PWR: Pressurized Water Reactor

RSV: Reheat stop valve; stop valve located in front of ICV

Re-generation of resin:	Cation resin is re-generated with HCl (Hydrochloric acid) and anion ion is re-generated with NaOH (Sodium hydroxide)
Reheat steam:	Steam dried and superheated by MSR supplied for LP turbine
SCC:	Stress corrosion cracking
Sea water:	Sea water for cooling the condenser
Seal welding:	Welding to connect tube to tube sheet
SG:	Steam generator
SGBD:	SG blow down; Blow down from SG for purification
T_{ave}:	Average temperature of reactor coolant
T_{ref}:	Reference average temperature programed corresponding to P_{1st}
TTD:	Terminal temperature difference; temperature difference between heating temperature and heated outlet temperature
Turbine bypass:	Bypass line of turbine which leads main steam directly to condenser using for stating up of the unit of load rejection.
Turbine inlet nozzle:	High pressure turbine first stage stator nozzle, the area of which is the minimum pass when GV fully open.
USC:	Ultra super critical

Chapter 1 Introduction

This study aims to develop design method for the two-phase flow behaviors based on the analysis and clarification, and its application to actual units in PWR turbine plant.

1.1 Nuclear steam turbine system

Birds-eye view of 1,200-MW-class large power nuclear steam turbine is shown in Fig. 1.1. Turbine is tandem compound, from the front to rear, of one cylinder double flow high-pressure turbine, three cylinders of low-pressure turbines and generator. Moisture separator reheaters are located both side of the turbine.

Fig.1.1 Birds-eye view of large power nuclear steam turbine and moisture separator reheaters

1.1.1 Steam condition and reheat cycle

Main steam and heat cycle

Unit thermal power control concept of PWR plant is shown in Fig. 1.2. Average temperature of reactor coolant (T_{ave}), which is the average temperature of hot and cold leg of the coolant, is program-controlled in relation to the thermal power as shown in Fig. 1.2 (a). HP-turbine first stage pressure (P_{1st}) is used as an indication of turbine load, because pressure at each turbine stage is proportional to its flow rate, which follows that the pressure at every stage is in proportional relation to turbine load as shown in Fig. 1.2 (b). Thermal power is controlled in a manner that the actual T_{ave} is controlled to be equal to T_{ref} which is the set value of T_{ave} to the turbine load as shown in Fig. 1.2 (c).

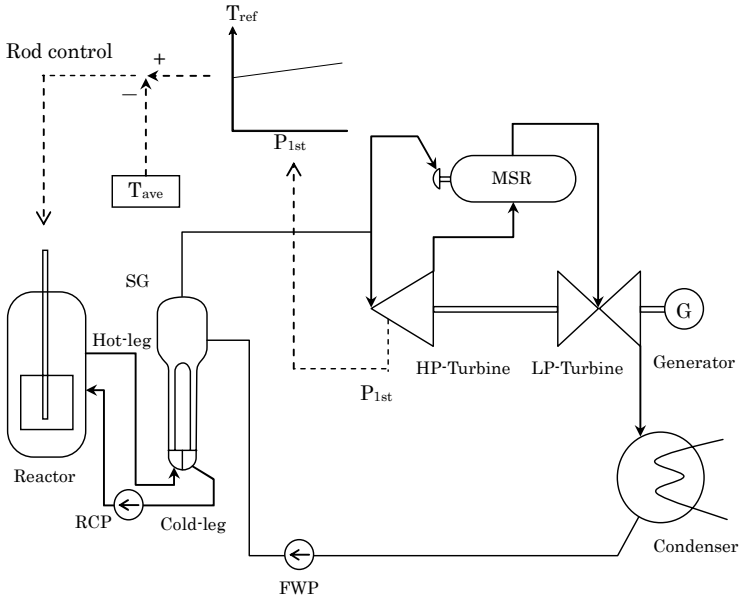

(c) Thermal power control diagram

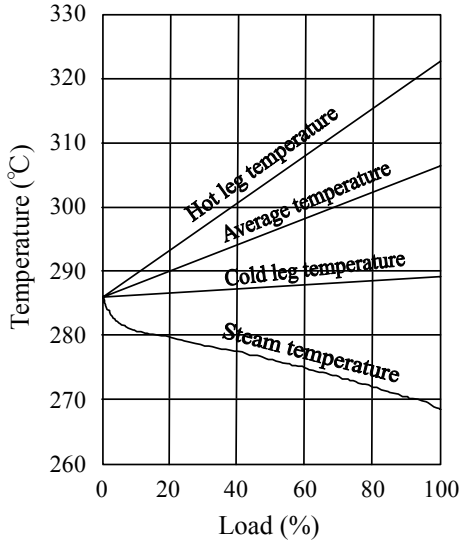

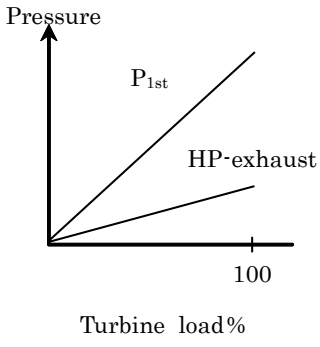

(a) Reactor coolant temperature control and main steam temperature (b) Turbine stage pressure

Fig. 1.2 Unit thermal power control concept

Main steam temperature for PWR turbine system is determined as followings.

The highest temperature of hot-leg at the rated power point is limited by fuel temperature. Heating temperature for steam generator is that of cold-leg of reactor coolant which is determined by the flow rate of the reactor coolant pump on the condition of the predetermined allowable highest temperature of hot leg. Main steam temperature is determined by the heat transfer tube surface of steam generator on condition of the given heating temperature.

Saturation condition main steam, derived from above manner, is 5.4 to 6.3 MPa of pressure and its corresponding temperature of 269 to 279˚C. The turbine system adopts steam-reheat cycle. On the other hand the fossil turbine system adopts main steam of of 24 to 31 MPa with temperature of nearly 600 ˚C associated with boiler-reheat cycle. Turbine expansion lines both of nuclear and fossil is shown in Fig. 1.3.

Lower temperature of main steam and reheated steam in nuclear turbine cycle causes lower heat cycle efficiency associated with large flow rates and consequent large capacity of equipments.

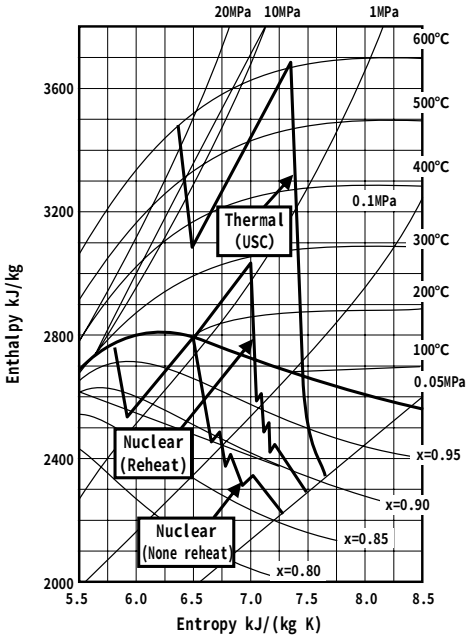

Fig. 1.3 Turbine expansion line both of nuclear and fossil

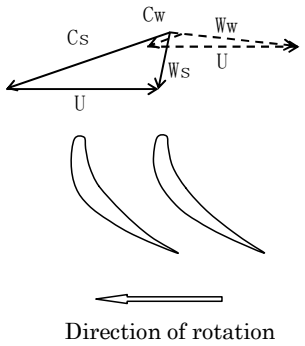

Note;
U: Blade tip speed
C_s: Inlet steam absolute velocity
W_s: Inlet steam relative velocity
C_w: Inlet water droplet absolute velocity
W_w: Inlet water droplet relative velocity

Fig. 1.4 Velocity triangles entering the turbine blade

Reheat cycle

The turbine cycle consists of high pressure turbine, reheat cycle by moisture separator reheater, low pressure turbines, condenser and regenerative cycle. Distinguishing cycle in nuclear steam turbine is reheat cycle by steam as follows.

Saturated main steam generated from a steam generator expands within a turbine, thus ingenerating rotational force associated with an enthalpy drop and a subsequent increase of wetness fractions. The velocity-triangles of steam and water droplet entering the turbine blades is shown in Fig.1.4, which explains an increase of wetness fraction adversely affects the mechanical efficiency of the turbine by inhibiting the rotational force caused by the speed gap between steam and water droplet.

The reheat cycle consists of mist separation and superheating in a turbine expansion process of high pressure turbine exhaust, where the steam condition is about 1.2 MPa, 187℃ and wetness fraction of 12%, respectively.

The heating steams are both high pressure turbine extraction steam and main steam, for the current double stage reheat system. This cycle contributes to an improve in turbine mechanical efficiency by overcoming the heat loss attributing to transferring the main steam at higher temperatures to the reheated cycle steam at lower temperatures, thus rendering a final improvement in turbine efficiency by 2.2% to 2.5%. Reheated steam super-heated by 70˚C expands in low pressure turbine to condenser vacuum with the wetness fraction of 12% which is nearly equal to that of high pressure turbine exhaust point.

This cycle also contributes to suppression of the FAC of the low-pressure turbines and their extraction system auxiliaries colored green in Fig.1.13, though the area colored red maintains wet steam and the colored yellow is the consequent scale adhesion region. Detail is described in Section 1.2.3.

1.1.2 System construction

Main steam of 6.0 MPa expands in high pressure turbine to about 1.2 MPa with 12% wetness fraction, then after dried and super-heated by 70 ˚C with MSR, is led to low pressure turbine expanding finally to condenser vacuum. Extraction steams from high pressure and low pressure turbine heat feedwater heaters (FWH). Steam turbine system flow diagram is shown in Fig. 1.8.

Main turbines and MSR

The turbine consists of a single cylinder of double flow high pressure turbine and two or three cylinders of double flow low pressure turbine, due to the large flow rate derived from the main steam condition of lower temperature and pressure. Moisture separator reheater is constructed with chevron vane type mist separator and double stage U-tube type heat exchanger located turbine operating floor.

Condensate and feedwater system

Regenerative cycle consists of four stage low pressure feedwater heater (FWH), a direct contact deaerator and one stage high pressure FWH, all of which are heated by extraction steam of low and high pressure turbines. Feedwater system consists of condensate pump, feedwater storage tank combined with deaerator (DTR-tank), feedwater booster pump and main feedwater pump. Feedwater booster pump is adopted to maintain the required NPSH of FWP for which is selected higher rotation speed for high efficiency.

Purification system

Purification concept, for preventing heat transfer tube of SG from corrosion is to eliminate impurities and to suppress corrosion in the cycle.

Condensate demineralizer purifies condensed water of low pressure turbine exhaust at the condenser outlet by ion exchange of cation and anion resins eliminating cation-ion like sodium (Na^+) and anion-ion like chlorine (Cl^-), respectively. Water seal valves and chemical dosing are adopted for suppression of corrosion. Water sealed valve in vacuum area is used against for air in-leakage. Ammonia is dosed for pH control and hydrazine is dosed both for deaeration and reducing atmosphere.

Turbine control and protection

Turbine control and protection system consists of turbine speed control system, turbine protection system and turbine over speed protection controller (OPC), all the system of which activates the turbine main valves.

Main valves for turbine consist of control valves and isolating valves. The control valves consist of Governing-valve (GV) installed at the inlet of high pressure turbine and Intercepter-valve (ICV) installed at the

inlet of each low pressure turbine. Isolating valves consist of Main-Stop-valve (MSV) installed in front of GV and Reheat-stop-valve (RSV) installed in front of each ICV. They are shown in Fig. 1.8. All the turbine main valves are designed to keep the position by oil pressure, which balances to the spring reaction during controlling, and to close quickly by the spring due to fail of oil pressure exhausted to drain.

Turbine speed control system throttles GV and ICV.

Turbine protection system trips the turbine on conditions of turbine over speed of 110% of the rated speed, lower condenser vacuum, lower bearing oil pressure and others.

OPC functions as precedent control to suppress the increase of turbine speed less than 110% of the rated, where over speed trip functions, by controlling both GV and ICV according to a preset deviation in power and rotation speed. The controlled lift of GV is designed smaller to that of ICV. The activation area of OPC is shown in Fig. 1.5. The deviation of power is the difference of actual load of turbine generator and generating capability of turbine indicated by P_{1st}. The deviation of rotation speed of $\Delta\omega$ (%) is the difference of actual speed from the rated.

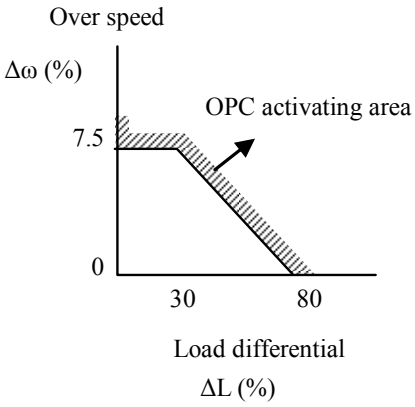

Fig. 1.5 Activation area of OPC system

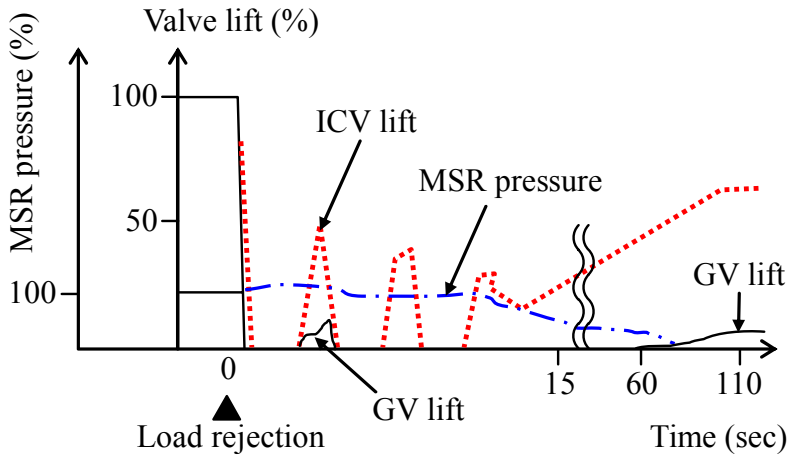

Fig. 1.6 Typical behaviors at OPC functioning

Typical behaviors of GV, ICV and pressure of MSR shell, when OPC functions at load rejection, are shown in Fig. 1.6. All the GV and ICV are closed instantaneously by exhausting the oil. ICV control the speed according to the activation area alternating opening and closing a few times in about 10 seconds and then fully open. GV opens hardly more than one time with a small lift until ICV fully opens in about 100 seconds. The pressure of MSR shell, which is the same pressure of HP-turbine exhaust, begins to fall in 10 seconds. The fall of pressure causes stoppage of extraction steam for Deaerator and DTR-tank.

System control

System control is shown in Fig. 1.8.

Feedwater flow rate is controlled to keep the pressure drop, which is programmed for turbine load, between SG outlet and feedwater header by adjusting the rotation speed of FWP through its driving turbine. Level of SGs is controlled by feedwater control valve furnished each feedwater line.

DTR-tank (feedwater storage tank) is level controlled by condensate flow control valve, functions of which are constant level control and NPSH control described in chapter 4.

MSR is controlled for the following two items.

One is low-pressure turbine inlet cycle steam temperature control, the scheme of which is shown in Fig. 1.7. The temperature is controlled in an indirect method by controlling the heating steam pressure and its saturation temperature which leads to the low pressure inlet temperature due to the constant value of terminal temperature difference (TTD). The temperature is program controlled to turbine load, where heating steam temperature is reduced by MSR temperature control valve in the region less than 50% turbine load and the heating steam temperature is not reduced in larger than 50% turbine load. Furthermore at start of reheating at 35% turbine load in case of turbine start, the temperature is feedback controlled in the allowable rate of temperature change prohibiting turbine casing from stress and strain indicated as dotted line.

The other is heat transfer tube ventilation control described in chapter 2.

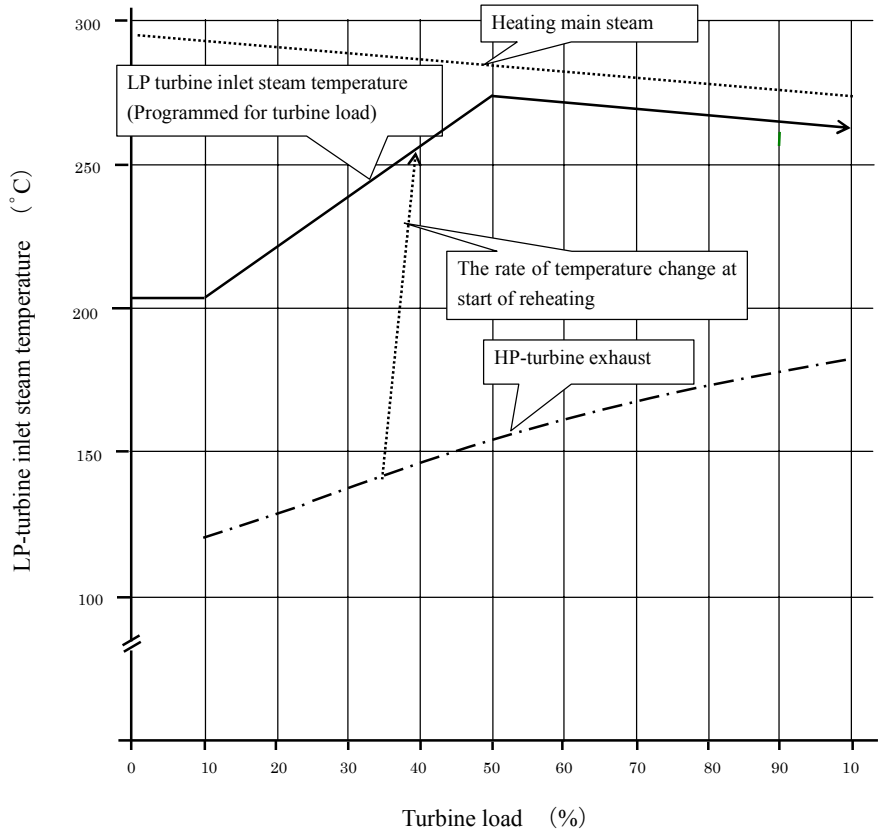

Fig. 1.7 Low pressure turbine inlet steam temperature scheme

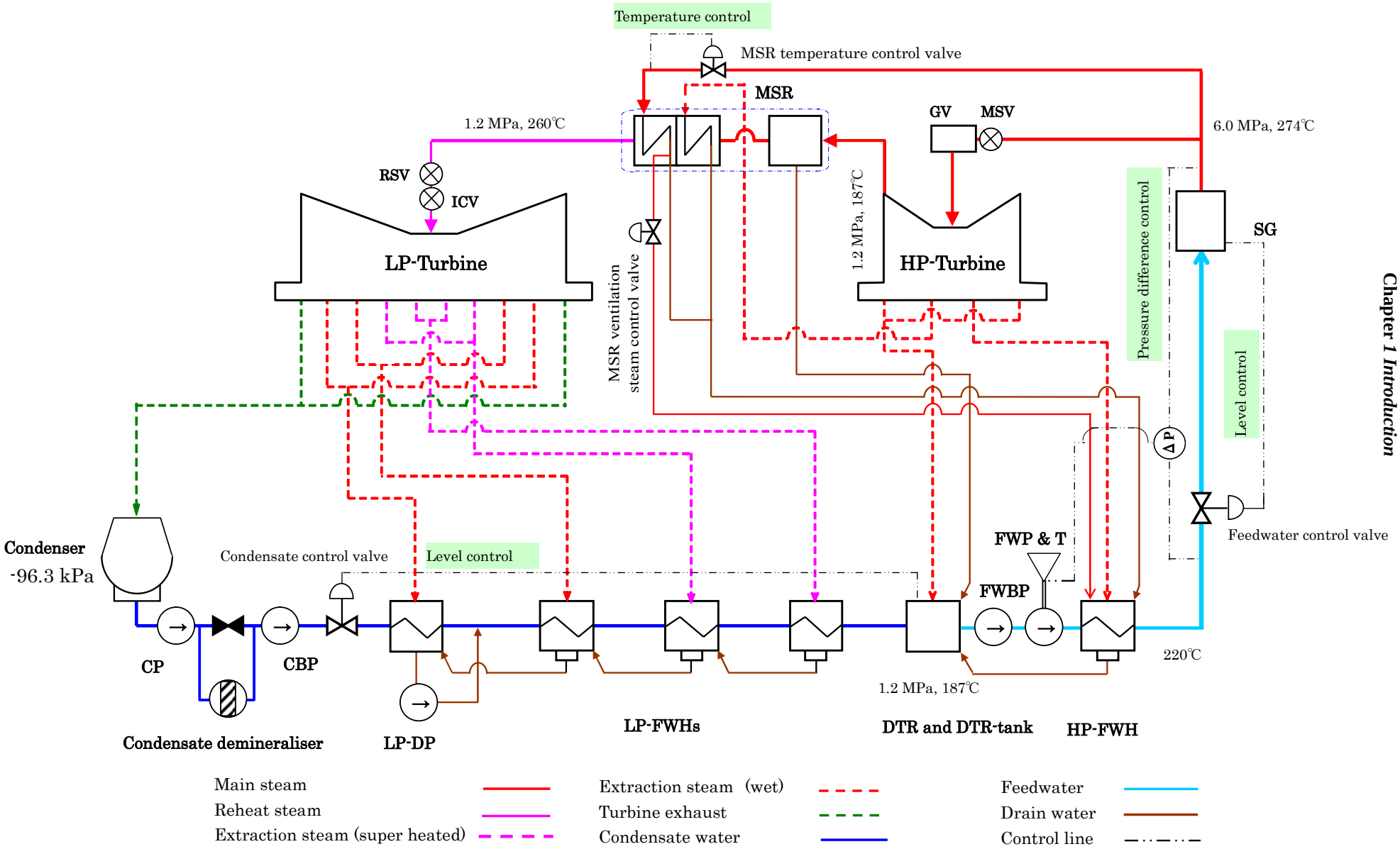

Fig. 1.8 Steam turbine system flow diagram

1.2 Surveillance of issues of the system

1.2.1 Performance of the unit

Following items have been adopted both along with development of technologies and in the acceptable range of economy.

Main steam condition

Main steam temperature increase, which improves turbine plant efficiency or heat consumption rate by 0.2% / ˚C, is available by increase of flow rate of reactor coolant pump (RCP), increase of heat transfer surface of steam generator (SG) and adoption of an economizer.

Average temperature of reactor coolant is program-controlled to the thermal power as shown in Fig. 1.2 (a), where the available highest temperature of hot-leg is limited by fuel temperature. Because the temperature difference between hot-leg and cold-leg is in inverse proportion to the flow rate of the reactor coolant, the increase of flow rate of RCP causes the temperature of cold-leg higher which brings the higher temperature of generating main steam. Steam generator with economizer has the construction firstly to preheat cold feedwater by cold-leg of reactor coolant then to heat almost all the recirculation water by hot-leg of the coolant, leading to temperature rise in generating main steam.

The effect of feasible main steam temperature rise is in range of 2 to 3 ˚C which brings comparatively smaller improvement for turbine plant efficiency.

Turbine

Current progressing three dimensional designed integral shroud blades (ISB), and the largest class low pressure turbine are shown in Figs. 1.9.

(a) Three dimensional flows designed Integral shroud blade (ISB)

(b) Low pressure turbine with 54 inch length last stage blade

Fig. 1.9 Current progress in turbine blade

Turbine blade has been developed in its performance and vibration characteristic. The performance increase was developed from two dimensional flow design to the recent three dimensional. Vibration characteristic was developed in construction aiming for increase of vibration dumping from conventional Grouped-Blades construction to the recent Integral-shroud-blade (ISB). The construction of Grouped-Blades was that many numbers of blades were connected each other with several numbers of stubs. The construction of ISB is that all the blades contact each other with reaction force by release of torsion along with rotation speed increase.

Furthermore last stage blade of low pressure turbine has progressed in its length for reducing the exhaust velocity loss to the condenser vacuum. The development is from 40 inches length to the recent 54 inches length with ISB construction.

On the other hand design against for wetness, water droplet gathered at the tip of the blade by centrifugal force is designed to be exhausted out of the casing to condenser, and recently hollow construction stator vane was developed which catches the mist in steam via slit into the vane exhausting out of the casing.

Reheat system

Current moisture separator reheater is shown in Fig. 1.10.

.

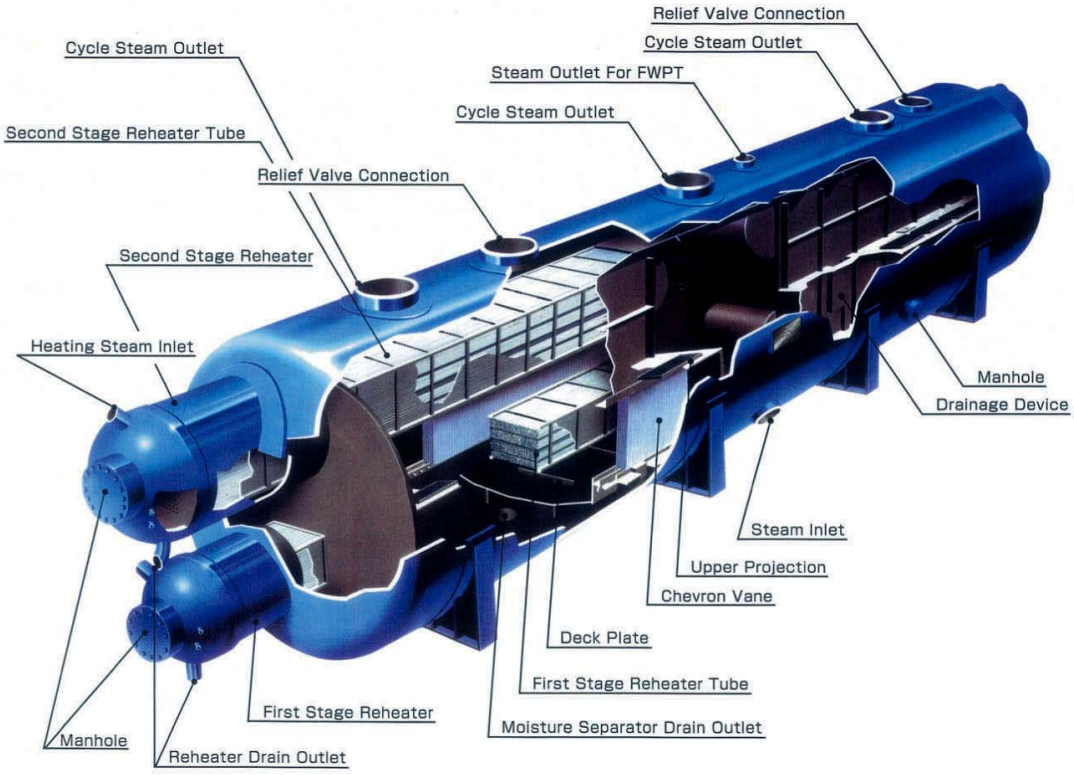

Fig.1.10 Current moisture separator reheater

The reheat system was progressed in heat cycle, from single-stage reheating heated by main steam, to the recent double-stages reheating heated both by high pressure turbine extraction for first stage and by main steam for second stage. Single stage and double stage reheat improves the turbine heat consumption rate by 2.0% and 2.5%, respectively.

The mist separator performance is the key item due to its high influence factors for turbine heat consumption rate of 0.2% for unit percent mist carryover, which corresponds approximately to the potential improvement attained by an additional feedwater heater of the seventh stage to the prevailing six stages regenerative cycle.

Terminal temperature difference (TTD) of heating steam and heated steam was adopted of 13.9 ˚C both for first and second stages.

Regenerative system

Number of regenerative cycle stage was 5 stages for 600 MW class units and has been increased to prevailing 6 stages along with the increase of generating power more than 800 MW class, improving the contribution to heat consumption rate by 0.6%. TTD had been selected for 2.8 ˚C, but last decade it was altered to 2.2 ˚C for 1,200 MW class units from economy evaluation.

Remained items for 1,500 - 1,700 MW class units are the number of the stage and TTD, both of which are to be evaluated only from economical point of view.

Feedwater pump (FWP) driving method

Turbine-driven method gives less generating power at generator-end but larger at transmission-end compared to the motor driven, because main turbine exhaust velocity loss reduces due to the consumption of driving steam for FWP and furthermore the driving energy for FWP, or the driving steam amount, could be adjusted to be minimum by controlling the rotation speed avoiding the surplus pressure drop in feedwater control valve. FWP is driven by electric motor for 600 MW class units and turbine-driven for larger than 800 MW class only based on economy evaluation.

Condenser vacuum

Aluminium brass tube had been adopted for sea water cooled condenser due to both its high performance of heat transfer capability and comparatively lower cost, but the vacuum in summer season became lower than designed resulting in the lack of rated generating power. The reason was ferrous sulphate injection to make protective coating for sea water in-leakage to the cycle, which on the other hand affected heat transfer coefficient.

Recent days all newly constructed units in Japan adopted titanium tube material and almost all the existing ones had been replaced for titanium tube resulting in high vacuum even in summer season by elastic ball cleaning aggressively. There remains no item for condenser.

Steam generator blow down (SGBD) heat recovery

Purification of steam generator had been conducted by blowing down a small ratio of feedwater at bottom of SG out of the cycle before full flow capacity condensate de-mineraliser was adopted. After the adoption of full flow condensate de-mineraliser, SG blow down of 1.5% feedwater has been recovered to condenser associated with purification of the contaminated SGBD by condensate de-mineraliser, but the heat energy of 270˚C has not been recovered. The remained only energy resource of SG blow down in turbine cycle is to be recovered.

Rated thermal power operation

Turbine generating power was restricted by rated generating power, which was determined maximum capable generating power through the year, resulting in the decrease of thermal power in winter season when the capability of turbine generating power could be larger than that of the rated power due to higher condenser vacuum. Rated thermal power operation, where thermal power was kept rated point through year, was recognized by authority and remains no problems because turbine system had been designed based on the rated thermal power.

1.2.2 Turbine load variation

Nuclear power plants in Japan have been operated in rated generating power or rated thermal power. Exceptions are design requirement for load rejection and daily load follow operation. Load rejection occurred once in a while and the daily load follow operation has not been conducted.

Load rejection

Turbine system and arrangement of FWBP and DTR-tank is shown in Figs. 1.11 and 1.12, respectively.

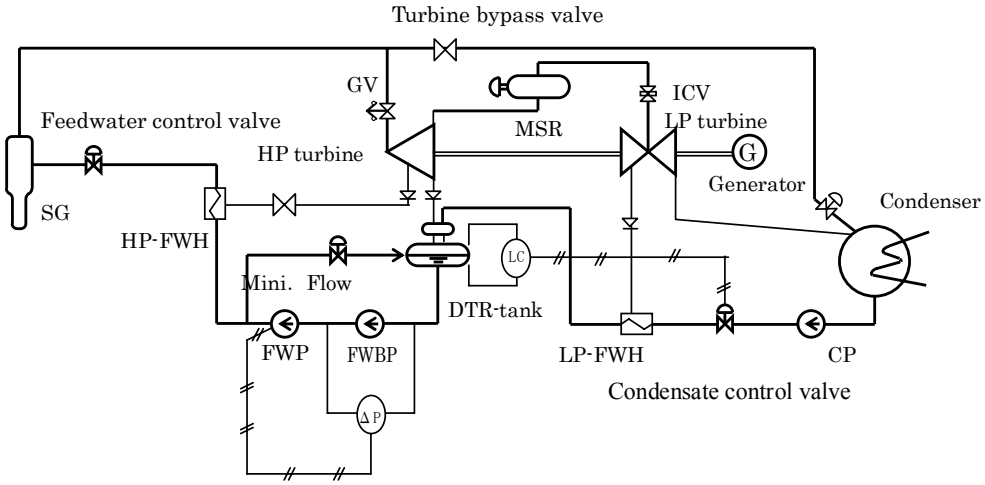

Fig. 1.11 Turbine system fundamental constructions

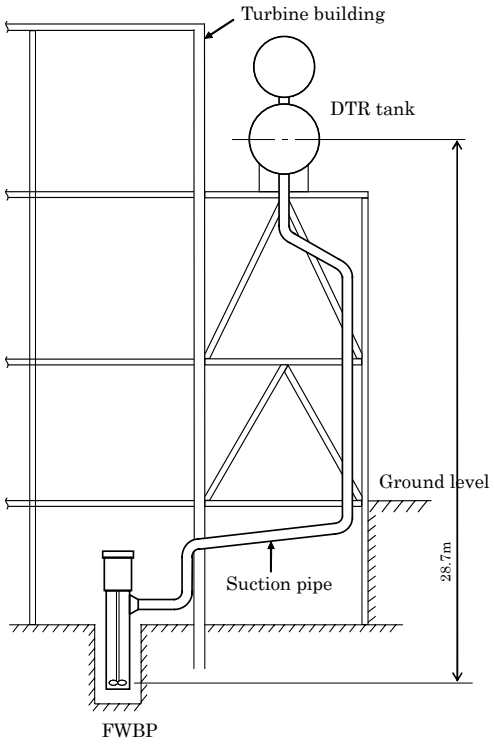

Fig. 1.12 Arrangement of FWBP and DTR-tank (Current design)

Turbine load reduces suddenly from full power to house load of about 5 %, which occurs especially in winter season by the accident of electricity transmission grid caused by lightning strike along the Sea of Japan.

In turbine system, OPC functions due to both the large load differential and increase of turbine speed. There remains no item for turbine because it had been confirmed in thermal units.

Feedwater is required for cooling the primary system for 10 to 15 minutes dumping the generated main steam to condenser via turbine bypass line. The requirement for feedwater system to continue operation is a critical issue for system design of FWBP (Feedwater booster pump) and DTR-tank (Feedwater storage tank combined with deaerator). Available NPSH ($NPSH_{av}$) for FWBP begins to reduce soon after the load rejection to the minimum value in a few minutes caused by the stoppage of turbine extraction heating steam for DTR-tank and retention time due to suction piping.

The current design for the system is that NPSHav is calculated by time-history analysis throughout the transient to figure out both the capacity of the DTR-tank and static head for FWBP enough for the required NPSH ($NPSH_{req}$) of the pump measured on condition of both room temperature and air saturated industrial water. This results in uneconomical design of large capacity and highly elevated location of the DTR-tank, and lower speed higher cost FWBP.

Load follow

Load follow operation is an operation with load variation between the rated to 50% load, of which the maximum load alteration rate is one hour for 50% load alteration band. Turbine system is capable for the operation except for the possible heat transfer tube drainage instability of MSR. Experiences overseas revealed the problem of unstable tube drainage especially in partial load accompanied by sub-cooling to the heating saturated steam temperature with temperature oscillation at the heat transfer tube outlet. The temperature oscillation resulted in thermal fatigue in the seal welding of tubes to tube-sheet at the end of the tubes.

1.2.3 Flow accelerated corrosion and succeeding scale adhesion

Erosion and corrosion, which is called flow accelerated corrosion (FAC), and consequent scale adhesion is the prevailing issue.

Wet steam distribution

Despite the reheat system there remains wet steam condition in a range both from high pressure turbine to MSR and from lower half stream of low pressure turbine to condenser, associated with their extraction line equipments of high pressure FWH, first stage reheater, deaerater and low pressure FWHs. Figure 1.13 shows the condition of the steam in the cycle, super-heated is colored green, wet steam colored red and consequent scale adhesion region colored yellow.

The remained wet steam condition causes FAC and consequent scale adhesion as follows.

Flow accelerated corrosion

Flow accelerated corrosion (FAC) ingenerates both in the gas-and-liquid two-phase region and liquid single-phase region of irregularly-shaped piping, for example of elbows and down stream of orifices and valves.

FAC develops rapidly especially in the annular flow piping because the ammonia distribution factor for gas to water is 30 times larger which causes reduction of pH of water on the surface of the equipments. High pressure turbine exhaust piping, where the velocity is about 40 m/s and the diameter of the piping is generally 1 m, is

plotted in the Baker chart, indicated as (＊) showing annular flow in Fig. 1.14.

Figures1.15 shows FAC in MSR where the wetness fraction is the maximum of about 12% in turbine system and the local velocity is considerably higher due to its complex construction.

Main steam pressure affected by scale adhesion to SG tubes

Addition to the lack of margin, having been pointed out commonly, on lower vacuum condition in summer seasons, possible drastic lack of generating power due to reduction in main steam pressure was revealed. The typical generating power capability of NPP turbine along with main steam pressure alteration is shown in Fig. 1.16(1). Main steam pressure had gradually declined as a result of scale adhesion over the steam generator tube surface, not only affecting the turbine efficiency by the rate of 0.2% per 0.1MPa but also requiring the turbine governing valves to be opened increasingly until they would be significantly open. After GV fully open, the admission steam would decline rapidly, which meant drastic lack of generating power, by the limitation of fully opened governing valves as a result of the increase in specific volume of main steam along with the main steam pressure drop. It was anticipated that the main steam pressure reduction rate with the current all volatile water treatment (AVT) would lead to the turbine inlet GV being fully open within the intended lifetime.

FWP driving power affected by scale adhesion and others

Scale adhesion to the surface of FWP impeller causes increase of steam consumption of its driving turbine or current electricity of its driving motor attributing to the reduction of head and efficiency.

The steam consumption of FWP is shown in Fig. 1.17(1), which illustrates the rapid increase of driving steam consumption soon after the start of operation to the saturation condition in 50 to 100 days. A few number of FWPs, C unit # 1, D unit # 1 and # 2 for example, had to change to minimum flow operation every 3 months to eliminate scale for prohibiting the increase of steam consumption by starting the stand-by motor driven FWP. The minimum flow rate is 40 % of the rated one, which alters the flow patter in the impeller eliminating the scale. In case of motor-driven FWP, the increase of current electricity causes possible thermal trip of the motor due to over current.

Scale adhesion on tube inner surface of high pressure FWH causes increases of pressure drop through the FWH over the design value.

Conventional countermeasures for FAC and scale adhesion

Countermeasures for FAC were adoption of erosion endurable materials, decrease of local velocity and alkalization by water treatment.

Erosion endurable material of stainless steel or low alloy steel have been adopted, due to its high cost, only to the area of both two-phase flow in relatively higher temperature and irregular shaped part where velocity is higher. Decrease of local velocity is also difficult because it causes scale up of the equipments and piping. Countermeasures of the materials and the local velocity could not be the final best method. Current water treatment could not raise pH in the system to the expected numerical value described as followings.

Current all volatile water treatment (AVT)

Current water treatment is all volatile water treatment (AVT) using ammonia for alkalization and hydrazine for deaeration and reducing atmosphere, respectively. The purification process of AVT is full flow condensate purification with condensate demineralizer. The maximum pH is 9.2 due to the restriction of copper carry-on to SG on condition of copper material heat transfer tubes in auxiliary heat exchangers. This treatment resulted in insufficient pH value for preventing FAC due to the reduction of pH value in water on the surface of equipment in

liquid-vapor two-phase flow region, derived from large distribution factor of ammonia for gas to water. The minimum pH through the system is 8.8 at separated drain line of MSR, which is not able to suppress FAC.

New concept water treatment

It was reported that raising pH numerical value was effective for suppressing erosion developing rate. The sample of the effect is shown in Fig. 1.18[(2)].

Raising pH is selected as a counter measure for FAC and consequent scale adhesion.

1.2.4 Remained items

The surveillance resulted in that remained items of the issues are performance prediction of mist separator of MSR, instable drainage of heat transfer tubes of MSR, flow accelerated corrosion (FAC) succeeded by scale adhesion in equipments and NPSH of FWBP, except for the issues of main steam temperature condition and turbine blade efficiency. The remained issues are behaviors of two phase flow themselves or phenomena derived from two phase flow such as mist flow in separator, annular and others in tube drainage, FAC attributing to reduction of pH in liquid of liquid-vapor two-phase flow and depressed boiling in the HPSH.

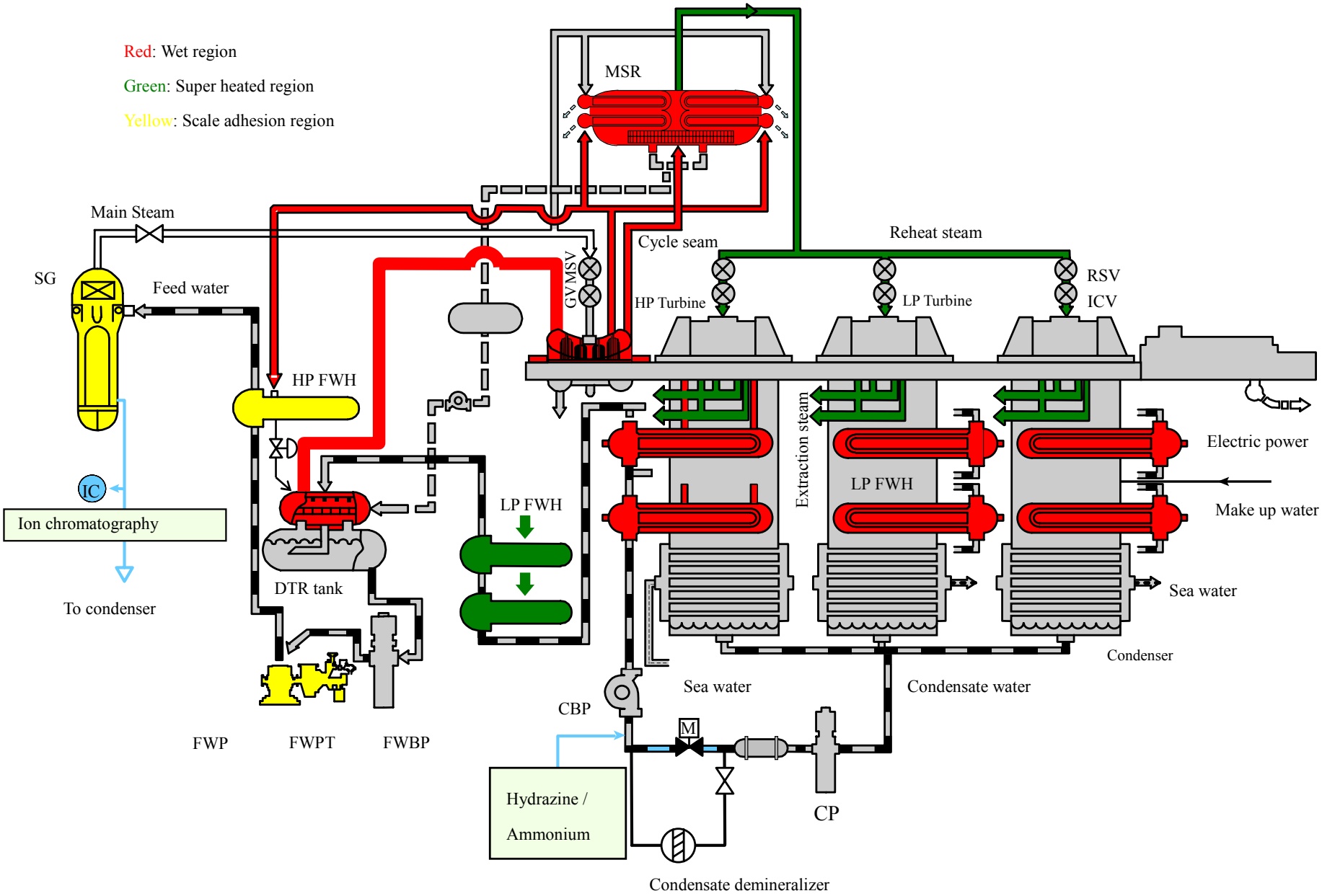

Fig. 1.13 FAC and scale adhesion region of NPP turbine system

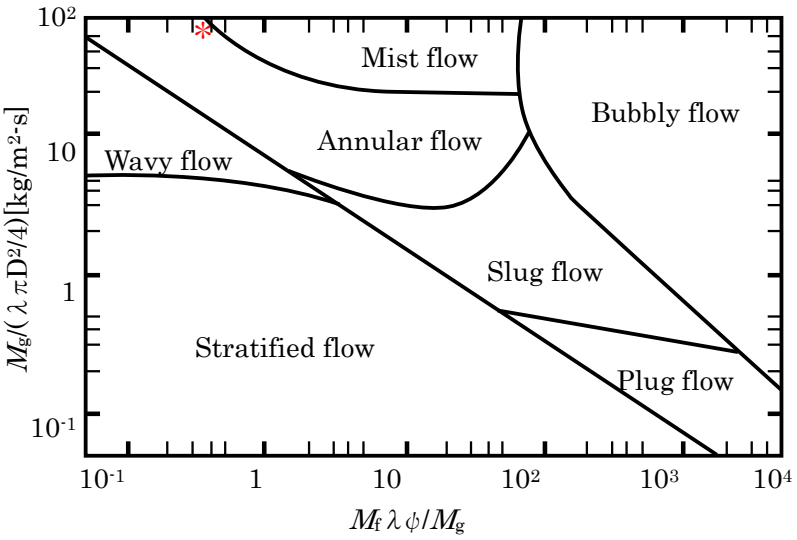

Fig. 1.14 Flow condition of turbine system

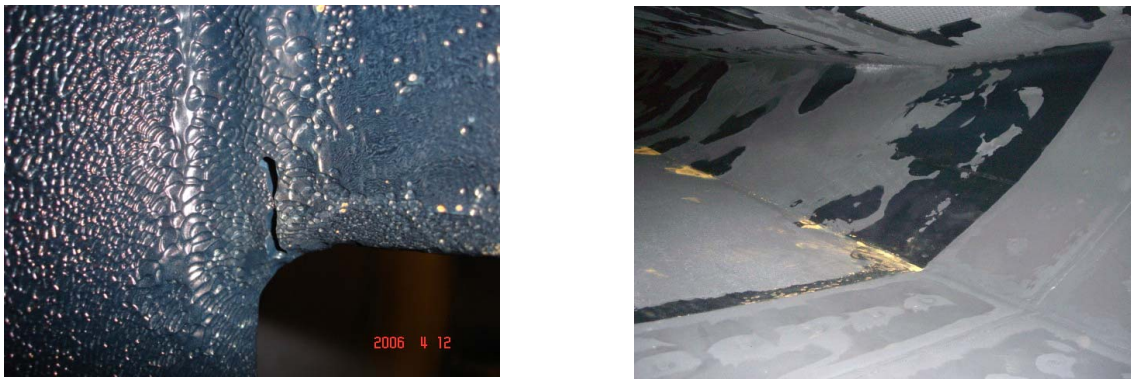

Fig. 1.15 FAC in moisture separator reheater

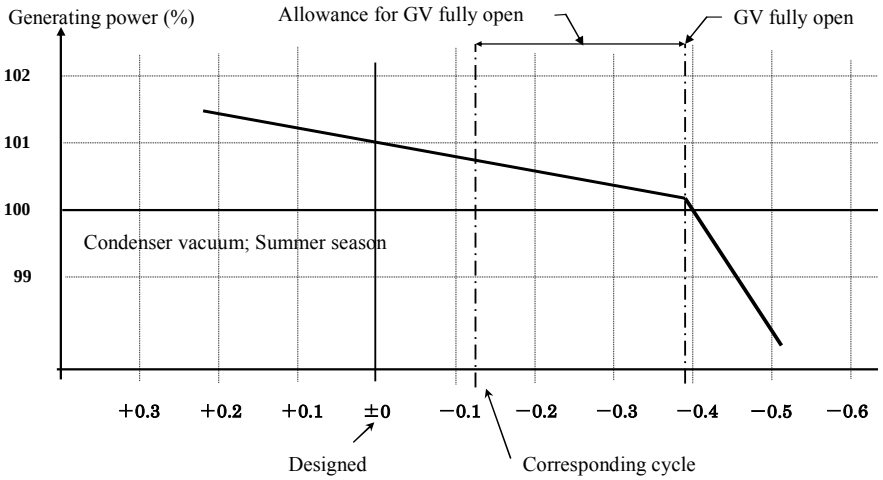

Fig. 1.16 Typical generating power capability

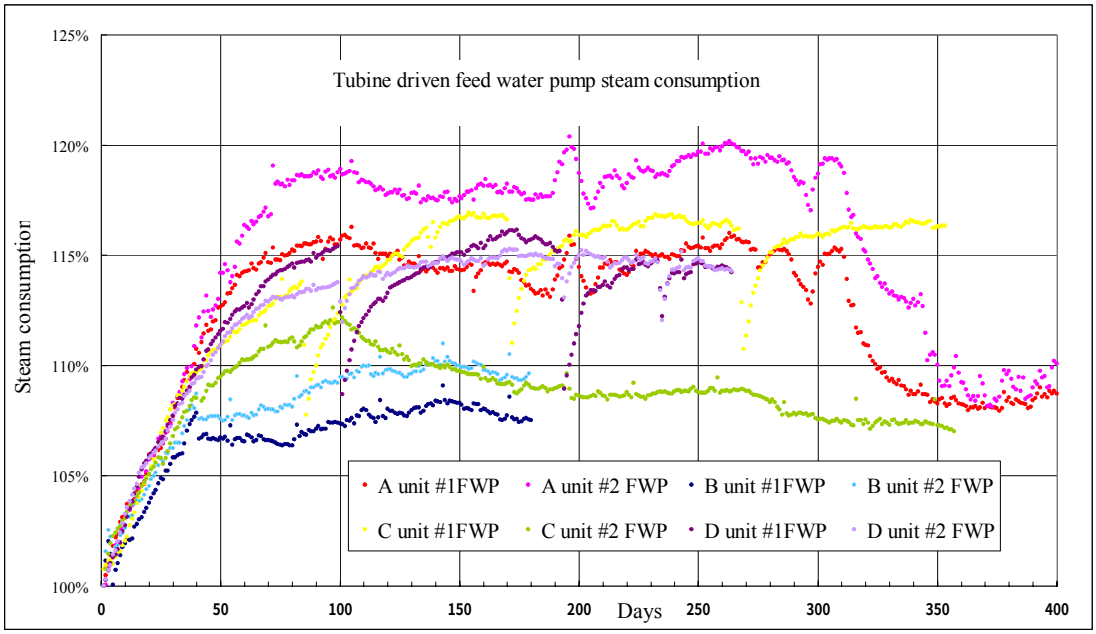

Fig. 1.17 FWPT steam consumption due to scale adhesion to the pump impeller

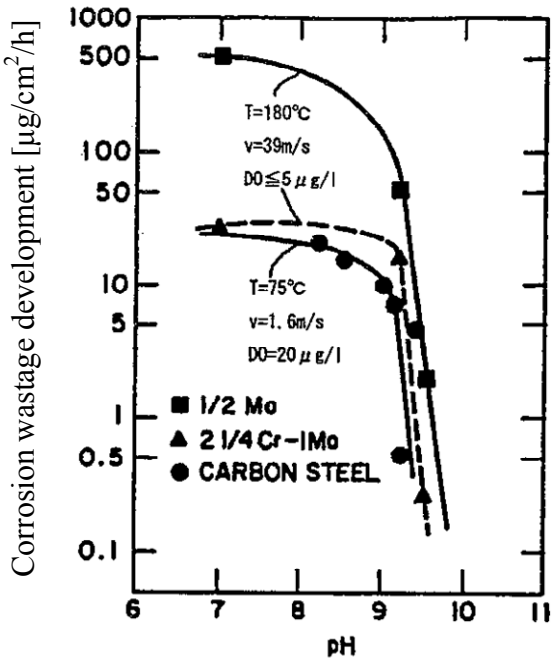

Fig. 1.18 Effects of pH for suppressing erosion developing rate.

(Codes for Power Generation Facilities, - Rules on Pipe Wall Thinning Management- , JSME S CA1-2005, 2005-3, JSME)

1.3 Issues studied in this thesis

The remained issues of the nuclear steam turbine system are derived from two-phase flow of mist, annular flow and depressed boiling condition described in the former section. Here the issues caused by two-phase flow in the system and auxiliaries are studied in this thesis. The traditional technologies and the prospect for the issues are as followings.

1.3.1 Moisture separator reheater in the reheat system

Construction of MSR

MSR is a complex heat exchanger facilitated with functions both of mist separation and superheating. The large-size current model MSR is applied to the 900 MW and 1,200 MW class units as shown in Fig. 1.19.

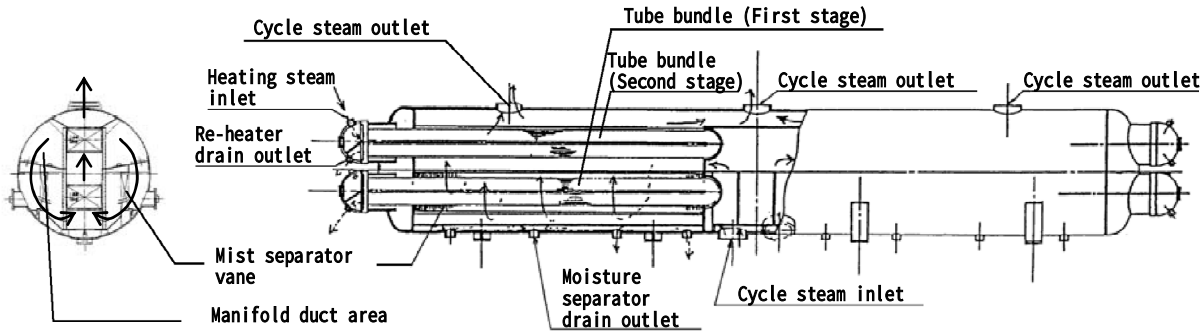

Fig. 1.19 Construction of current model MSR

The MSR of current model is constructed with chevron vane type mist separator and double stage heat exchanger. The first stage is heated by high pressure turbine extraction steam and the second stage by main steam.

Cycle steam at pressure of 1.2 to 1.3 MPa, which is high pressure turbine exhausting steam, with wetness fraction of about 12%, is channeled into the MSR from the inlet nozzles located at the center of the vessel. Then the steam is subsequently channeled into both wings of the vessel through each manifold duct area and delivered uniformly to the mist separator vane assemblage which is located longitudinally along the tubes in the bottom of the vessel.

The mist separated and dried cycle steam is led to the tube outer side of the tube bundle and super heated. The heating steam is deprived of its latent heat by condensing in tubes with transferring its heat to colder cycle steam. Low finned tube is adopted for compensating the poor heat transfer coefficient of tube outer side super heated condition.

Ventilation steam is utilized for exhausting tube inner side condensed drain by friction between the ventilation steam and the drain for smooth drainage for MSR of PWR in Japan and popularly overseas. The ventilation steam needs to be distributed appropriately for each tube, of which the heat transfer load or ingenerating drain quantity is distributed along the cycle steam direction. The necessary ventilation steam for each tube is distributed using the orifice plate installed at the inlet of the tube bundle, facilitated with

different size orifice hole for each tube which corresponds to the sum of condensate drain and inevitable ventilation steam for exhausting the drain.

An example of operating condition at 100% load is shown in Fig. 1.20, which is a single stage reheat system heated with main steam commercially put in operation in 1980s.

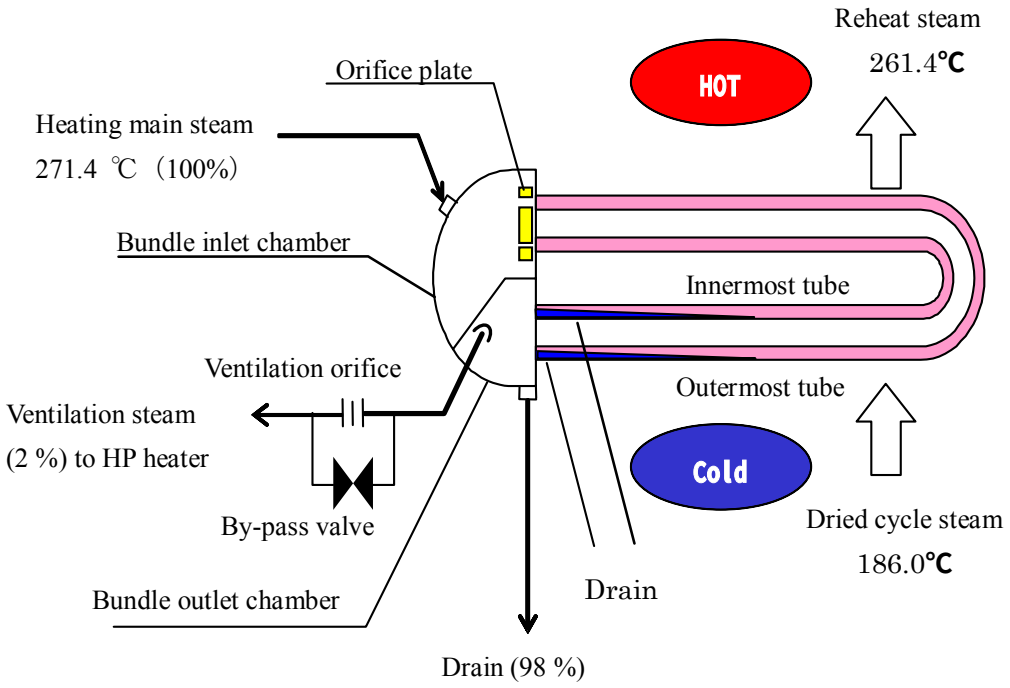

Fig. 1.20 Drainage of MSR heat exchanger tube

Mist separator

Construction of chevron type mist separator vane (Conventional) is shown in Fig. 1.21.

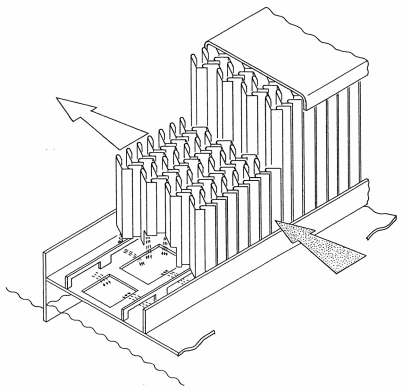

Fig. 1.21 Construction of chevron type mist separator vane (Conventional)

The performance prediction is very important not only from the influence for the turbine heat consumption rate but also from the determination of pressure vessel diameter. The cycle steam flow to the vane is not in direction of right angle to the vane face but in oblique, which makes the velocity in the vane bottom higher than that of the average one. This leads that the performance prediction of the separator must be conducted on condition of the actual arrangement in the pressure vessel with drainage devices of weir and exhausting mouth in the vane bottom.

Performance test on actual steam condition could be executed only one time from economy point of view. Separator performance prediction method on actual steam condition from the air-water test is studied in this thesis.

Heat transfer tube drainage

Heat transfer load at 100% and 50% turbine load is shown in Fig.1.22. The heat transfer load of the tubes, which corresponds to the quantity of ingenerating drainage, alters from the bundled outer tubes to the inner tubes due to a temperature rise in the cross-flow cooling cycle steam along the tubes despite the constant heating temperature of steam inside the tubes.

The ratio of heat transfer loads on the outermost tube to the innermost tube is roughly estimated to be 1.3 under a 100% turbine load. The load ratio increases to 2.1 at a 50% turbine load, caused by both an increase of the heating temperature of main steam and a fall in the temperature of cooling cycle steam due to the steam generator and turbine characteristics, respectively. This may result in inadequate ventilation steam for the outermost tubes due to improper distribution by fixed-sized orifice plate and others. Inadequate ventilation steam will result in the instable drainage of the sub-cool state with temperature oscillation, which may adversely affect the tubes to tube sheet seal welding with thermal fatigue.

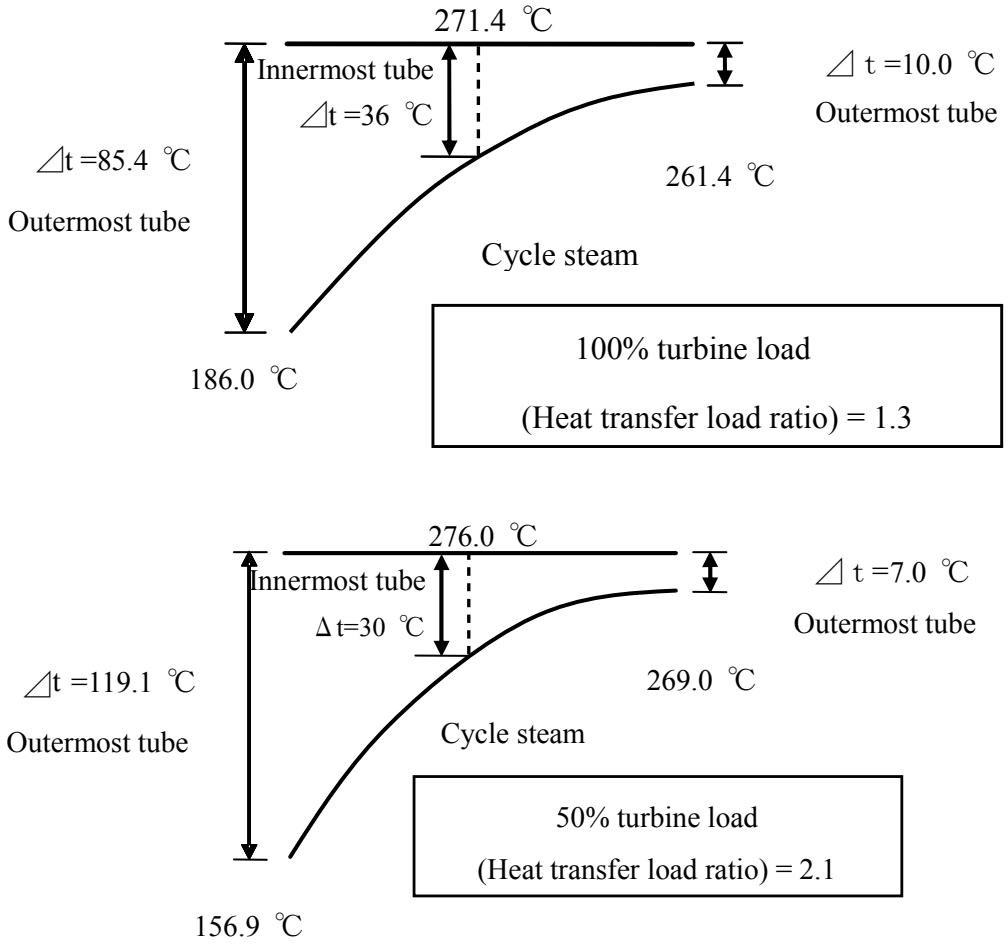

Fig. 1.22 Heat transfer load at 100% and 50% turbine load

The counter measures are as followings;

Four-path-bundle design which exhausts the drain from both the outer half the bundle and the inner half one separately which increase the ventilation steam for each bundle without increase of total venting steam despite complexity of construction, shown in Fig. 1.23. The other is smaller temperature raise bundle by reducing both the ingenerating drain quantity and the heat transfer loads ratio despite the cut of the heat cycle efficiency. The unique exception is Europeans-manufacture design with vertically located one-pass tube bundle.

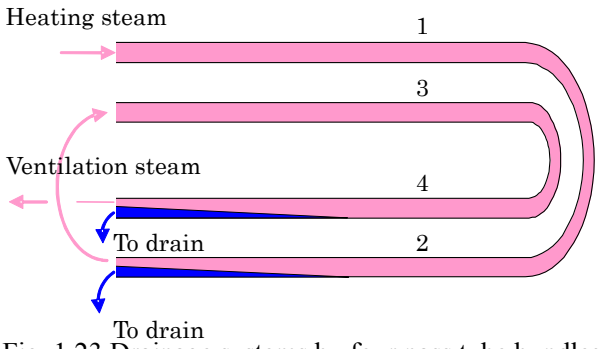

Fig. 1.23 Drainage systems by four pass tube bundles

A method for suppressing the instability in the current model MSR, which was designed larger temperature rise and two pass bundle construction is studied in this thesis.

1.3.2 High all volatile water treatment

Fundamental requirement for water treatment

The requirement for water treatment is for preventing the corrosion of SG heat transfer tube and others. Fundamental design concept for preventing corrosion is as followings;

- Preventing impurities in the cycle adopting leak tight condenser, condensate demineraliser and others.
- Suppression of corrosion in the system by dosing ammonia for pH control and hydrazine for deaeration and reducing atmosphere.

Other than corrosion, water level oscillation and concentration of impurities, both derived from deposit of iron particle to the gap space between tube and tube-plate, are to be prevented by reducing iron concentration in feedwater which is the same way for scale adhesion.

Additionally in recent days for prohibiting from IGA (Inter granular attack), followings are required base on the SG tube corrosion susceptibility diagram which was investigated in the "Investigation of Improving Future Reliability on Secondary water Chemistry Environment" sponsored by JPEIC (Japan Power Engineering and Inspection Corporation) shown in Fig. 1.24[(3)].

- To keep $pH_{300\,^{\circ}C}$ is in range between 5 and 10.
- To prevent ingress of oxidizing materials such as copper.

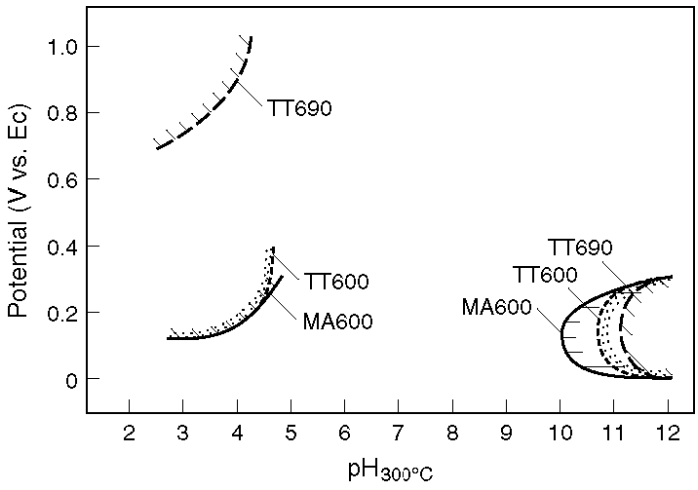

Fig. 1.24 IGA susceptibility for Alloy 600MA, 600TT and 690TT

Requirement for water treatment for preventing FAC and succeeding scale adhesion (HAVT)

(1) Minimum pH value in the system

Minimum pH value is to be elevated to the value where the FAC progress rate reduces enough. And the feedwater iron concentration is small enough to keep the main steam pressure enough for the generating power through unit lifetime.

(2) System requirement for sea-water cooled unit

Purification concept of HAVT is requested both to treat high concentration ammonia, and to be able to operate full capacity condensate demineraliser at sea-water in-leakage, which is the last protection despite the adoption of leak tight condenser.

1.3.3 High temperature NPSH

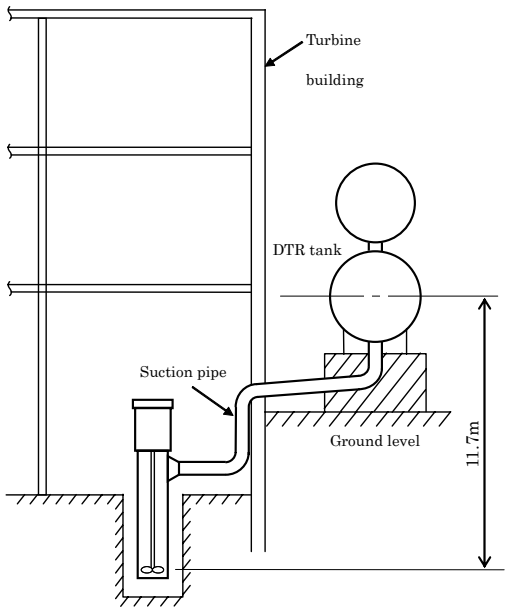

Fig.1. 25 Arrangement of FWBP and DTR-tank

Two similarly designed second generation 800MWe class units, of which the available NPSH ($NPSH_{av}$) was designed insufficient for the transient due to lack of the requirement for the operation function, maintained smooth operation at the load rejection test from full power to house load during their trial operations in the 1970s, followed by neither complete loss of the FWBP head nor the succeeding tripping of the FWP by a protection interlock. This datum suggests that the NPSH of FWBPs was maintained through the transitions. Arrangement of the FWBP and DTR-tank is shown in Fig. 1.25, static head of which is less than half of the current design shown in Fig. 1.9. This may follow the reduction of required NPSH in higher temperature contributing to cost reductions of lower elevation of DTR-tank and others.

Definition of NPSH here is not the NPSH adopted by industry, which maintains head over 97% head or 3% head loss, but the suction head which gives nearly half of the rated head due to the reduction of required NPSH of FWP in partial flow condition. NPSH depends on both dissolved gas and temperature. It increases by dissolution of dissolved air along with static pressure reduction and decreases along with temperature rise by mechanism of thermal effect of cavitation. Dependency of required NPSH ($NPSH_{req}$) on temperature is presented by Stepanoff [(4), (5)], Ruggeri-Moore [(6)] and others. Ruggeri also stated that pump may keep a range of 0.85 to 0.97 head coefficient with $NPSH_{req}$ of nearly zero in a higher temperature, may it be a foretelling of negative $NPSH_{req}$. On the other hand according to Minemura [(7)] and others, increase of the gas to gas-water mixture ratio up to range of 6 to 7 % reduces head gradually to several percentages and then reduces the head rapidly to zero head within the ratio nearly 10% in case of a centrifugal pump.

NPSH in actual high temperature condition with insufficient $NPSH_{av}$ is studied in this thesis based on actual unit data and prediction method by Ruggeri.

1.4 Composition of the thesis

Based on the surveillance and the prospect for the issues, followings are studied in this thesis.

In chapter-2 "Reheat system and moisture separator reheater", separator performance prediction method on actual steam condition from air-water test, method for suppressing the instability of tube drain in partial turbine load associated with clarification of temperature oscillation of condensing water and new design concept for larger capacity unit are studied.

In chapter-3 "High all volatile water treatment", concept of HAVT complying with sea water cooled unit in Japan and prediction both for reduction of FAC rate and scale adhesion attribute to suitable selection of pH in feedwater are studied.

In chapter-4 "High temperature NPSH and its application to a feedwater system", design theory for high temperature NPSH is described based on clarification of experiences in actual units by bringing the concept of NPSH in negative area based on both simulation of available NPSH and prediction of required NPSH at actual high temperature.

References

(Ex. 1) J. Manabe, K. Yamakami, S. Hiraoka, T. Kawai, A Lifecycle Management Program for NPP Turbine Balance of Plant, JSME Journal of Power and Energy Systems, Vol. 3, No. 2, 2009

(Ex. 2) Codes for Power Generation Facilities, - Rules on Pipe Wall Thinning Management-(in Japanese), JSME S CA1-2005, 2005-3, JSME

(Ex. 3) Y. Shoda, M. Sato, H. Fujiwara, R. Kamio, T. Hattori, Improvement of SG Crevice Environment Estimation, 1998 JAIF International Conference of Water Chemistry in NPP at Kashiwazaki, Japan

(Ex. 4) Stepanoff, A.J., Cavitation Properties of Liquids, Journal of Engineering for Power, April, 1964 / 195

(Ex. 5) Stahl, H.A., Stepanoff, A.J., Thermodynamic Aspects of Cavitation in Centrifugal Pumps

(Ex. 6) Ruggeri, R., Moore, R., Method for Prediction of Pump Cavitation Performance for Various Liquids, Liquid Temperatures, and Rotative Speeds, NASA TN D-5292, 1969, Lewis Research Center Cleveland Ohio NASA

(Ex. 7) Minemura, K., Uchiyama, T., Shoda, S., Egashira., K., Prediction of Air-Water Two-Phase Flow Performance of a Centrifugal Pump Based on One-Dimensional Two-Fluid Model, Journal of Fluids Engineering, ASME, JUNE 1998, Vol. 120, pp 327-334

Chapter 2 Reheat System and Moisture Separator Reheater

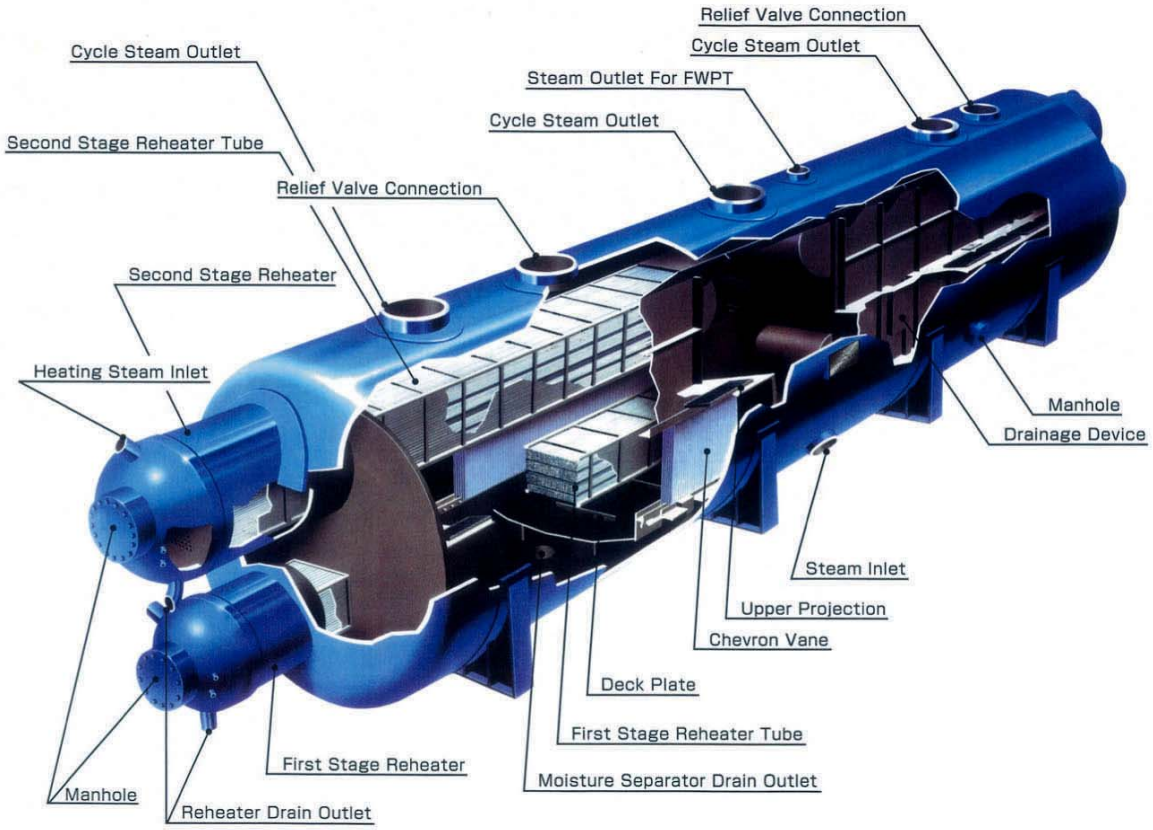

Fig. 2.1 Current model Moisture Separator Reheater

2.1 Introduction

2.1.1 Reheat cycle

Current moisture separator reheater is shown in Fig. 2.1, which was adopted for the units of 800 MW and 1200 MW class, number of which is 11 units.

Wetness fraction in steam

Saturated main steam generated from a steam generator for a light-water reactor expands within a turbine, thus ingenerating rotational force associated with an enthalpy drop and a subsequent increase of wetness fractions. The velocity-triangles of steam and mist entering the turbine blades is shown in Fig. 2.2, which explains an increase of wetness fraction adversely affects the mechanical efficiency of the turbine by inhibiting the rotational force caused by the speed gap between the steam and mist. As shown in Fig. 2.3, the wetness fraction results in FAC over all the auxiliaries of the turbine extraction piping and heat exchangers.

The wetness fraction in a reheat turbine system reaches 12% at high-pressure turbine exhaust and finally reaches the same level at low-pressure turbine exhaust. On the other hand, the value would exceed 12% in a non-reheat system as shown in Fig. 2.4.

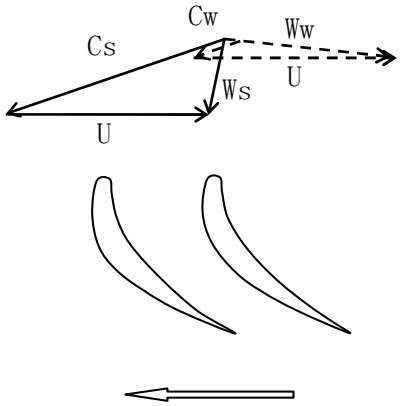

Note;

U: Blade tip speed

C_s: Inlet steam absolute velocity

W_s: Inlet steam relative velocity

C_w: Inlet water droplet absolute velocity

W_w: Inlet water droplet relative velocity

Fig. 2.2 Velocity triangles entering the turbine blades

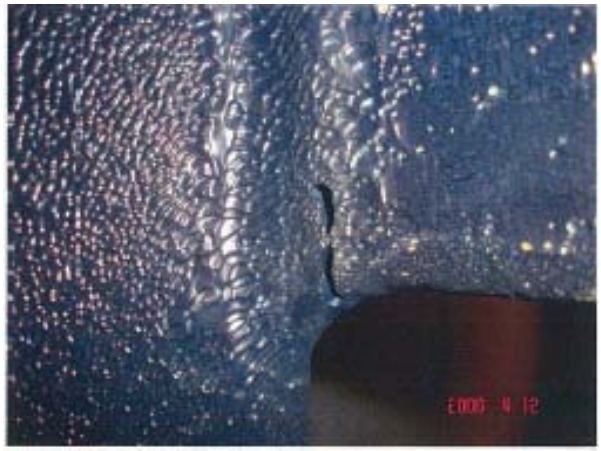

Fig. 2.3 FAC in the inner construction of MSR

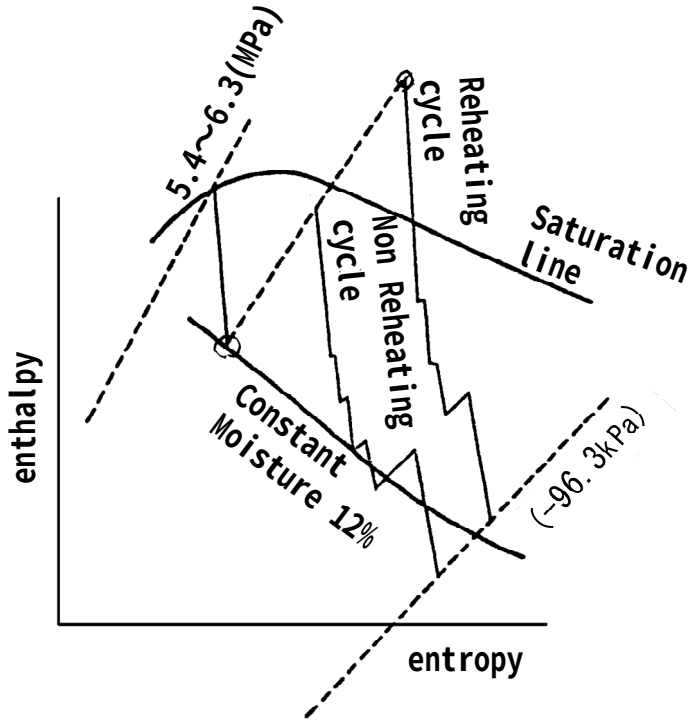

Fig. 2.4 Steam turbine expansion diagram

Improvement of turbine mechanical efficiency

A reheat cycle consists of mist separation and superheating in a turbine expansion process. This cycle contributes to an improve in turbine mechanical efficiency by overcoming the heat loss by transferring the main steam at higher temperatures to the reheated cycle steam at lower temperatures, thus rendering a final improvement in turbine efficiency by 2.2% to 2.5%.

Influence factor for turbine heat consumption rate of MSR performance

MSR performance is defined by both TTD of the first and second stages respectively and the cycle steam pressure drop through the vessel, as well as the separator mist carryover rate of the cycle steam.

Influence factor for the turbine heat consumption rate are about 0.02% and 0.01% for unit TTD in the second stage and the first stage respectively, 0.1% for unit pressure drop percentage of the inlet cycle steam and 0.2% for the unit percent mist carryover from the separator. The separator performance is the key item due to its high influence factor, which corresponds approximately to the potential improvement attained by an additional regenerative FWH of the seventh stage to the prevailing six stages regenerative cycle.

Contribution to suppression of the FAC

This cycle also contributes to the suppression of the FAC of the low-pressure turbines and their extraction system auxiliaries colored green in Fig. 2.5, though the area colored red maintains wet steam and the colored yellow is the consequent scale adhesion region. The remained red colored area, containing MSR pressure vessel and its inner construction, must be applied other measure of HAVT water treatment argued in Chapter 3.

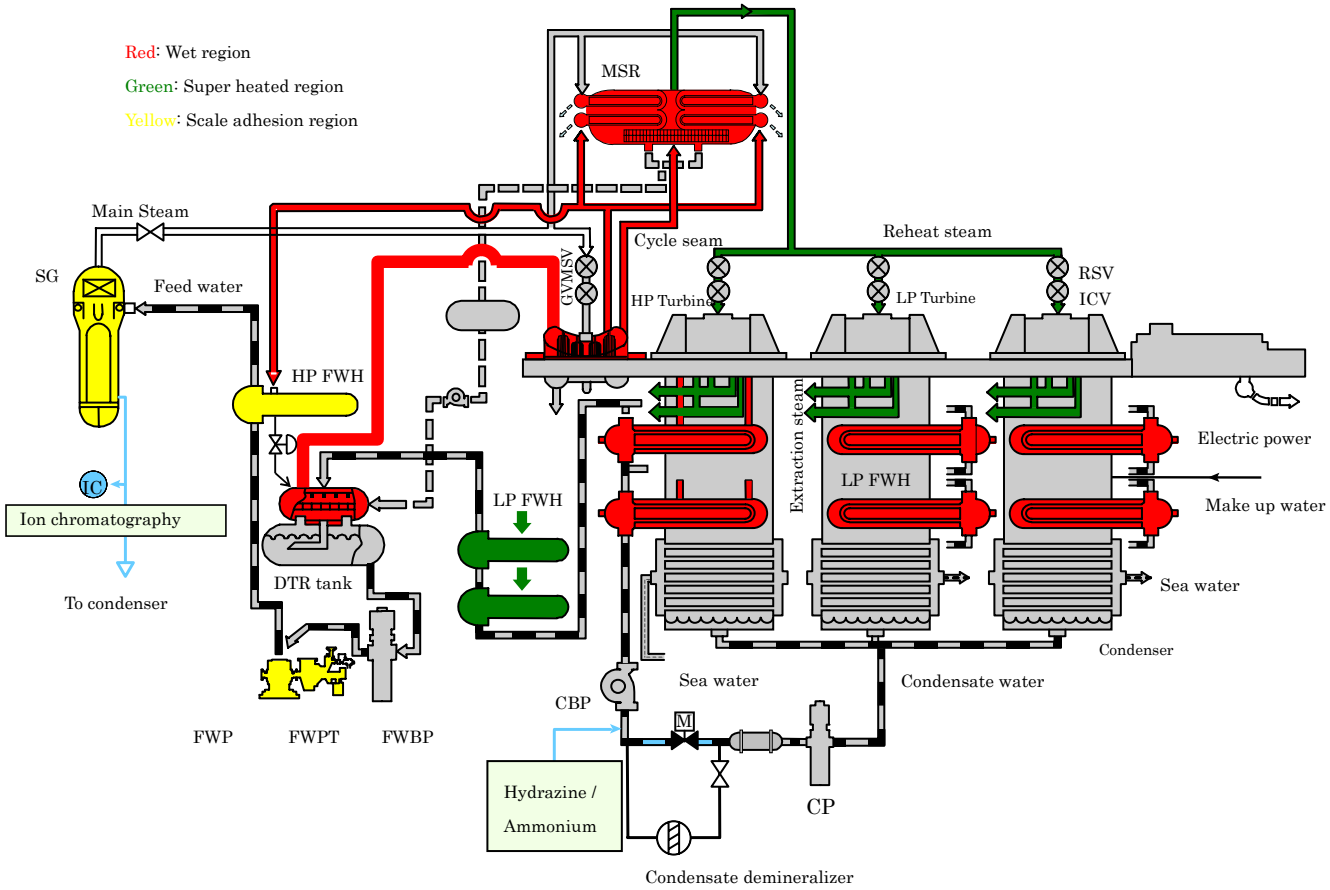

Fig. 2.5 System and equipments

2.1.2 Reheat pressure

Heat cycle efficiency

Heat cycle efficiency is affected by increase of wetness fraction in steam along with the expansion in turbine. The maximum efficient reheating pressure point with mist separation is in the middle of main steam and turbine exhaust because the efficient is zero in the both points. The lower the reheat point moves the larger the wetness fraction in high pressure turbine becomes affecting the efficiency of high pressure turbine despite the wetness in low pressure turbine becomes lower increasing the efficiency in low pressure turbine on the condition of a constant reheat temperature.

The study for selecting the reheat pressure was reported by R.C. Spencer and J.A. Booth [(1)] stating the most efficient pressure was around 20 to 30% of main steam pressure despite its sensitivity was relatively low.

MSR

Higher reheat pressure is better for MSR component due to both compact design and reliability. Higher reheat pressure contributes to smaller pressure vessel, easy for chevron vane mist separation and lower cycle steam pressure drop both of which the performances are restricted by dynamic pressure. The higher pressure also contributes to the reliability derived from both smaller thermal deformations [(2)] of the vessel by lower cycle steam temperature rise and lower heat exchange load distribution for heat transfer tubes.

Turbine

Lower reheat pressure is advantageous for compact design of low pressure turbine, which attributes to reduction of blade tip leak loss caused by reduction of blade stages of low pressure turbine. The blade tip leak loss is reduced by reduction of flow passes because the low pressure turbine has six path of three cylinders construction despite the high pressure turbine has two path of one cylinder.

Current design pressure

The above follows that the optimum reheat pressure is to be evaluated comparing the total efficiency of turbine system with cost of component design of turbine and MSR associated with the reliability. The current reheat pressure, except for one Europe manufacturer, is selected 1.0 to 1.4 MPa which corresponds to roundly 20% of the main steam pressure of 5 to 7 MPa.

2.1.3 Current model MSR for PWR in Japan

Construction of MSR

The large-size current model MSR was applied to the second-generation PWR units in the 900 MW class units, which started commercial operation in the 1980s, and to those in the 1,200 MW class in the 1990s as shown in Figs. 2.1 and 2.6.

The MSR is constructed with chevron vane type mist separator and double stage heat exchanger. Heat transfer tube bundle is constructed of 2 pass U tube. Low finned tube is adopted for compensating the poor heat transfer coefficient of tube outer side super heated condition. The first stage is heated by high pressure turbine extraction steam and the second stage by main steam.

Cycle steam at pressure of 1.2 to 1.3 MPa, which is high pressure turbine exhausting steam, with wetness fraction of about 12%, is channeled into the MSR from the inlet nozzles located at the center of the vessel as shown in Fig. 2.6 section A-A. Then the steam is subsequently channeled into both wings of the vessel through each manifold duct area and delivered uniformly to the mist separator vane assemblage which is located longitudinally along the tubes in the bottom of the vessel as shown in Fig. 2.6 section B-B. Chevron vane type mist separator catches water droplet by pocket located at the chevron corner. The mist separated and dried cycle steam is led to the tube outer side of the tubes of the tube bundle and super heated. The heating steam is deprived of its latent heat by condensing in tubes transferring its heat to colder cycle steam.

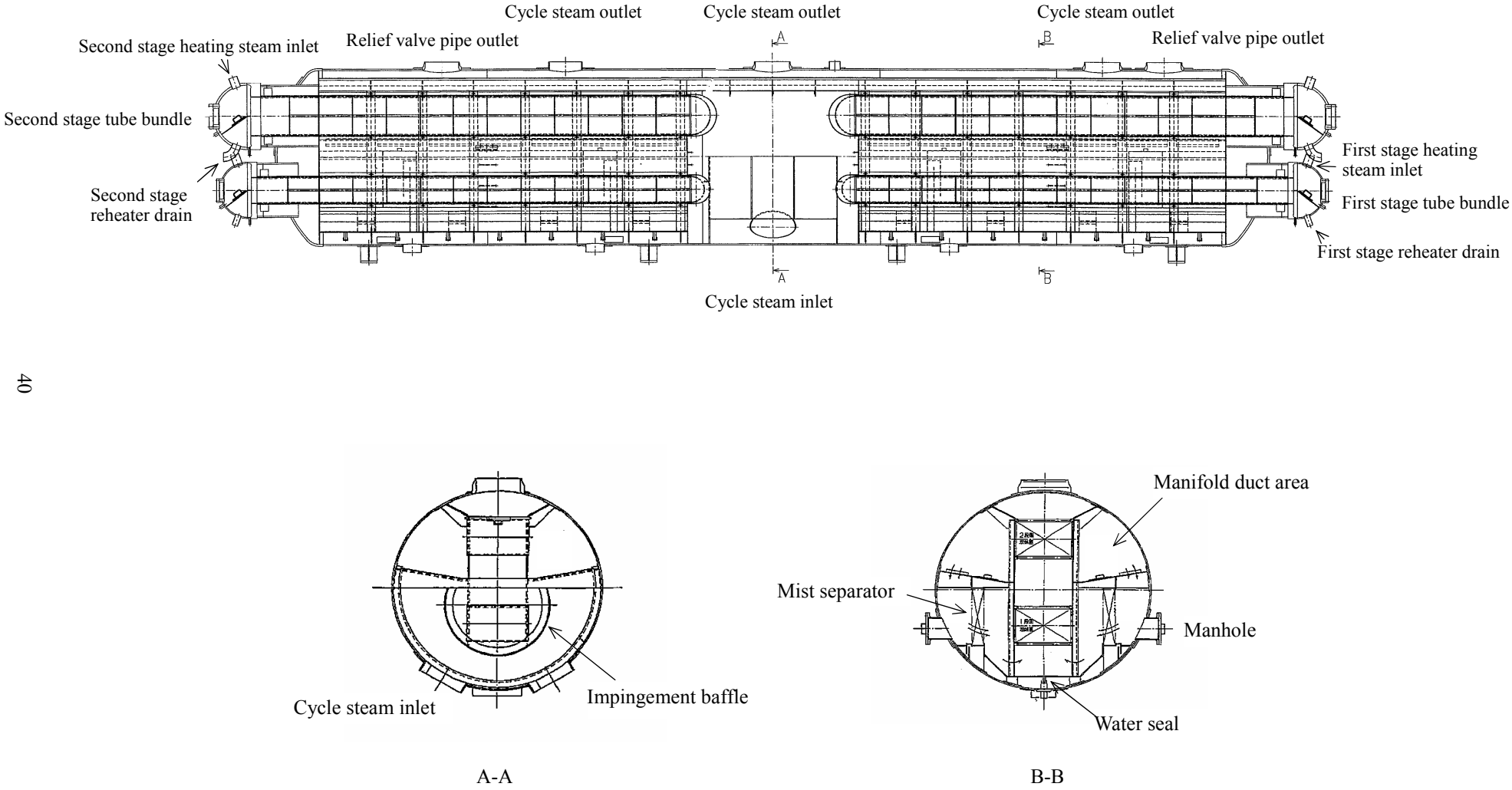

Fig. 2.6 Current model MSR in Japan

Performance of the MSR

The performance of the current model MSR is shown in Table 2.1, stating the achievement of the expected TTD values of 13.9˚C, the separator mist carryover of 0.25%, the cycle steam pressure drop of 4% and suppression of the tube drainage instability.

Table 2.1 Performance of the current model MSR

	900-MW class	1200-MW class
Second stage TTD(˚C)	8.7	8.0
ΔP (% ratio to inlet pressure)	2.1	2.6
Carried over mist (%)	Less than 0.1	Less than 0.1
Sub-cool (˚C)	0.8	Not measured

Here the mist carryover performance of the advanced type vane for 1200 MW class was predicted from air-water test data by the developed method without actual steam test as shown in Table 2.2. The tube drainage instability was suppressed by another developed new method.

Table 2.2 Performance prediction for separator vanes

	900 MW class	1200 MW class
Separator vane type	Conventional	Advanced
Laboratory verification	*Air-water* and *Actual steam*	*Air-water* and *Prediction* under actual steam by the developed method

2.1.4 Comparison of MSRs overseas and in Japan

Comparison of MSRs overseas and in Japan is shown in Table 2.3 [(5), (6) and (7)]. The PWR turbine system adopted reheat system from their first commercial construction with single and then double stage reheat processes, alongside their increase of generating power. Prevailing reheat process is double-stage reheating for both PWR and BWR. Number of MSR pressure vessel is two with current large-size model for 2 to 3 low pressure turbine cylinders. Type of the vessel is generally horizontal which is easy both for construction and maintenance despite the difficulty of tube drainage.

Ventilation steam is adopted popularly for smooth drainage of heat transfer tubes. There are other procedures currently adopted for smooth drainage overseas. One is the 4 path bundle design which exhausts the drain from both the outer half the bundle and the inner half one separately, increasing the ventilation steam for each without increase of total ventilation steam, as shown in Fig. 2.7. The other is smaller temperature raise bundle by reducing both the drain quantity and its distribution despite the cut of the heat cycle efficiency. The unique exception is Europeans-manufacture design, which is vertical vessel with one pass tube bundle located vertically as shown in Table 2.3 E. The feature of the design is easy for tube drainage by gravity, despite the complicated inner construction in narrow vessel bottom especially for mist separator which requires relatively lower steam velocity.

Table 2.3 Comparison of MSRs overseas and in Japan

Manufacture	A (Japan)	B (Japan)	C (Japan)	D (Japan)
Configuration	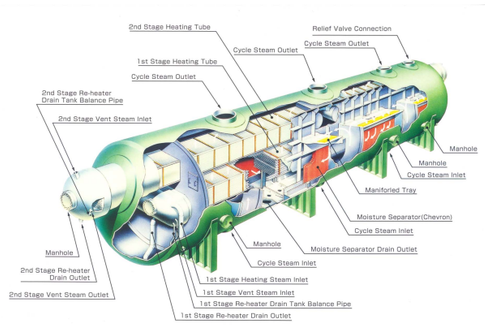	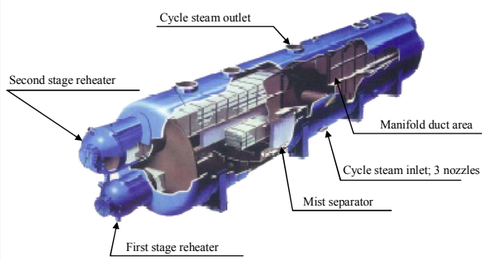	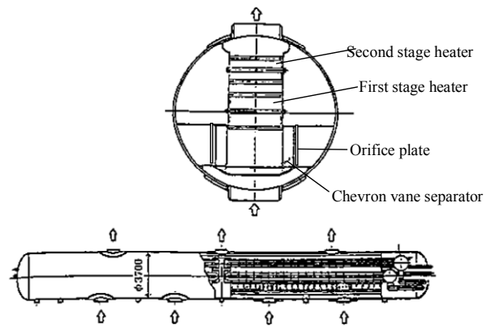	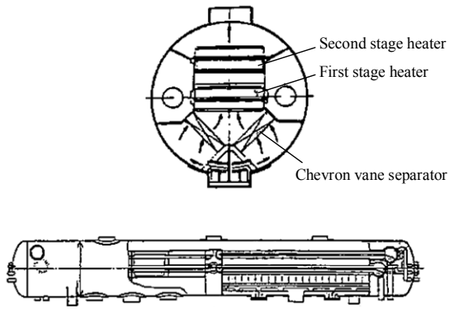
Features	(1) Horizontal vessel double stage reheat (2) Two pass tube (3) Vertically arranged chevron type mist separator	(1) Horizontal vessel double stage reheat (2) Two pass tube (3) Vertically arranged chevron type mist separator	(1) Horizontal vessel double stage reheat (2) Two pass tube (3) Vertically arranged chevron type mist separator	(1) Horizontal vessel double stage reheat (2) Two pass tube (3) Aslant arranged chevron type mist separator

Manufacture	E (Europe)	F (Europe)	G (USA)	H (Japan)
Configuration	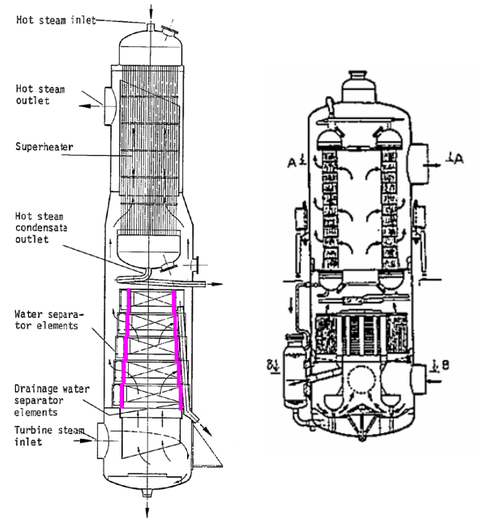	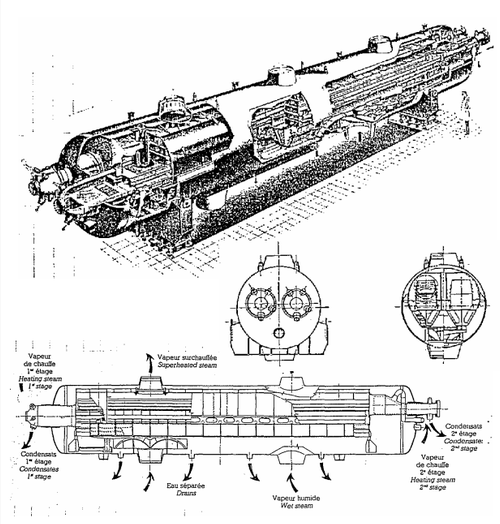	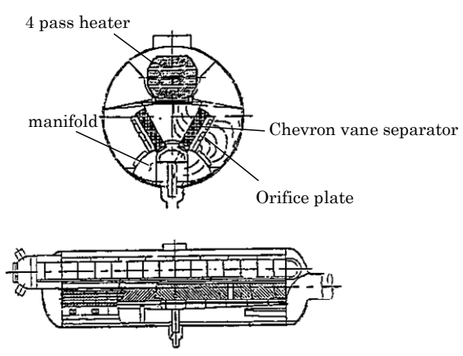	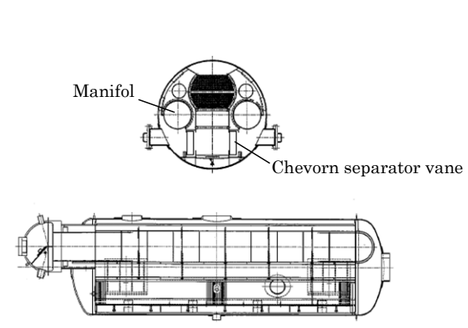
Features	(1) Vertical vessel single stage reheat (2) One pass tube (3) Vertically arranged chevron type mist separator	(1) Horizontal vessel double stage reheat (2) 2 pass tube (3) Aslant arranged chevron type mist separator	(1) Horizontal vessel single stage reheat (2) 2 pass tube (3) Aslant arranged chevron type mist separator (4) Model for retrofit	(1) Horizontal vessel single stage reheat (2) 2 pass tube (3) Vertically arranged chevron type mist separator (4) Model for retrofit

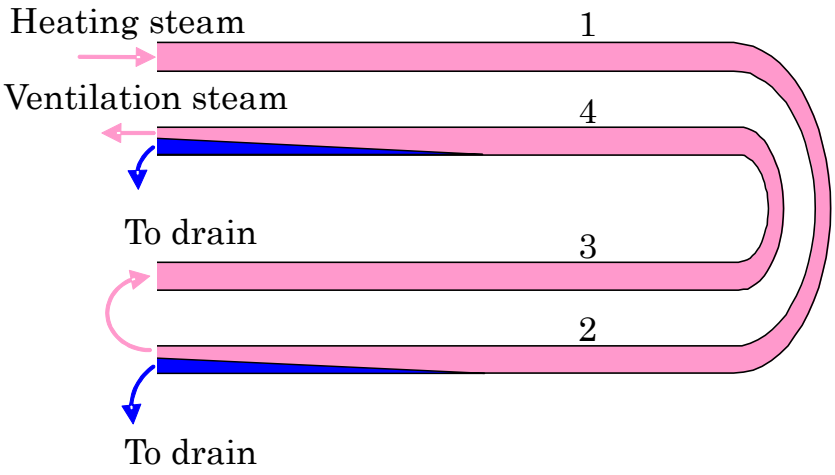

(a) Four pass system of proto type

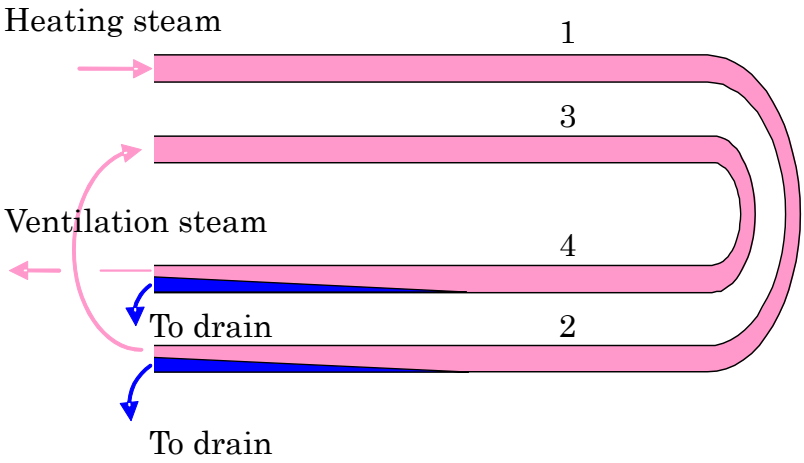

(b) Four pass system of recent days

Fig. 2.7 Drainage system by four path tube bundles

2.1.5 Mist separator

Performance of separator vane

MSR separator system requires a drainage device with weir and exhausting mouth in the vane bottom, where the velocity is relatively higher than average. It leads to the necessity of separator performance prediction on actual steam condition from the air-water test with actual arrangement in the vessel.

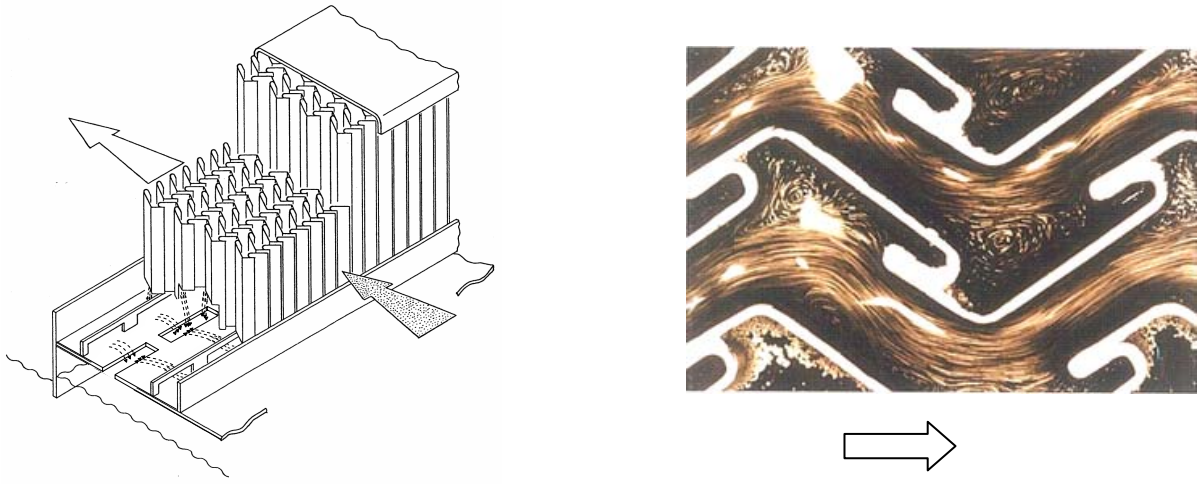

Fig. 2.8 Conventional type mist separator and its observation in shallow-water tank test

A bird eye view of conventional type mist separator is shown in fig. 2.8, the construction of which is 7 turns with pocket at each corner. Observation in shallow-water tank test of the conventional vane showed vortexes at the corner, which anticipated that a part of mist flow did not caught by the pocket.

Advanced type vane with higher performance was developed, shown in Fig. 2.9, of which the construction is 3 turns and a mist catch pocket at each turn leading smooth flow without vortexes. Flow resistance coefficient was 19 in definition of right angle flow, which was comparatively smaller to that of 41 of the conventional.

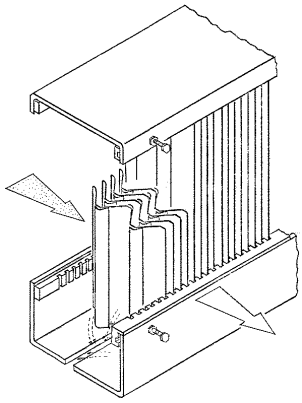

Fig. 2.9 Advanced type mist separator vane

It was prospected that the advanced vane would bring the higher performance on the condition that the final performance of the separator system would be ruled not by vane element but by accumulated water level which might depend on the pressure drop through the vane.

Velocity distribution around the mist separator

The uniformly delivered cycle steam in direction of vessel longitude to the chevron vane assemblages enters into each vane affected adversely for its favorable approaching velocity. The cycle steam flow is not in direction of right angle to the vane face but in oblique because the flow enters from manifold duct area located upper side of the vane, which makes the velocity in the vane bottom higher than that of the average one. Velocity distribution of the separator vane is evaluated as following.

Nomenclature

U_1: Velocity discharging out from the manifold duct area to the space in front of the separator vane

U_2: Velocity discharging out from the space rear of the separator vane

P: Static pressure

V: Steam velocity in direction of right angle to the separator vane face

ζ: Flow resistance coefficient of the separator vane

ρ: Density of steam

g: Acceleration of gravity

Subscript

1: Cross section 1 (Top of the vane)

2: Cross section 2 (Bottom of the vane)

m: Average

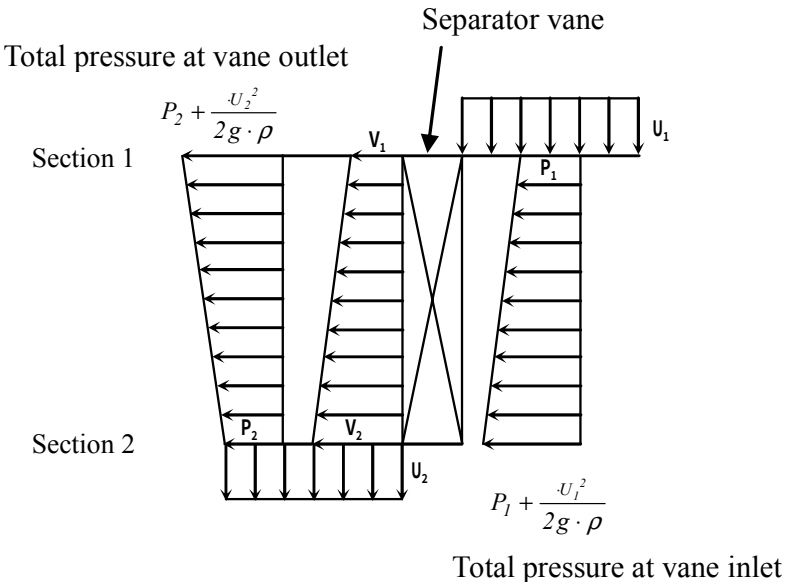

Fig. 2.10 Velocity distribution of mist separator vane

Static pressure and vane velocity (V), in direction of right angle to the vane face, distribute in vertical direction as shown in Fig. 2.10, on the assumption of both static pressure of P_1, P_2 and velocity of U_1, U_2 at vane inlet and outlet, respectively. U_1 is the discharging velocity out from the manifold duct area to the space in front of the vane, and U_2 is the discharge velocity out from the vane rear space, respectively.

Bernoulli's theorem applied to the cross section of 1 (Top of the vane), 2 (Bottom of the vane) of vane and through vane from inlet to outlet leads Eqs. (2.1), (2.2) and (2.3), respectively.

$$\frac{P_1}{\rho}-\left(\frac{P_2}{\rho}+\frac{{U_2}^2}{2g}\right)=\zeta\cdot\frac{{V_1}^2}{2g} \tag{2.1}$$

$$\left(\frac{P_1}{\rho}+\frac{{U_1}^2}{2g}\right)-\frac{P_2}{\rho}=\zeta\cdot\frac{{V_2}^2}{2g} \tag{2.2}$$

$$\left(\frac{P_1}{\rho}+\frac{{U_1}^2}{2g}\right)-\left(\frac{P_2}{\rho}+\frac{{U_2}^2}{2g}\right)=\zeta\cdot\frac{{V_m}^2}{2g} \tag{2.3}$$

Ratio of the velocities through the vane on cross section 2 to 1 is described as Eq. (2.4). The equation explains that the velocity at the bottom of the separator vane is larger than that of the top. Because mist carryover performance is subject to the vane bottom velocity of V_2, described in the latter section, the velocities of U_1 and U_2 are to be limited. Especially too higher velocity of U_1 causes adverse direction flow in upper area of the vane.

Vane average velocity of V_m is to be designed not to ingenerate the carryover throughout the vane considering the velocity distribution, especially the vane bottom velocity of V_2.

$$\frac{V_2}{V_1}=\sqrt{\frac{\zeta+\left(U_2/V_m\right)^2}{\zeta\ -\left(U_1/V_m\right)^2}} \tag{2.4}$$

Not only the velocity of V_m but also the velocities of U_1 and U_2 influence the vessel diameter. Thus the prediction for the critical velocity of separator vane is very important not only for the turbine heat consumption rate but also for the compact vessel design of MSR.

2.1.6 Tube drainage and ventilation steam

Heat transfer of MSR is a deprivation of latent heat of condensing heating steam inner side of the tubes. Figure 2.11 shows estimate of one condition in horizontally located tube, where heating steam condenses by cooling from tube outer side, explaining possible several kinds of flow conditions.

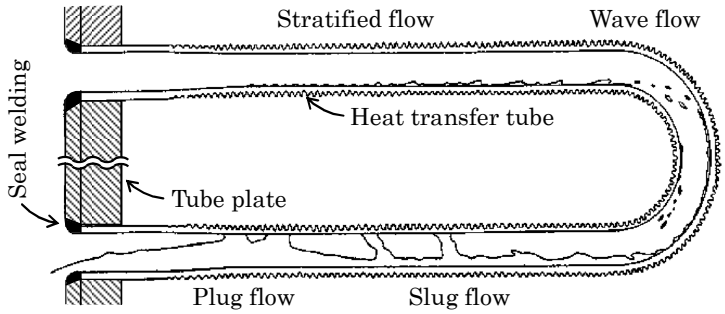

Fig. 2.11 Estimate of one condition in tube inside

One of the operating condition is shown in Fig. 2.12, which is a single stage reheat system heated with main steam commercially put in operation in early 1980s as the last unit with single reheat.

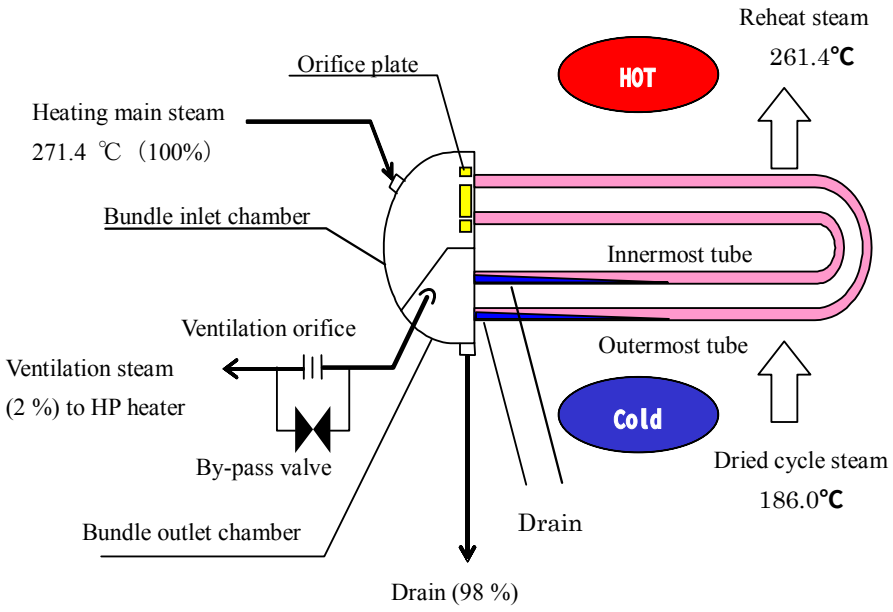

Fig. 2.12 Drainage system of PWR in Japan

Mist separated and dried cycle steam of 1.2 MPa and 186.0 ℃ enters into the tube outer side of the heat transfer tube bundle, where the heating main steam transfers its latent heat by condensing itself in the tubes to a colder cycle steam.

Ventilation steam of about 2% to 3% of the total heating steam is utilized for exhausting tube inner side

condensed drain by friction between the ventilation steam and the drain for smooth drainage. Ventilation steam flows into tubes, then gathers together at the bundle outlet chamber and controlled its flow rate to be constant by ventilation orifice which is operated in critical pressure ratio.

The ventilation steam needs to be distributed appropriately for each tube because the heat transfer load of the tubes, which corresponds to the quantity of ingenerating drainage, alters from the bundled outer tubes to the inner tubes due to a temperature rise in the cross-flow cooling cycle steam along the tubes despite the constant heating temperature of steam inside the tubes.

The necessary ventilation steam for each tube is distributed using the orifice plate installed at the inlet of the tube bundle. The orifice plate is facilitated with different size orifice hole for each tube which corresponds to the sum of condensate drain and inevitable ventilation steam for exhausting its drain.

On the other hand, experiences overseas revealed a problem of instable tube drainage especially in partial load accompanied by sub-cooling to the heating saturated steam temperature with temperature oscillation at the heat transfer tube outlet, resulting in thermal fatigue in the seal welding of tubes to tube-sheet at the end of the tubes, as described in Section 1.3.1.

Heat condition around the MSR in partial turbine load

Heat condition around MSR in partial turbine load is described for analysis of unstable drainage in partial load.

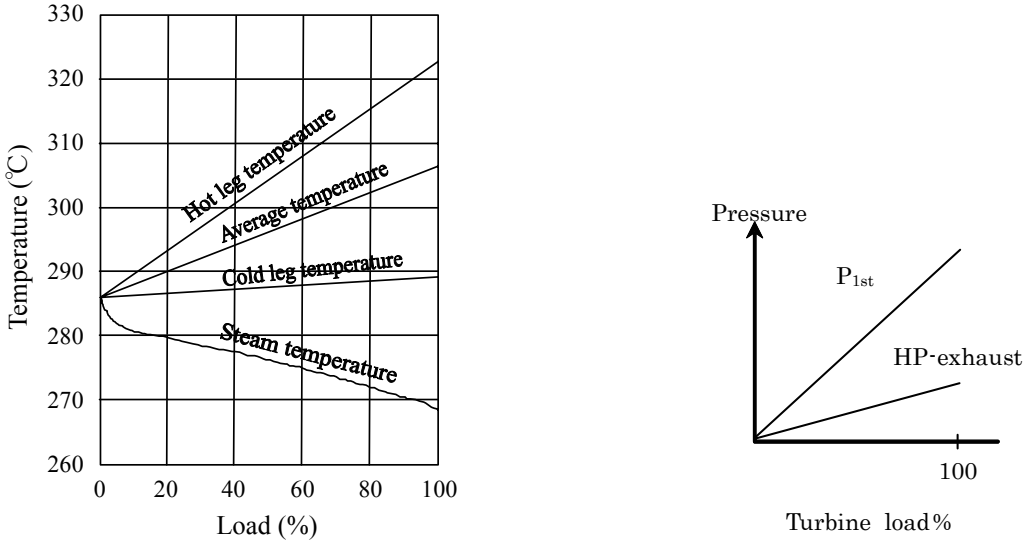

(a) Reactor coolant temperature control and main steam temperature (b) Turbine stage pressure

Fig. 2.13 Pressure in turbine stage vs. load and T_{ave} control

Heat condition around MSR in a partial turbine load is determined by unit thermal power control, as described in Section 1.1.1.

-Temperature of heating main steam is higher than that of turbine rated power by several ˚C due to the reactor coolant temperature control, as illustrated in Fig. 2.13 (a).

-Temperature of cycle steam is saturation temperature of the pressure which is in proportional relation to the turbine load, as illustrated in Fig. 2.13 (b).

Thus the pressure and temperature around MSR is as shown in Table 2.4 which is the actual value of the measured unit.

Table 2.4 Heat condition around MSR

Measured point	50% turbine load	100% turbine load
Main steam pressure at SG outlet (MPa)	6.15	5.69
Heating steam temperature for MSR (°C)	276.0	271.4
HP-turbine exhaust pressure (MPa)	0.57	1.13
HP-turbine exhaust temperature (°C)	158.2	186.5

Heat transfer load and tube drainage in partial turbine load

Heat transfer load alteration along the bundle is shown in Fig. 2.14 for 100% and 50% turbine load, respectively. Sequential computation attained the temperature of cycle steam on the assumption that the inner side of the tubes was condensing without sub-cooling.

The ratio of heat transfer loads on the outermost tube to the innermost tube is roughly estimated based on the temperature difference between the heating steam and cooling cycle steam, shown in Fig. 2.14(a), to be 1.3 under a 100% turbine load by Eq. (2.5).

$$(Heat\ transfer\ load\ ratio\ ) = \frac{(Outermost\ tube)}{(Innermost\ tube)} = \frac{85.4℃ + 10.0℃}{36℃ + 36℃} = 1.3 \tag{2.5}$$

Furthermore, the load ratio varies showing an increase under a partial turbine load, caused by both an increase of the heating temperature of main steam and a fall in the temperature of cooling cycle steam due to the steam generator and turbine characteristics described in former section. It is 2.1 at a 50% turbine load as shown in Fig. 2.14(b), which may result in inadequate ventilation steam for the outermost tubes, derived from improper distribution by both fixed-sized orifice plate and reduction of the flow resistance coefficient of the innermost tube by reduced ingenerating drain. Inadequate ventilation steam will result in the instable drainage of the sub-cool state with temperature oscillation, which may adversely affect the tubes to tube sheet seal welding with thermal fatigue.

Increasing the ventilation steam rate under a partial load was presented to suppress possible instable drainage for the intended load follow-up operation.

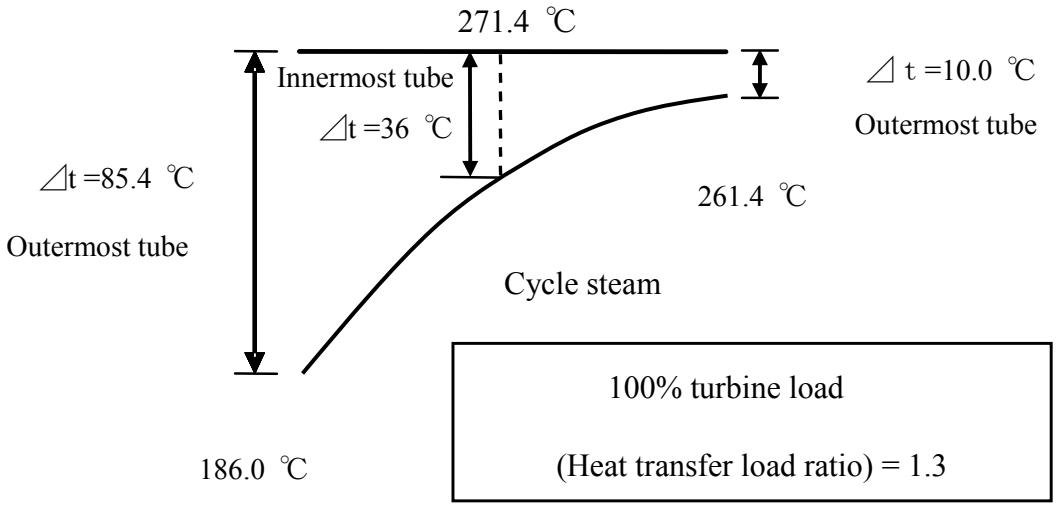

(a) 100% turbine load

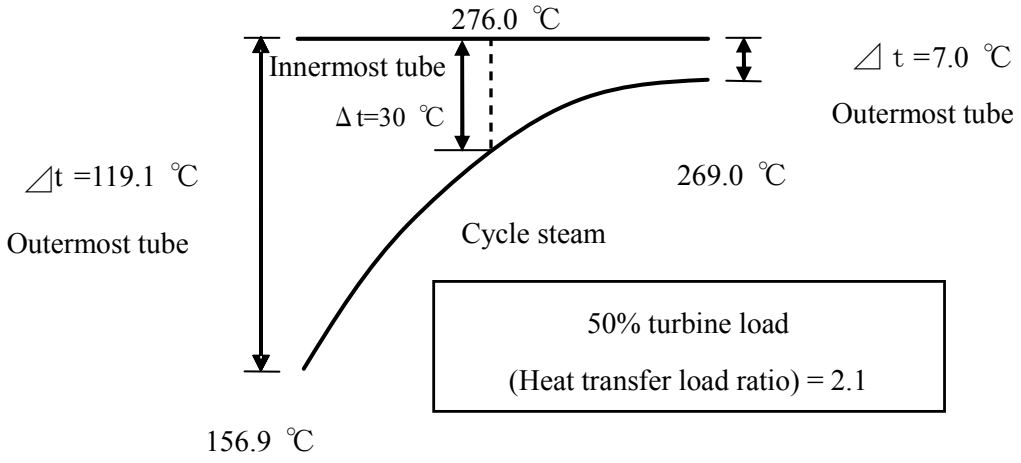

(b) 50% turbine load

Fig. 2.14 Heat transfer load distribution at 100% and 50% turbine load

2.1.7 Vessel diameter of 1,500 MW class units

The pressure vessel diameter for 1,500 MW class units increases to more than 5 m so far as using the current model concept, in which the heating steam chambers of both first stage and second stage are distributed at out of the vessel, due to the regulation for pressure vessels. The regulation requires to keeping a space between the steam chambers, which results the large space between the bundles in the vessel.

2.1.8 Core design issues

PWR turbine systems placed in service in the 1980s required the ability of daily load follow-up operation and the adoption of large-size current model MSR.

The core issues for the MSR were as follows:

(1) A prediction method of the mist separator performance under actual steam conditions based on air-water two-phase condition test data, with no steam condition tests, had to be developed in immediate preparation for 900 MW class units, followed by 1200 MW and higher class units.

(2) A suppression method of instable tube drainage based on the clarification of behaviors had to be developed as well, for the preparation of daily load follow up operation with the simple construction of two pass bundle.

(3) Additionally the planned 1,500 MW class and more required the new concept for compact vessel design.

.

2.2 Mist separator performance prediction

Nomenclature

g: Acceleration of gravity
V: Average gas velocity in direction of right angle to the separator vane face
Y: Wetness fraction of steam or air entering separator vane
ρ: Density
ζ: Flow resistance coefficient for average gas velocity of *V*, measured as 41 and 19 for conventional and advanced vanes, respectively.

Sub-script
a: air
g: steam
w: water in air-water test
l: liquid in steam test
c: Critical condition where carryover starts

2.2.1 Air-water two-phase flow test

Test facility and separator vanes

An air-water two-phase flow test was implemented to check the carryover performance of separator vane as well as the distribution of velocity using a rotatable Pitot tube and a precision minute pressure gage. The test facility construction, as shown in Figs. 2.15 and 2.16, was an actual-sized one-quarter sector model of the MSR vessel. The facility covered the manifold duct area, and was equipped with actual size separator vanes, a water spray system and a measuring cylinder for carryover mist. The tested separator vanes were of conventional type with 7 turns and of advanced type with 3 turns, and both of them were equipped with a mist catch pocket at each turn as shown in Fig. 2.17.

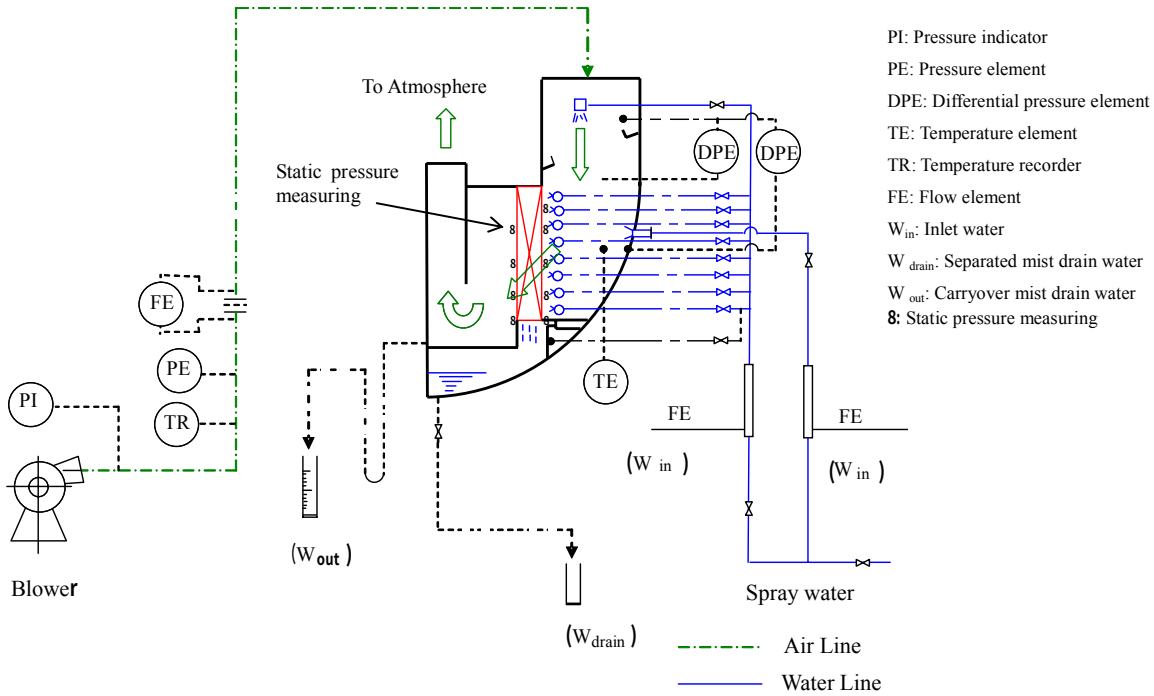

Fig. 2.15 Test facility flow diagram of air-water test

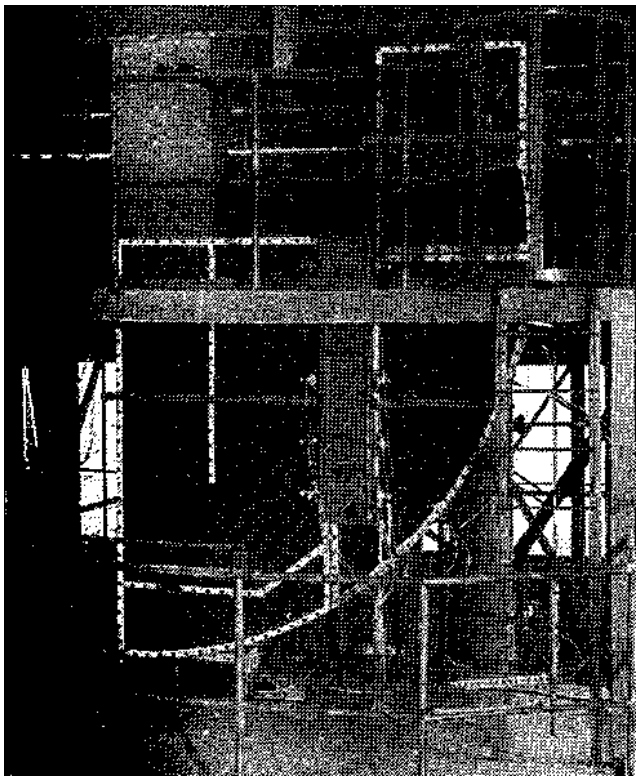

Fig. 2.16 Photo view of the test facility

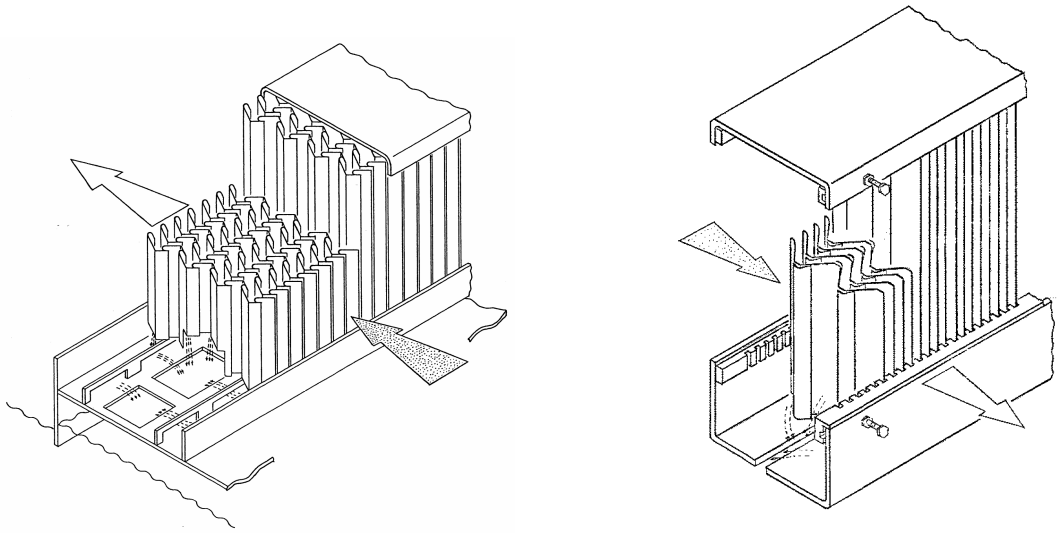

Fig. 2.17 Chevron type mist separator vane of conventional (left) and advanced one

Observation of the test

Figure 2.18 shows the results of observation revealing that the condition of the bottom drain box of the separator vane when the carryover departed. The down stream of the drain box was filled with accumulated drain water with upward slope to the weir and the mist was entrained to the main stream of the air near at the top of the weir. This showed a possible mechanism whereby the critical velocity was determined by the pressure difference of the separator vane in a range of the average velocity where the mist carryover started at drain box and not at the mist catch pocket of the vane.

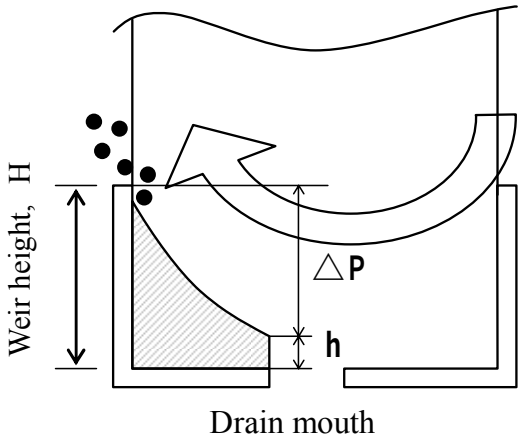

Fig. 2.18 Entrainment of the accumulated drain over the weir

Test results of the critical velocities

The results of the test are shown in Fig. 2.19 on both types of vanes under conditions of inlet wetness fraction at 20% and the weir height in separator vane bottom box with 60 and 150 mm, respectively

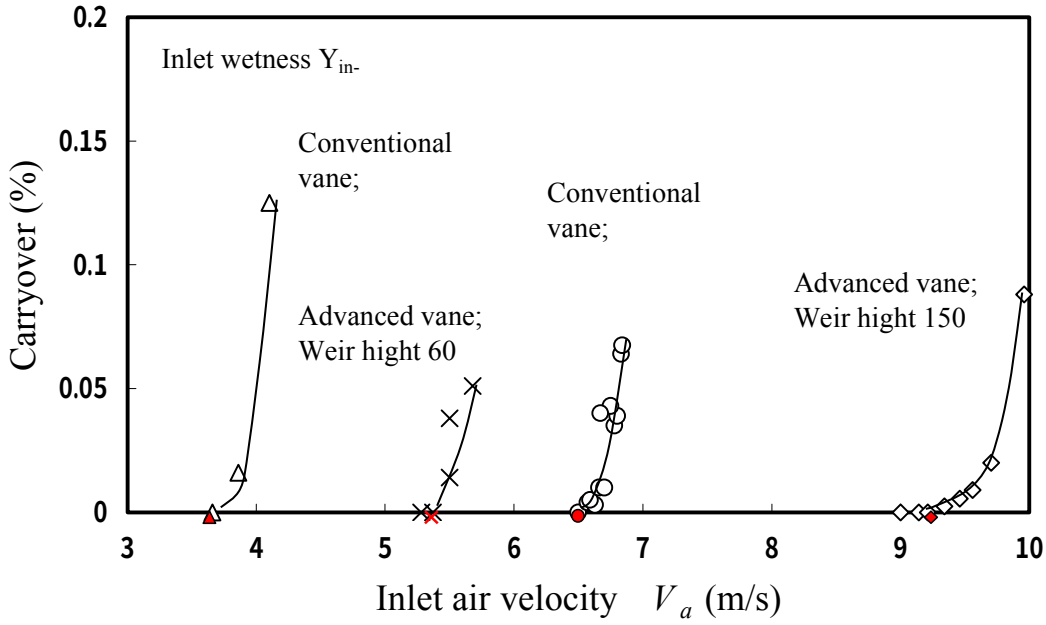

Note; Carry over (%) is the wetness fraction of separator vane outlet.

Fig. 2.19 Separator performance of air-water model test

2.2.2 Prediction formula for critical velocity

Here the prediction formula of Eq. (2.6) for critical velocity is presented. The formula means that the accumulated drain level is the sum of the water level by a pressure drop through the bottom of the separator vane in the range down stream of the drain mouth to the weir and the critical water depth *h* to exhaust the separated drain from the drain mouth of the vane.

$$H = C\ \zeta \frac{\rho_a V_a^{\ 2}}{2g\rho_w} + h \tag{2.6}$$

Where,

C: Coefficient to correct the pressure drop through separator vane on the condition of average velocity to get the pressure drop through the bottom of separator vane in the range of down stream of the drain mouth to the weir, which depends on flow pattern through the separator vane and the location of the drain mouth.

h: The critical water depth to exhaust the separated drain, where the Froude number (*Fr*) is kept 1.0, as shown in Eqs. (2.7-a) and (2.7-b).

$$Fr = \frac{u}{\sqrt{g \cdot h}} \tag{2.7-a}$$

$$h = \left(\frac{Q^2}{g \cdot B^2} \right)^{1/3} \tag{2.7-b}$$

Where,

u: Velocity of drain water

B: Drain mouth width (16.57 mm), illustrated in Fig. 2.20

g: Gravity acceleration

Q: Separated drain flow rate exhausted from the drain mouth (3.57×10^{-5} m^3/s)

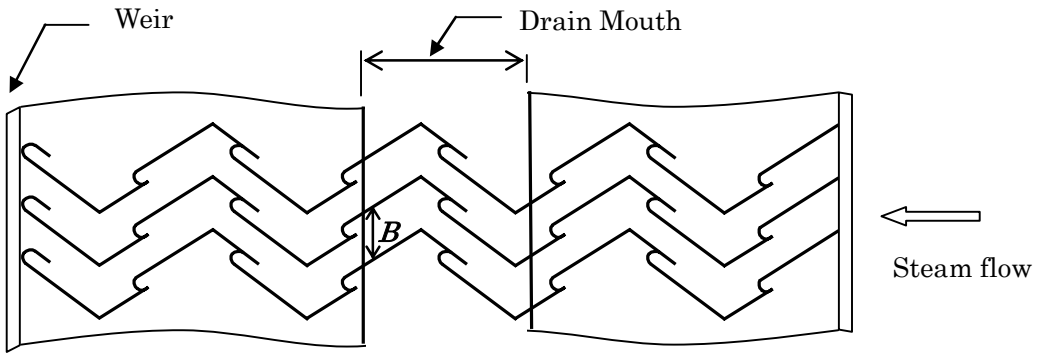

Fig. 2.20 Model of critical water depth to separated drain

The prediction formula was verified by comparing the ratio of the critical velocities, which were the

velocities when carryover started, of the air-water test results in Fig. 2.19 with the predicted one.

The prediction manners of the velocity ratio are as followings.

Coefficient *of C* is treated as identical on the assumption that the flow pattern is influenced neither by the weir height nor the separator vane types with different flow coefficient. The calculated value of *h* is 9 mm. The flow coefficient of the vane is 41 for the conventional one and 19 for the advanced one, respectively.

Equation (2.6) leads to Eq. (2.8) in case of different type of separator vane which has different flow resistance coefficient on condition that *C*, ρ_a and ρ_w are identical.

$$\frac{V_2}{V_1} = \sqrt{\frac{\zeta_1}{\zeta_2}} \tag{2.8}$$

Equation (2.6) leads to Eq. (2.9) in case of different height of weir on condition that *C*, ρ_a and ρ_w are identical, with additional neglect of *h* because it is small enough comparing to the weir height of 60 mm and 150 mm.

$$\frac{V_2}{V_1} = \sqrt{\frac{H_2}{H_1}} \tag{2.9}$$

Prediction for critical velocity ratio of different flow resistance vanes

The critical velocity ratios of the test results, for the advanced vane V_{ca} to the conventional type V_{cc}, with weir height of 60 and 150 mm, respectively, are as follows.

$$\frac{V_{ca}}{V_{cc}} = \frac{5.3m/s}{3.7m/s} = 1.4 \quad \text{(Weir height 60 mm)} \tag{2.10}$$

$$\frac{V_{ca}}{V_{cc}} = \frac{9.2m/s}{6.4m/s} = 1.4 \quad \text{(Weir height 150 mm)} \tag{2.11}$$

The predicted velocity ratio is 1.5 from Eq. (2.8) using the measured values of each ζ (ζ_1=41, ζ_2=19), showing a good coincidence to those of the test results.

Prediction for critical velocity ratio of different weir heights

The critical velocity ratios of the test results, for weir height of 150 mm (Vc_{150}) to 60 mm (Vc_{60}), with vane type of conventional and advanced vane, respectively, are as follows:

$$\frac{V_{c150}}{V_{c60}} = \frac{6.4m/s}{3.7m/s} = 1.7 \quad \text{(Conventional vane)} \tag{2.12}$$

$$\frac{V_{c150}}{V_{c60}} = \frac{9.2m/s}{5.3m/s} = 1.7 \quad \text{(Advanced vane)} \tag{2.13}$$

The predicted velocity ratio is 1.6 from Eq. (2.9) using each weir height (H_1 = 60mm, H_2 = 150 mm), showing a good coincidence to those of the test results.

2.2.3 Steam test

An actual steam condition test was implemented with an actual size conventional separator vane with a weir height of 60 mm and a blow-by inhibiting partition plate installed for the sake of performance improvement as shown in Fig. 2.21.

The test facility is shown in Fig. 2.22 equipped with a steam distributing orifice plate and water spray system. Both of them simulated the flow pattern attained by the air-water model test. Carryover mist of separator vane was measured by sodium tracing.

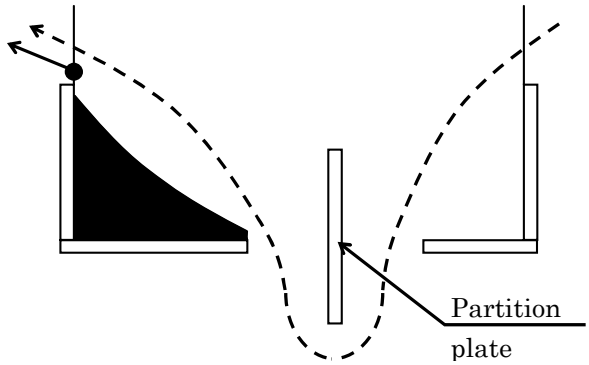

Fig. 2.21 Blow-by inhibiting partition plate

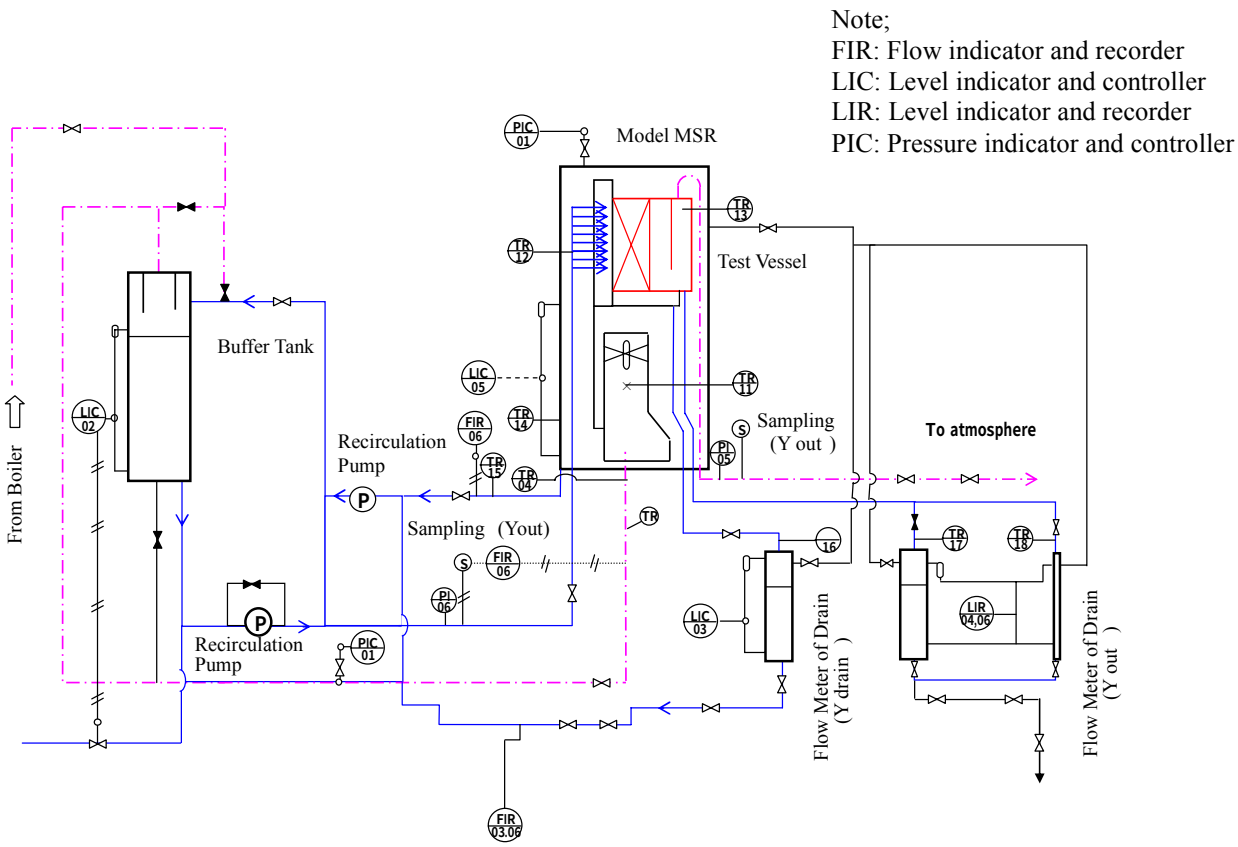

Fig. 2.22 Steam model test facility flow diagram

2.2.4 Prediction for the critical velocity under actual steam condition based on air-water condition

Carryover model

The carryover model of the steam condition is identical to that of the air-water condition shown in Figs. 2.18 and 2.21. The condition of the down stream of the drain box is filled with accumulated drain water and the mist is entrained to the gas flow (air or steam) nearly at the top of the weir.

Prediction manner

The carryover model requires simultaneously both the accumulated drain water level described in Eq. (2.6) and the separated drain volume flow rate are identical in the condition of air-water model and steam model.

The identity of the accumulated drain water level leads to Eq. (2.14), using density of air, steam, water in air water test, liquid in steam test (Nomenclature in top of this section), on the assumption in Eq. (2.6) that C is identical and the h is negligible because it is small enough to the weir height of 60 mm and 150 mm.

$$\frac{V_g}{V_a} = \sqrt{\frac{\rho_l}{\rho_g}} \Bigg/ \sqrt{\frac{\rho_w}{\rho_a}} \tag{2.14}$$

The identity of the separated drain volume flow rate leads to Eq. (2.15) using the inlet wetness fraction (Y_g, Y_a) and velocity of both steam and air-water conditions (V_g, V_a).

$$Y_a = \frac{\dfrac{Y_g}{1-Y_g}\cdot K}{1+\dfrac{Y_g}{1-Y_g}\cdot K} \quad , \quad K = \left(\frac{\rho_g \cdot \rho_w \cdot V_g}{\rho_a \cdot \rho_\ell \cdot V_a} \right) \tag{2.15}$$

Verification

The prediction method is verified by comparing the predicted steam condition with the actual steam condition as explained below.

Result of the actual steam condition test at a pressure of 1.3MPa is shown in Fig. 2.23 along with an inlet wetness fraction of 11% to 15%. The result of the air-water test on the blow-by prohibiting partition plate model of the same construction to the steam condition is shown in Fig.2.24.

The prediction from the result of the air-water test with wetness fraction of 33%, which corresponds to 16% of the steam condition, is additionally plotted in Fig. 2.23, showing the prediction for the critical velocity gives about 20% less than that in the actual steam condition. The presented prediction manner is useful for a design that has a certain margin despite lack of precision.

Supplementary explanation

It is explained that the wetness fraction of 16% in steam test corresponds to that of 33% in air-water condition as followings.

Test conditions both for air-water and steam were;

Air-water test condition Atmospheric pressure, $\rho_w = 998.3$ kg/m^3, $\rho_a = 1.163$ kg/m^3

Steam test condition 1.3 MPa, $\rho_l = 873.5$ kg/m^3, $\rho_g = 6.619$ kg/m^3

Equation (2.14) leads the velocity ratio as following.

$$\frac{V_g}{V_a} = \sqrt{\frac{\rho_l}{\rho_g}} \Big/ \sqrt{\frac{\rho_w}{\rho_a}}$$
$$= \sqrt{\frac{873.5}{6.619}} \Big/ \sqrt{\frac{998.3}{1.163}}$$
$$= 0.392$$

Equation (2.15) leads the corresponding wetness fraction of air-water as 33 % to that of 16 % steam.

$$K = \left(\frac{\rho_g \cdot \rho_w \cdot V_g}{\rho_a \cdot \rho_\ell \cdot V_a} \right)$$
$$= \frac{6.619 \times 998.3}{1.163 \times 873.5} \times 0.392$$
$$= 2.55$$

$$Y_a = \frac{\frac{Y_g}{1 - Y_g} \cdot K}{1 + \frac{Y_g}{1 - Y_g} \cdot K}$$
$$= \frac{\frac{0.16}{1 - 0.16} \times 2.25}{1 + \frac{0.16}{1 - 0.16} \times 2.25}$$
$$= 0.33$$

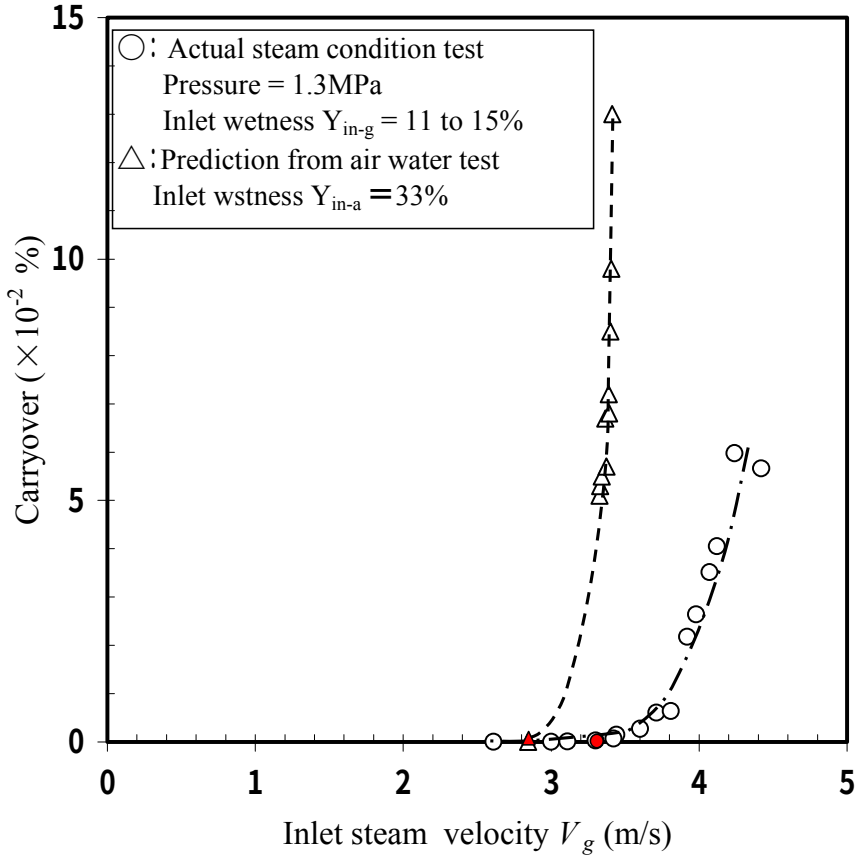

Fig.2.23 Actual steam condition test result and the prediction from air-water

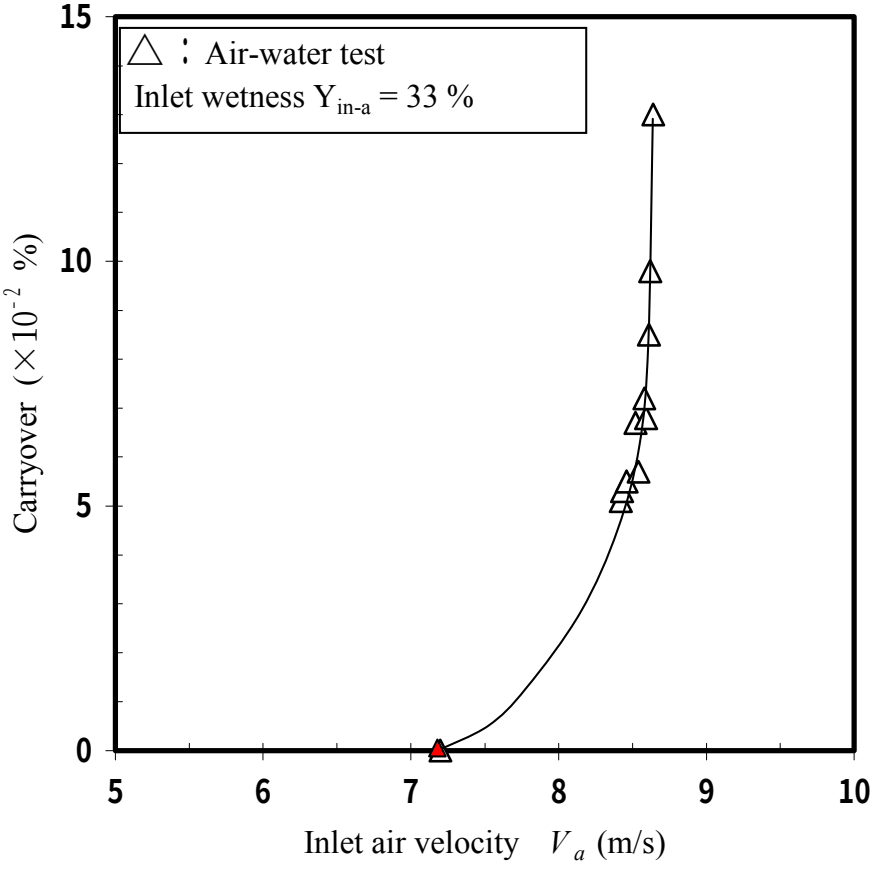

Fig. 2.24 Air-water test result with blow-by prohibiting partition plate

2.2.5 Evaluation of the prediction

The prediction method for actual steam condition considers pressure drop through the separator vane and volume flow rate of the accumulated drain, consisting of formulas of Eqs. (2.6), (2.14) and (2.15).
The prediction method is evaluated here from view points, other than the pressure drop, of flooding of the accumulated drain, shearing stress on the boundary of gas and water and entrainment of droplet considering viscosity. The evaluation refers to "Revised, Gas-Liquid two-phase flow handbook"[10], edited by JSME, Corona Co. (2006).

Nomenclature

A: Boundary surface of gas and liquid (m^2)

C: Value of ($J_L^{*1/2} + J_G^{*1/2}$)

C_L: Particle velocity of liquid on the boundary of gas and liquid, treated as zero for it is small enough compared to the gas velocity.

$(C_f)_i$ Frictional shearing stress coefficient on the boundary of gas and liquid

D: Diameter of pipe (m)

g: Acceleration of gravity 9.8 (m/s^2)

J_G: Apparent gas velocity (m/s)

J_L: Apparent liquid velocity (m/s)

J_{GC}: Critical gas velocity for entrainment of droplet (m/s)

Re_F (= Re_{L0}): Reynolds number of water film, $Re_F \equiv \dfrac{J_L \cdot D}{\nu_L}$

t_F: Thickness of liquid film (m)

U_G: Velocity of gas (m/s)

τ_i: Frictional shearing stress on the boundary of gas and liquid (kg/ms^2)

ν_L : Kinematic viscosity of liquid (m^2/s)

ν_w: Kinematic viscosity of water at the temperature of 15˚C

ρ_G: Density of gas (kg/m^3)

ρ_L: Density of liquid (kg/m^3)

$\Delta\rho$: Difference of densities between liquid and gas (kg/m^3)

μ_L: Viscosity of liquid (kgs/m^2)

σ: Surface tension (kg/m)

Conditions of air-water test and actual steam test

Table 2.5 shows the conditions on the air-water test and actual steam test, respectively.

Table 2.5 Conditions on the air-water test and actual steam test

	Air-water test	Actual steam test
Pressure (MPa)	Atmosphere	1.3
Temperature (˚C)	Room temperature (20.0)	191.8
Wetness fraction (%)	33	16
U_G (m/s)	7.2	3.3
ν_L (m^2/s)	1.0×10^{-6}	0.160×10^{-6}
ρ_G (kg/m^3)	1.163	6.619
ρ_L (kg/m^3)	998.3	873.5
σ (kg/m)	7.39×10^{-3}	3.89×10^{-3}
μ_L (kgs/m^2)	1.022×10^{-4}	0.143×10^{-4}

Model

The separator vane bottom was modeled in two cases as followings.

Model-1

Model-1 is shown in Fig. 2.25.

The accumulated drain water at the weir surface is a liquid film of annular flow condition with gas flow in a direction parallel to the weir surface in vertical pipe, using average drain flow rate.

-Distance in direction of cycle steam flow from inlet to outlet of the separator vane, indicated as D in the figure, is selected as the diameter of pipe.

-The modeled velocity in pipe is selected as that of average velocity in front of the separator vane but the flow direction is selected as parallel to the modeled pipe length direction.

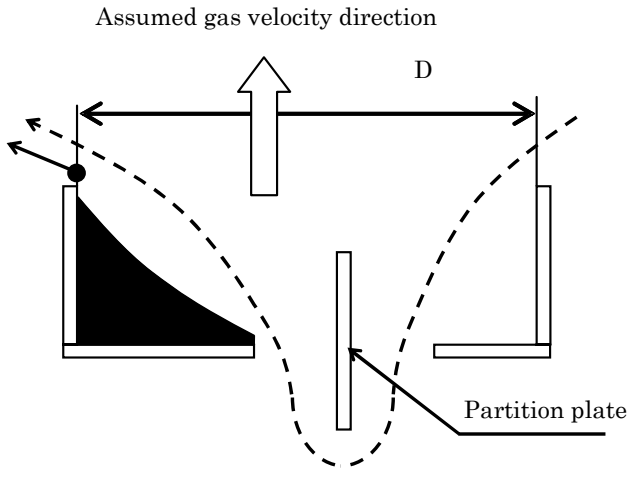

Fig. 2.25 Model-1

Model-2

Model-2 is shown in Fig. 2.26.

The accumulated drain water at the top of the weir is a liquid film of annular flow condition with gas flow in a direction parallel to the weir surface in vertical pipe, using equivalent flow rate of drain.

-Distance of separator vane plates of 0.01657 m is selected as the diameter of pipe indicated as red-circle which is equal to the drain mouth width B.

-The modeled velocity in the pipe is selected as that of average velocity in front of the separator vane but the flow direction is selected as parallel to the modeled pipe length direction.

-The drain water flow rate is modified in relation to the distance from vane inlet to outlet as following.

The modified wetness fraction of the model-2 is

(Wetness fraction %) ×（D / Distance of separator vane）

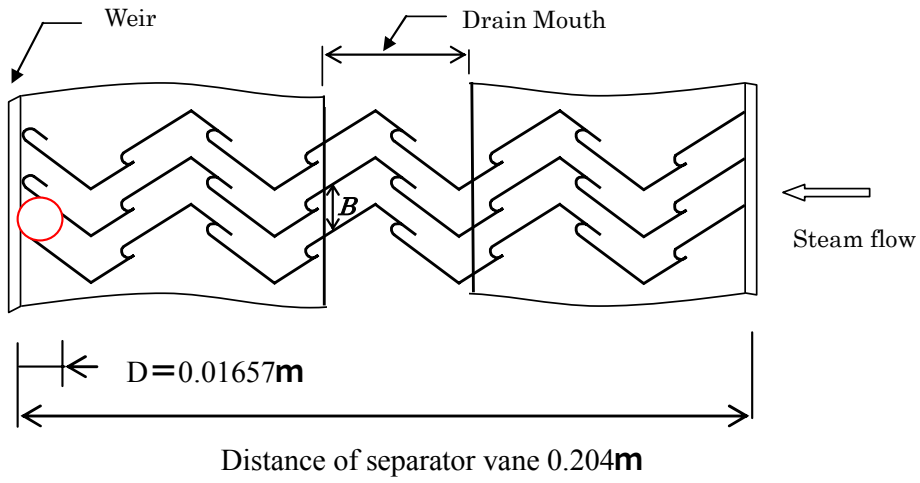

Fig. 2.26 Model-2

Flooding

Starting of flooding is presented by Wallis as Eqs. (2.16), (2.17) and (2.18), referred to the "Revised, Gas-Liquid two-phase flow handbook"[10], "8.4.3 Flooding" p. 262-263.

$$J_L^{*1/2} + J_G^{*1/2} = C \tag{2.16}$$

$$J_L^{*} = J_L\left(\frac{\rho_L}{g \cdot D(\rho_L - \rho_G)}\right)^{1/2} \tag{2.17}$$

$$J_G^{*} = J_G\left(\frac{\rho_G}{g \cdot D(\rho_L - \rho_G)}\right)^{1/2} \tag{2.18}$$

Numerical value of ($J_L^{*1/2} + J_G^{*1/2}$) is stated to be 0.8 to 1.0.

The result in case of model-1 is shown in Table 2.6. The value of ($J_L^{*1/2} + J_G^{*1/2}$) is nearly equal to 0.5 and flooding is not generated in this model both for air-water and actual steam test.

Table 2.6 Review of flooding (Model-1)

	Air-water test	Actual steam test
J_G m/s	7.2	3.3
J_L m/s	4.14×10^{-3}	4.91×10^{-3}
$J_L^{*1/2} + J_G^{*1/2}$	0.466	0.511

The result in case of model-2 is shown in Table-2.7, where the wetness fraction is modified as described above. The value of ($J_L^{*1/2} + J_G^{*1/2}$) is larger than 0.8 and flooding may generate in this model both for air-water and actual steam test.

Table 2.7 Review of flooding (Model-2)

	Air-water test	Actual steam test
Wetness fraction %	2.7	1.3
J_G m/s	7.2	3.3
J_L m/s	2.33×10^{-4}	3.29×10^{-4}
$J_L^{*1/2} + J_G^{*1/2}$	0.807	0.855

Shearing stress on the boundary of gas and water

Liquid film thickness and frictional shearing stress is evaluated on the assumption that liquid film begins adversely up-flowing due to the acceleration of gas velocity succeeding to the flooding. Liquid film thickness and frictional shearing stress coefficient on the boundary of gas and water are presented by Fukano and others considering the viscosity as Eqs. (2.19), (2.20) and (2.21), referring to the "Revised, Gas-Liquid two-phase flow handbook"[(10)], "8.3 Features of Liquid film flow in vertical pipe", p. 254-260.

$$\tau_i = \left(C_f\right)_i \cdot \frac{\rho_G}{2} \cdot \left(u_G - C_L\right)^2 \tag{2.19}$$

$$\left(C_f\right)_i = 0.425 \cdot \left(12 + \frac{\nu_L}{\nu_W}\right)^{-1.33} \left(1 + 12\frac{t_F}{D}\right)^8 \tag{2.20}$$

$$\left(\frac{t_F}{D}\right) = 0.0594 \cdot exp\left(-0.34 \cdot Fr_{G0}{}^{0.25} \cdot Re_{L0}{}^{0.19} \cdot x^{0.6}\right) \tag{2.21}$$

Where

$$Fr_{G0} \equiv \left(\frac{j_G}{\sqrt{gD}}\right) \tag{2.22}$$

$$Re_{L0} \equiv \frac{j_L D}{\nu} \tag{2.23}$$

$$x \equiv \frac{j_G \rho_G}{j_G \rho_G + j_G \rho_G} \tag{2.24}$$

The result of the calculation of liquid film thickness divided by pipe diameter D and frictional shearing stress is shown in Table 2.8 in the case of model-1. Additionally was calculated the ratio of the frictional shearing force to the weight of liquid film which is to be pulled up by the frictional shearing force. As flooding was already evaluated not to generate in this model, the evaluation of this frictional shearing force also brings that it is too small to maintain annular flow condition.

Table-2.8 Frictional shearing stress (Model-1)

	Air-water test	Actual steam test
J_G m/s	7.2	3.3
J_L m/s	4.14×10^{-3}	4.91×10^{-3}
Fr_{G0}	5.09	2.33
Re_{L0}	0.845×10^{3}	0.626×10^{4}
x	0.67	0.84
t_F / D	0.0141	0.0080
$(C_f)_i$	0.0497	0.0330
τ_i kg/ms^2	1.50	1.19
$(\tau_i \cdot A) / (t_F \cdot A \cdot \rho_L \cdot g)$	0.0531	0.085

The result of the calculation in the case of model-2 is shown in Table 2.9. The ratio of the frictional shearing force to the weight of liquid film is nearly 1.0, which leads, succeeding to the flooding, to possible annular flow condition in the upper area of the weir.

Table-2.9 Frictional shearing stress (Model-2)

	Air-water test	Actual steam test
J_G m/s	7.2	3.3
J_L m/s	2.33×10^{-4}	3.29×10^{-4}
Fr_{G0}	17.8	8.18
Re_{L0}	3.86	3.41×10
x	0.973	0.987
t_F/D	0.0245	0.0194
$(C_f)_i$	0.109	0.0808
τ_i kg/ms^2	3.29	2.91
$(\tau_i \cdot A) / (t_F \cdot A \cdot \rho_L \cdot g)$	0.829	1.06

Entrainment

Ishii and others presented formula for starting of entrainment as Eqs. (2.25) and (2.26), referring to the "Revised, Gas-Liquid two-phase flow handbook"[10], "8.7.2 Entrainment of water droplet and its incidence", p. 287.

For $Re_F \leqq 1635$

$$\frac{J_{GC}\cdot\mu_L}{\sigma}\left(\frac{\rho_G}{\rho_L}\right)^{1/2} = 11.78\cdot N\mu_L{}^{0.8}\, Re_F{}^{-1/3} \qquad \left(N\mu_L \leq \frac{1}{15}\right)$$

$$= 1.35\cdot Re_F{}^{-1/3} \qquad \left(N\mu_L \geq \frac{1}{15}\right) \qquad (2.25)$$

For $Re_F \geqq 1635$

$$\frac{J_{GC}\cdot\mu_L}{\sigma}\left(\frac{\rho_G}{\rho_L}\right)^{1/2} = N\mu_L{}^{0.8} \qquad \left(N\mu_L \leq \frac{1}{15}\right)$$

$$= 0.1146 \qquad \left(N\mu_L \geq \frac{1}{15}\right) \qquad (2.26)$$

Where,

$$N\mu_L \equiv \frac{\mu_L}{\left(\rho_L\cdot\sigma\sqrt{\frac{\sigma}{g\cdot\Delta\rho}}\right)^{1/2}} \qquad (2.27)$$

The result in case of model-1 is shown in Table 2.10. The actual velocities in test condition which is assumed to be about 50% larger than the average velocity ($1.5 \times J_G$ m/s) nearly equal to those of the calculated velocities which generate the entrainment of droplet. The entrainment may generate in the model.

Table 2.10 Review of entrainment

	Air-water test	Actual steam test
J_G m/s	7.2	3.3
J_L m/s	4.14×10^{-3}	4.91×10^{-3}
Re_F	0.845×10^{3}	0.626×10^{4}
Σ kg/m	7.39×10^{-3}	3.89×10^{-3}
$N_{\mu L}$	1.28×10^{-3}	2.98×10^{-4}
J_{GC} m/s	12.8	4.7
$1.5 \times J_G$ m/s	11.0	5.0

Results of the evaluation

The evaluation for the prediction method was carried out from view points of flooding, shearing stress on the boundary of gas and liquid and entrainment of droplet considering viscosity.

The result is that the accumulated drain in whole is not under condition of flooding and its slope was caused by the pressure drop through the separator vane, but at the top of the weir flooding and succeeding annular flow may generates. Entrainment of droplet may also generate. The evaluation results are in accordance with the test results that weir height or the pressure drop is dominant for the critical velocity, and entrainment of droplet is observed at the critical velocity.

This leads to the result that the performance is dominated by pressure drop and viscosity does not significantly influence the performance of the separator. The error of the prediction for actual steam condition by about 20% is estimated to attributing to the error of the measurement and a little deflection of the vane location between air-water and actual steam.

2.3 Tube drainage suppression method

Nomenclature

TI: Temperature at internal outlet of heat transfer tube

TO: Temperature at outer surface of heat transfer tube

2.3.1 Measurement on an existing unit

Increasing the ventilation steam rate was conducted on a single-stage MSR of an existing 600 MW class unit to verify its effect and clarify instable behaviors. Specification of the MSR was as follows;

The bundle was of the multi-U tube and cross-flow type. The bundle construction was 8400 mm in effective tube length, 35 rows by 40 tiers, and 690 U-tubes in total. Tube was copper-nickel alloy material with nominal diameter of 19.05mm and 19-fin/inch low-finned tubes. Mass velocity in the tube outer side gap was 1.95×10^5 kg/m^{2}h.

Measured items

The following items were measured as shown in Figs. 2.27, 2.28 and 2.29.

(1) The drain two-phase temperatures of both the upper and lower halves at the internal outlet of tube. The outermost and innermost tubes were selected for measuring as shown in Fig. 2.27 (b) as the measured points of *TI-1* to *TI-6*. Thermocouples are shown in Fig. 2.28(a).

(2) The outer surface temperatures of one tube at three points longitudinally displaced along the tube as shown in Fig. 2.27 (a) as the measured points of *TO-1* to *TO-3*. Thermocouples are shown in Fig. 2.28(b).

(3) The pressure difference between the inlet and outlet of the heating steam chamber.

(4) Besides the above, process data items on the heating steam temperature and the drain temperature at the outlet of the steam chamber and the cycle steam (inlet and outlet temperatures) were measured with permanently installed instruments.

(5) The measured point of the pressure difference and process data are illustrated in Fig. 2.29.

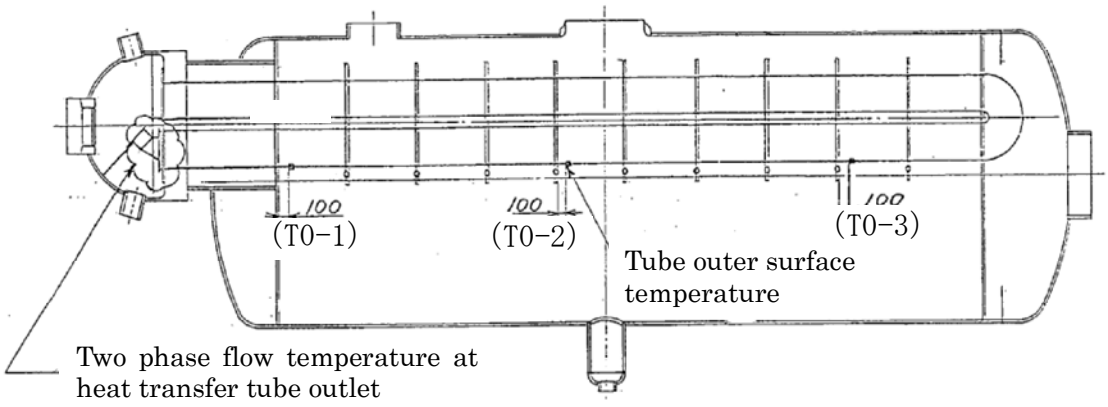

(a) Side view of the measuring items

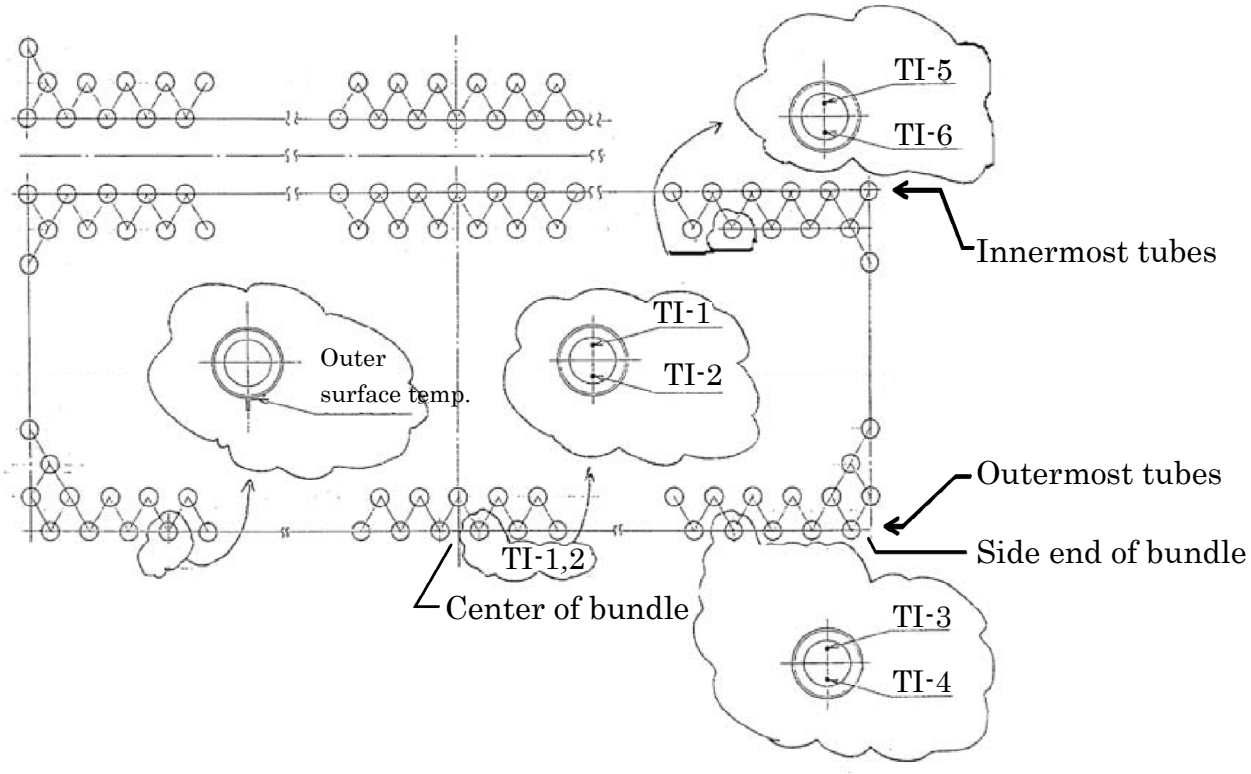

(b) Two-phase flow temperature of heat transfer tube internal outlet

Fig. 2.27 Measured items for tube drainage

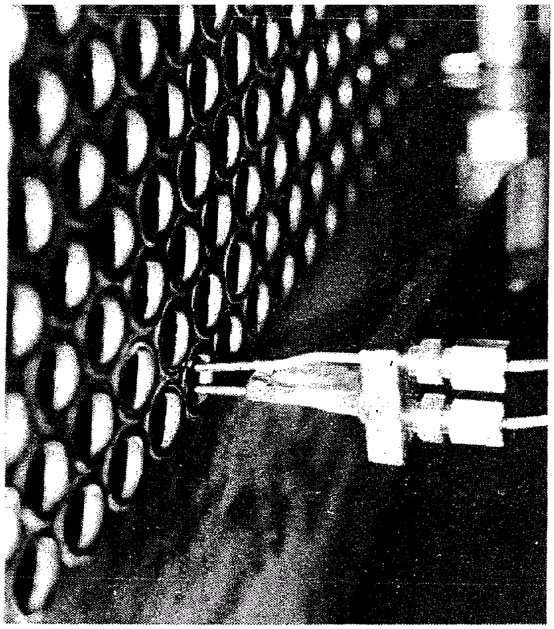

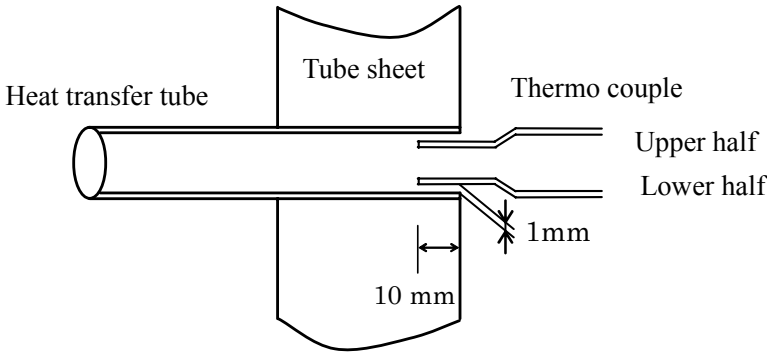

(a) Photo view and concept of thermocouples for upper and lower halves at the tube internal outlet

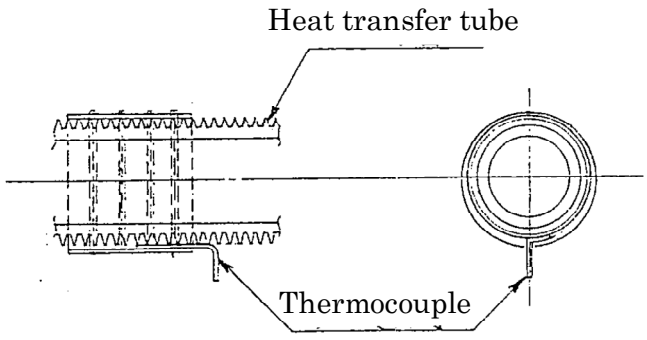

(b) Thermocouples for tube outer surface

Fig. 2.28 Thermocouples for the measuring

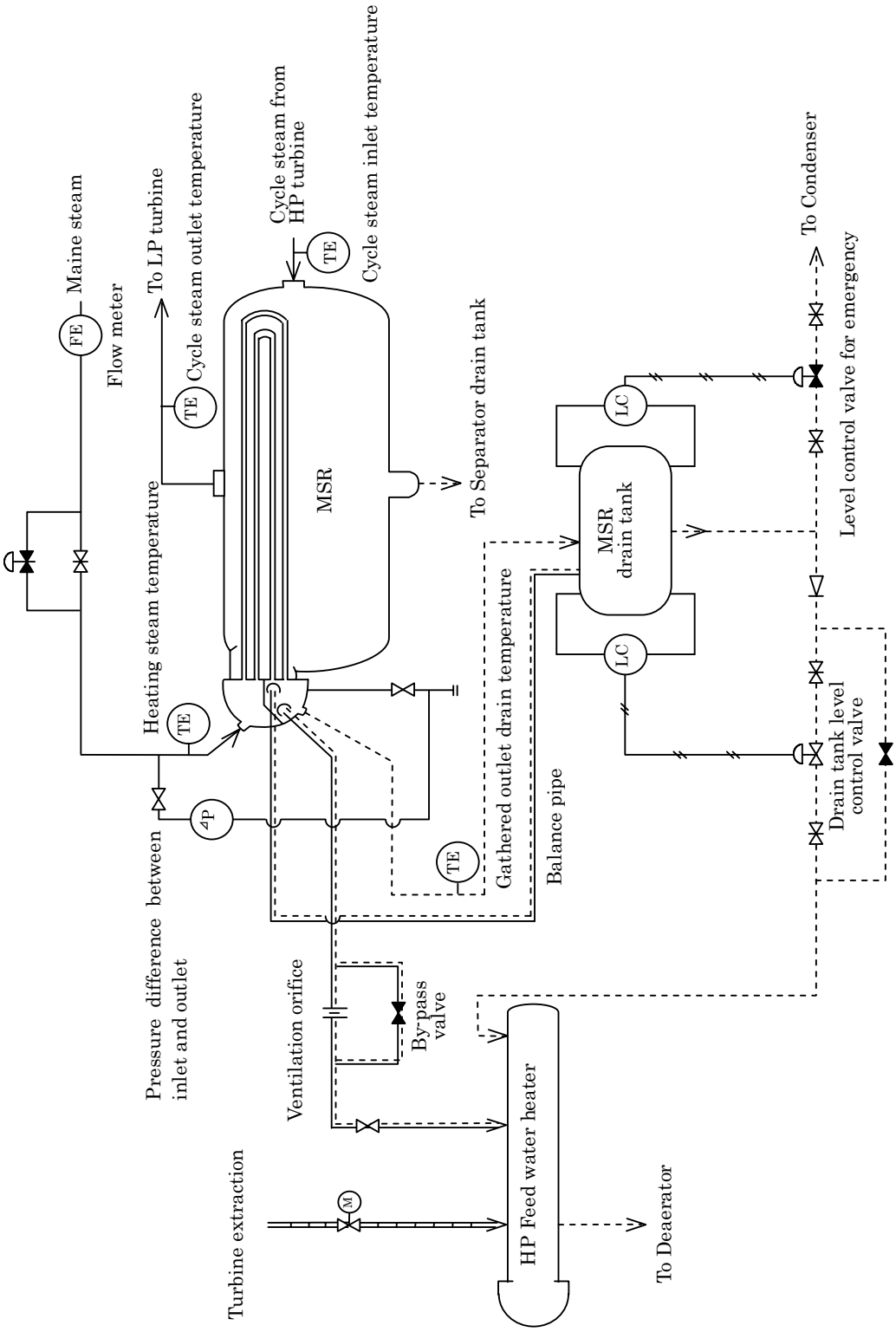

Fig. 2.29 Flow diagram of the MSR

Measuring procedure

The measuring process took place under stabilized turbine load conditions of both 50% and 100%, the details of which are as follows.

(1) Operation without an increase of ventilation steam rate with turbine loads of 50% and 100%, respectively. Here the ventilation steam ratio to the total heating steam was 2.0% at 100% turbine load, which corresponded to 3.3% at 50% turbine load due to the reduction of the cycle steam flow.

(2) Operation with an increase of ventilation steam rate at 50% load. The rate of ventilation steam was increased from 3.3% to 10% of the total heating steam by opening the by-pass valve of the excess steam ventilation orifice.

2.3.2 Results of the measurement

The measured temperatures of tube outlet ends (*TI-1* to *TI-6*), outer surface temperatures of the tube (*TO-1* to *TO-3*), and pressure difference through the steam chamber are shown in Figs. 2.30 and 2.31 for turbine loads of 50% and 100%, respectively.

The data on the 50% turbine load shows the behaviors beginning on the condition of increasing the ventilation steam to the condition without increment. The data on the 50% load shows the following items.

(1) Some of the drains show the sub-cool state with oscillation compared with both the saturation temperature (276.0°C) of heating steam and the chamber outlet drain temperature (275.7°C), where all the tube drains gather. The sub-cool state peaks at the outermost ends of *TI-3* and *TI-4* in comparison with the innermost side of *TI-5* and *TI-6* and the center outermost side of *TI-1* and *TI-2*.

(2) The upper half of *TI-3* exhibits a maximum sub-cool temperature of 49°C with an oscillation amplitude and cycle of 37°C and 55 seconds, respectively.

(3) The temperature alteration of the tube surface is distributed longitudinally along the tube, which peaks at the tube end (*TO-1*) and decays lengthwise along the tubes (*TO-2* and *TO-3*).

(4) The temperature of the tube outer surface was measured at the bottom of the tube, as shown in Fig. 2.28 (b), with downward bias through thermal resistance of contact between top of the tube fin and thermocouples. The numerical value of the resistance is roughly estimated as 35 to 40 ˚C by comparing the temperatures of bottom side of tube between *TI-4* and *TO-1*, on the assumption that these tubes showed same condition due to location in symmetrical position as shown in Fig. 2.27 (b).

(5) All the parameters oscillate in a synchronized manner, thus increasing gradually to peak and returning suddenly. The peak pressure difference corresponds to that in the drain sub-cool state.

(6) An increase of ventilation steam rate suppresses both the drain sub-cool state and oscillation.

The data on 100% load is described as follows:

(1) All the measured parameters show similar behaviors to those of 50% load though the figures are reduced. The upper half of TI-3 exhibits a maximum sub-cool temperature of 33°C to the heating steam of 271.4°C with an oscillation amplitude and cycle of 9°C and 27 seconds, respectively.

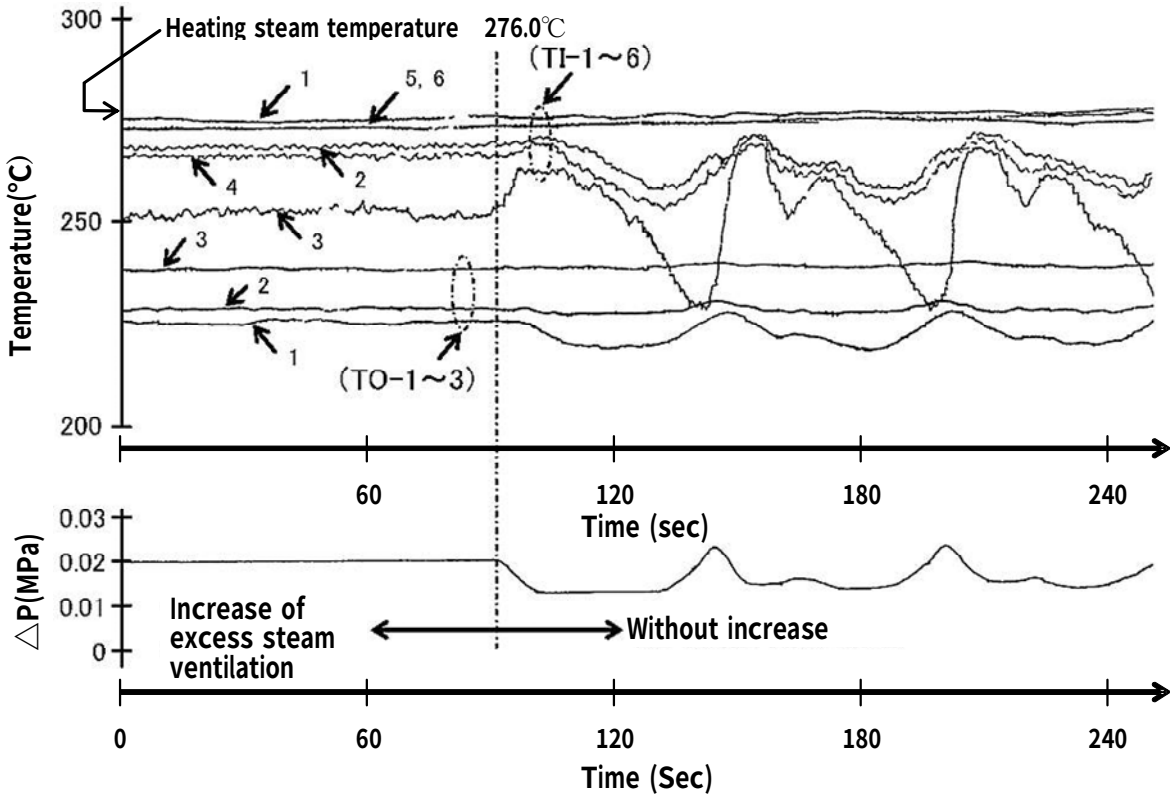

Fig. 2.30 Tube drain instability with and without increase of excess steam ventilation at 50% turbine load

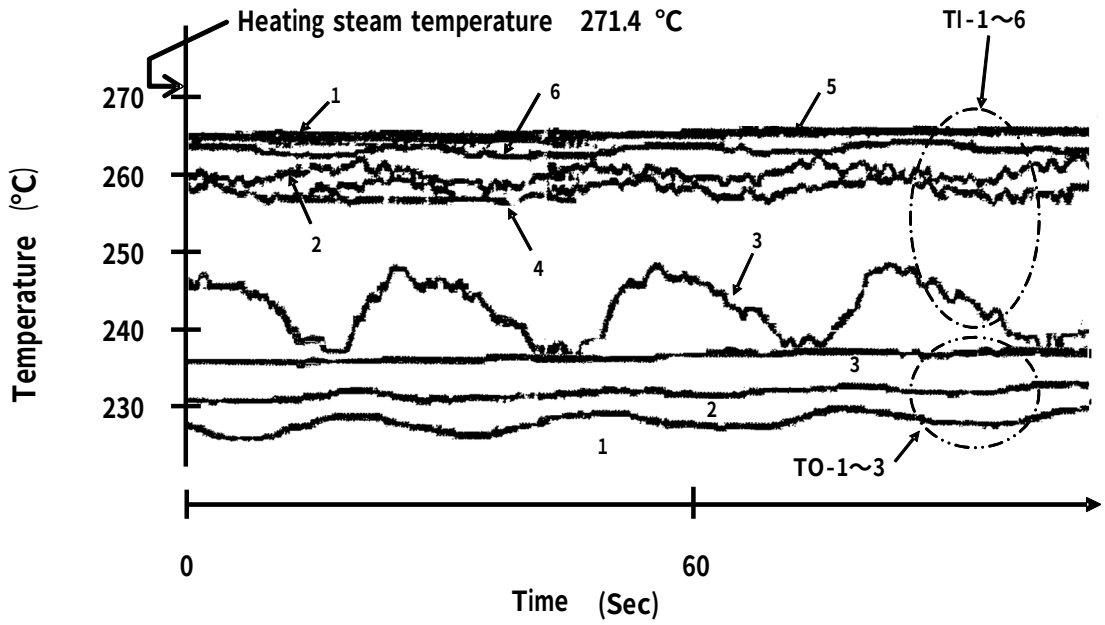

Fig. 2.31 Tube drain instability at 100% turbine load without increasing excess steam ventilation

2.3.3 Distribution of heat transfer resistance

Tube specification

Low finned heat transfer tube construction is shown in Fig. 2.32.

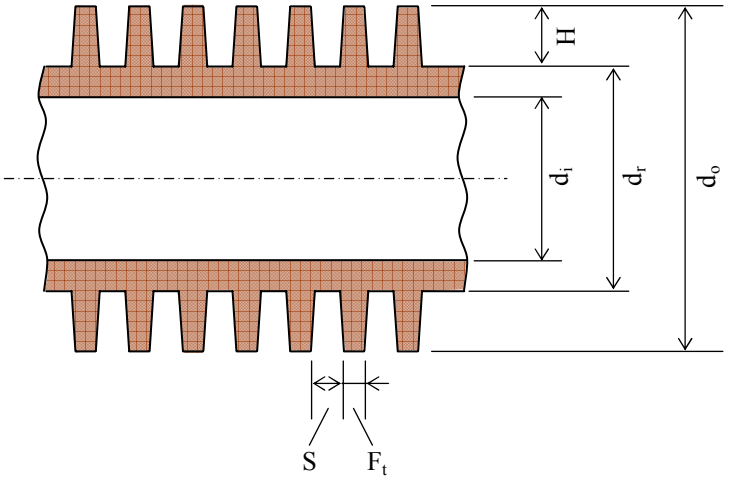

Fig. 2.32 Low finned heat transfer tube construction

The specification of the low finned copper-alloy material tube is as shown bellow.

d_i: Inner diameter;:12.12mm

d_o Fin out diameter; 19.05mm

d_r: Fin root diameter; 15.88mm

Fin number; 19 fin/ 25.4mm

F_t: Fin thickness; 0.31mm

H: Fin height; 1.59mm

S: Fin space; 1.03mm

Surface ratio of outer tube to inner; 4.13

Heat transfer

Heat transfer coefficient of tube outer side super heated steam condition is calculated from Briggs-Young experimental formula shown in Eq. (2.28).

$$St \cdot Pr^{2/3} = 0.134 / Re^{-0.319} \cdot \left(\frac{S}{H}\right)^{0.200} \cdot \left(\frac{S}{F_t}\right)^{0.1134} \tag{2.28}$$

Where;

$$Re = \frac{d_r \cdot V_{max}}{\nu} \tag{2.29}$$

d_r: Fin root diameter

V_{max} : Tube outer side velocity

Tube metal resistance is calculated using tube metal thermal conductivity of 77.9 W/m^{2}K, tube inner side condensing heat transfer coefficient defined for tube inner surface of 15,000 W/m^{2}K and fouling of tube outer surface defined for tube outer surface of 0.52×10^{-4} m^{2}K / W, respectively.

Distribution of heat transfer resistance

The calculated heat transfer resistance defined for tube outer surface and its distribution is shown in Table 2.11, on the 100% turbine load condition with the average cycle steam temperature of 223.7˚C and on the 50% turbine load with 213.0˚C for the operating condition shown in Fig. 2.14.

Table 2.11 Heat transfer resistance and its distribution on 100% and 50% turbine load

(a) 100% turbine load

100% turbine load	Heat transfer resistance (m^{2}K/W)	Resistance distribution (%)
Tube outer side	1.90×10^{-3}	78.9
Fouling of tube outer side	0.53×10^{-4}	2.2
Tube inner side	2.79×10^{-4}	11.6
Tube metal	1.74×10^{-4}	7.3
Total	2.41×10^{-3}	100.0

(b) 50% turbine load

50% turbine load	Heat transfer resistance (m^{2}K/W)	Resistance distribution (%)
Tube outer side	3.25×10^{-3}	86.5
Fouling of tube outer side	0.53×10^{-4}	1.4
Tube inner side	2.79×10^{-4}	7.4
Tube metal	1.74×10^{-4}	4.7
Total	3.76×10^{-3}	100.0

The resistance of heat transfer distribution is, with adequate ventilation steam, 80 to 90% for super heating condition on the outer side of the tubes, 7 to 12% for inner tube condensation and others.

2.3.4 Mechanism of the drainage instability

Based on the data in Section 2.3.2 and 2.3.3, the drainage mechanism is presented as follows, and illustrated in Fig. 2.33.

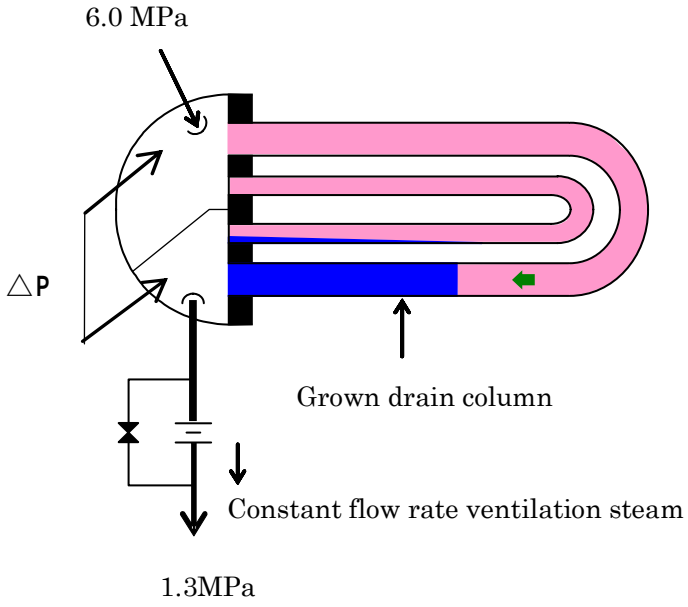

Fig. 2.33 Mechanism of drainage instability

(1) The resistance of heat transfer on the inner side of the tubes becomes 10 to 20 times larger than that of condensing when the drain column is retained. This keeps the overall heat transfer coefficient to the level of one half of that of adequate ventilation.

(2) The flow rate of total ventilation steam, being led to the high-pressure feedwater heater of 1.3 MPa, is kept constant by the ventilation orifice operated in a critical condition.

(3) The ingenerating drain water on condition of inadequate ventilation steam is retained, and grows due to loss of frictional shearing force for exhausting.

(4) The grown and retained drain water column is deprived of its heat by the overall heat transfer coefficient at the same level as that of adequate ventilation.

(5) Along with an expansion of the drain-plugged tube numbers, the pressure difference between the tube inlet and outlet increases by both a reduction in the un-plugged tube numbers and a constant flow rate of ventilation steam.

(6) Finally, the drain column is rapidly exhausted by the increased pressure difference overcoming the flow friction loss for the retained and grown drain water column to be exhausted.

(7) The behaviors stated in (3) to (6) bring down the sub-cool state and oscillation as shown in Fig. 2.33.

(8) The above estimation is supported by the data of tube outer surface temperatures as follows.

- The amplitude of tube surface temperature oscillations shows distribution, which show maximum value at TO-1 and decay as TO -2 and TO-3 along the tube.
- The temperature oscillation synchronizes with the tube end inner sub-cool state and oscillation.
- Tube end inner temperatures show the retention time by transportation of drain column.

2.3.5 Results in application to newly constructed units

The application of the suppressing method, to the current model MSR of newly constructed double stage reheat 900 MW class units, showed the expected results and demonstrated effectiveness of the method.

The measurement was implemented with the same method to that of 600 MW class unit described in Section 2.3. The measured point is shown in Fig. 2.34, which shows the outlet end of heat transfer tube distribution looked from steam chamber in the direction of the indicated red arrow.

The results showed the suppression of maximum temperature oscillation at the outermost tube, TI-5 as shown in Fig. 2.34, from 5˚C to 1°C at a 50% load by increasing the excess ventilation steam as shown in Fig. 2.35. The amplitude of the oscillation is comparatively small because of the smaller ratio of heat transfer load due to smaller temperature rise by double stage reheat. The oscillation at 100% turbine load was 0.8°C at a 100% load as shown in Fig. 2.36.

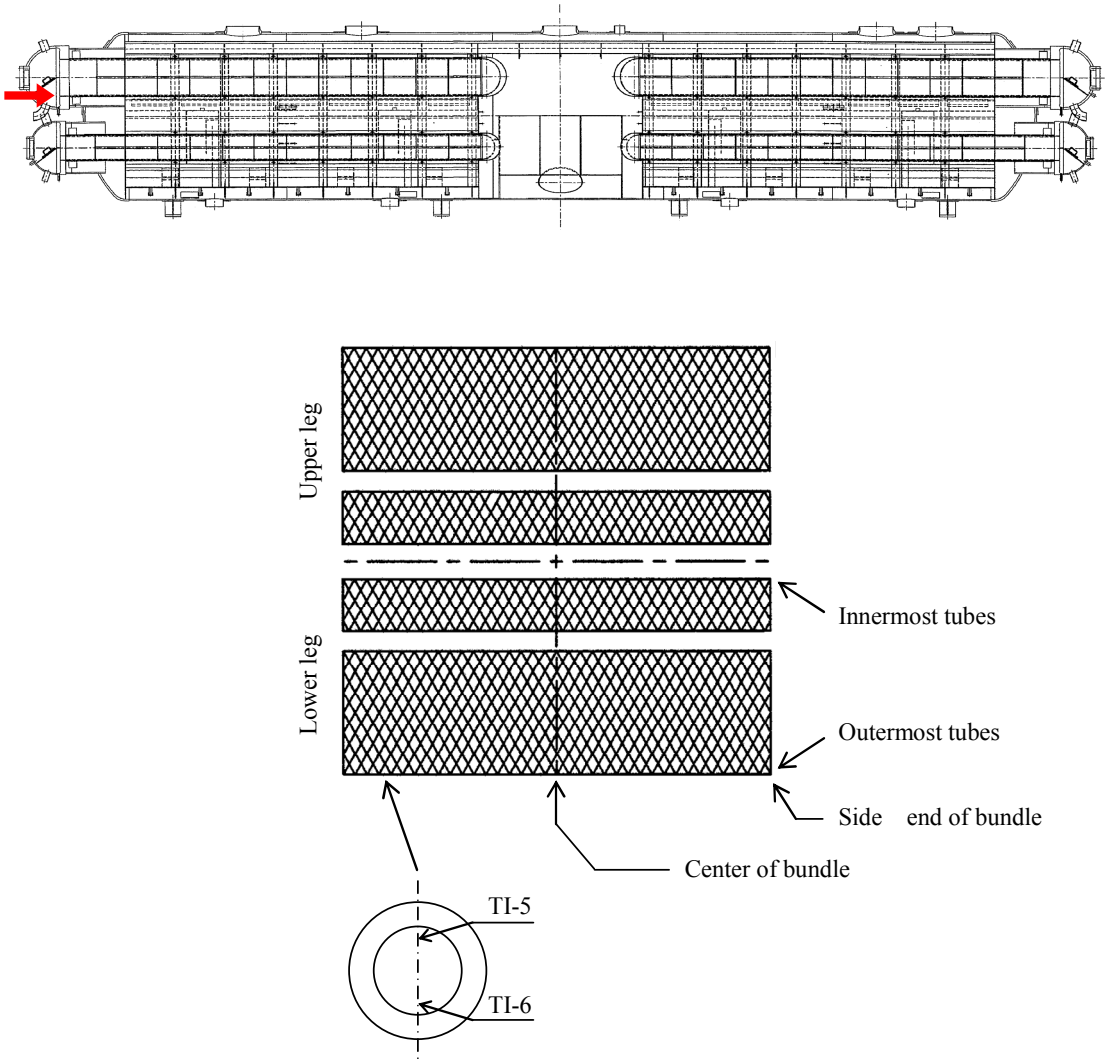

Note: The crossing point is location for tubes.

Fig.2.34 Measured tube at the internal outlet

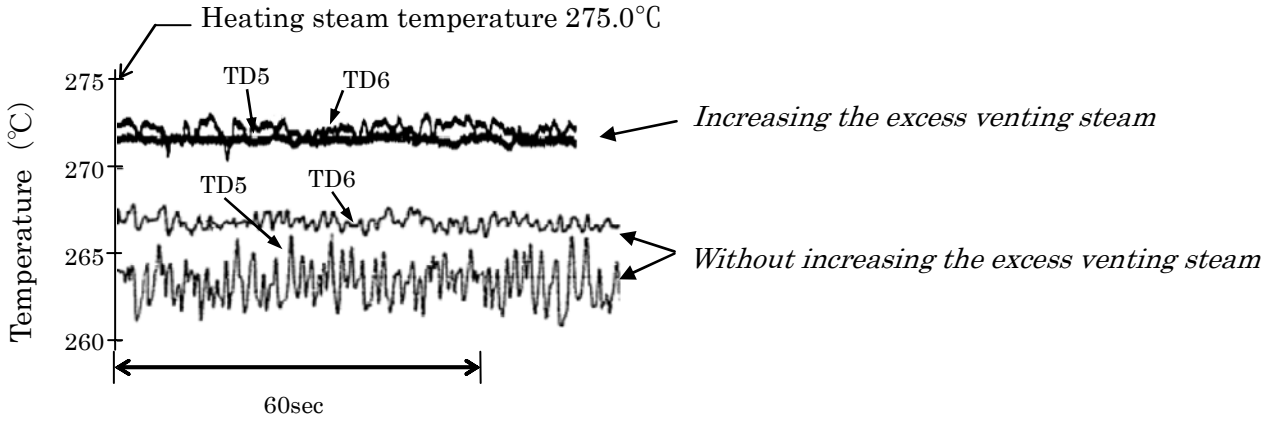

Fig. 2.35 Tube drain instability with and without excess steam ventilation at 50% turbine load

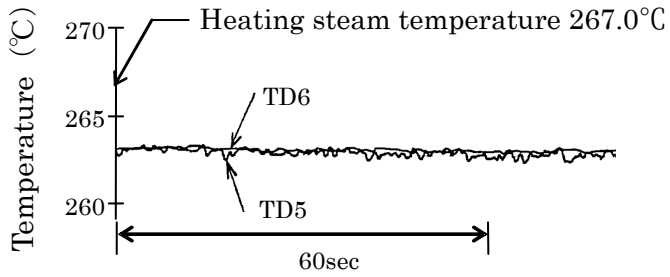

Fig. 2.36 Tube drain instability without excess steam ventilation at 100% turbine load

2.4. Design concept for 1,500 to 1,700 MW Class Units

Design concept of high-capacity 1,500 to 1,700 MW class MSR is adopted a coupled developed items of a containing the first stage reheater steam chamber in the pressure vessel and a distribution of the cycle steam inlet nozzle longitudinally along the vessel.

The first stage steam chamber is contained in a pressure vessel to eliminate the space between the first and second stage steam chambers which considerably contributes to a smaller vessel diameter. The smaller vessel diameter, on the other hand for mist separation performance, requires that the cycle steam inlet nozzles are to be distributed longitudinally, despite the nozzles were concentrated at the vessel center for the current model, to ensure uniform static pressure distribution in the vessel longitudinal direction by reducing the velocity in the manifold duct area, as shown in Fig. 2.37.

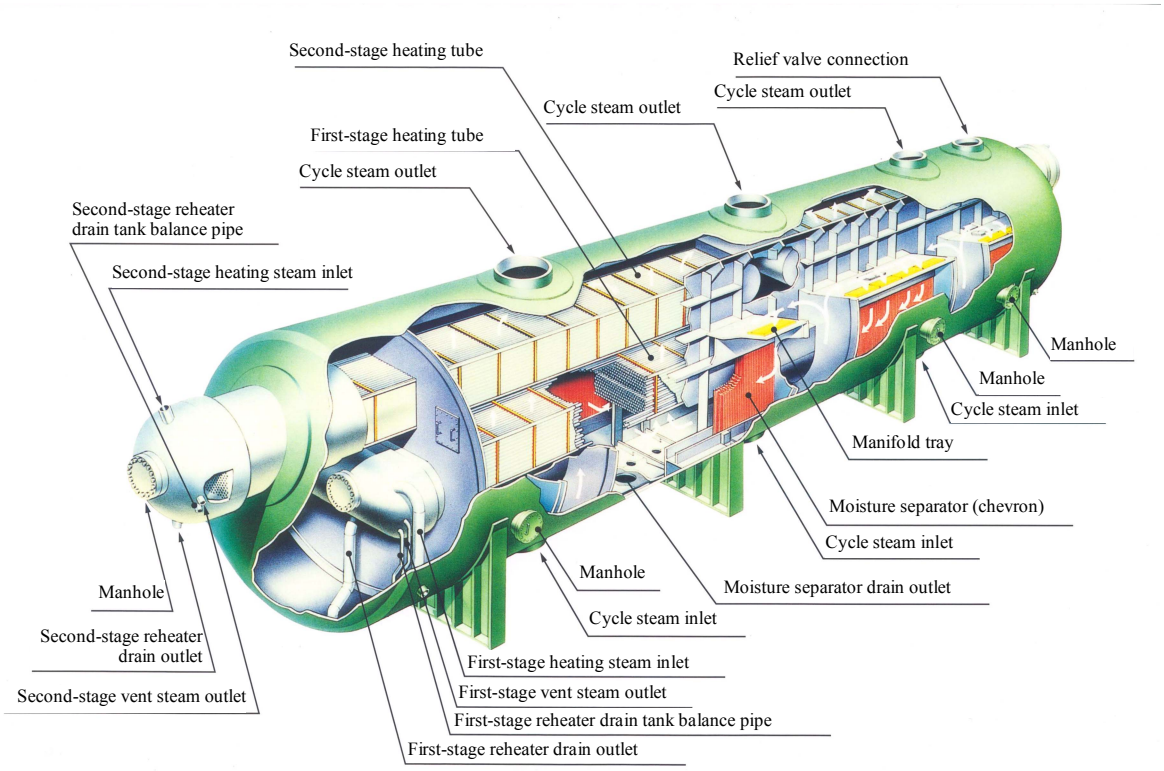

Fig. 2.37 New concept MSR for 1500 -1700 MW class unit

2.4.1 Cycle steam flow pattern

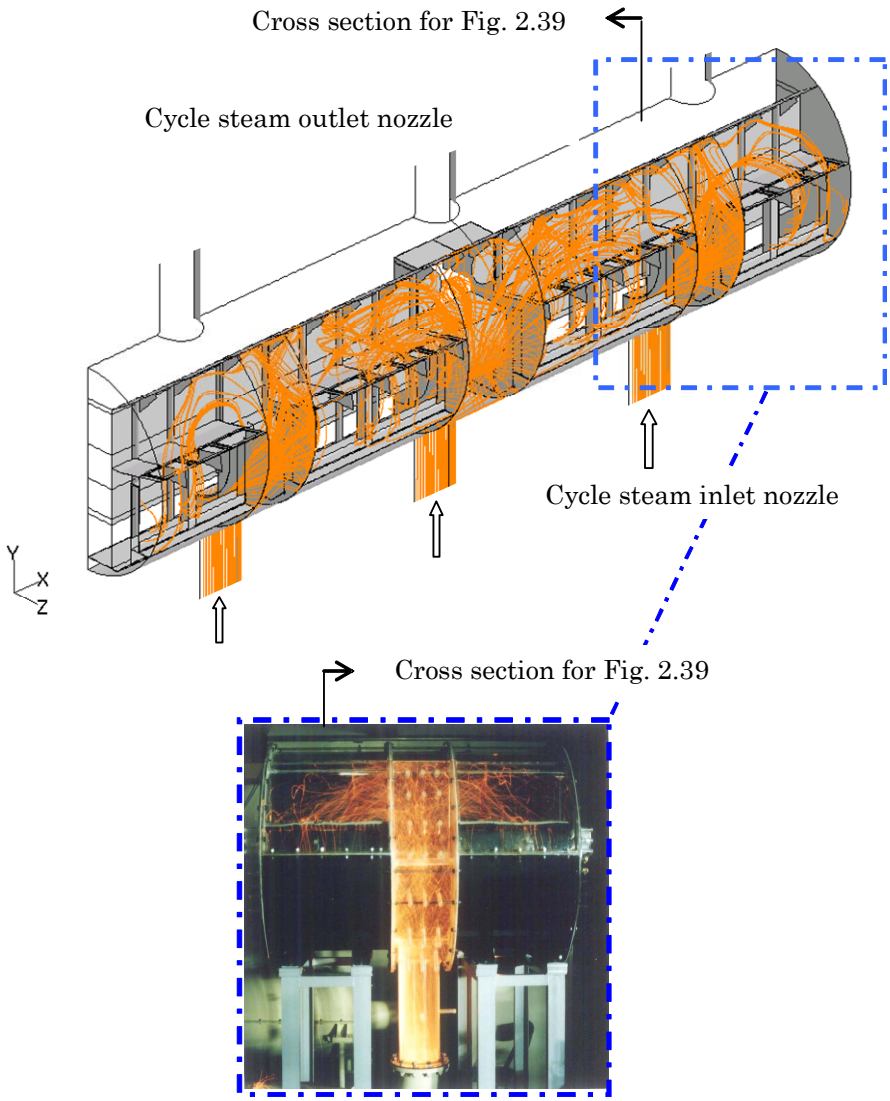

Fig. 2.38 Cycle steam flow pattern CFD (Upper) and observation (Lower)

The cycle steam flow pattern was analyzed by CFD alongside the coincidence to the observation of the experiment, shown in Fig. 2.38, because the distributed cycle steam inlet nozzles extend the strongly disordered flow area along the manifold duct. Succeeded analyses of flow pattern around the separator vane and the velocity distribution at the inlet of it, shown in Figs. 2.39 and 2.40, give the velocity which is allowable with additional device of the vane bottom for the advanced vane. The separator critical velocity of improved vane was predicted in actual steam condition by the method described in Section 2 based on the air-water test.

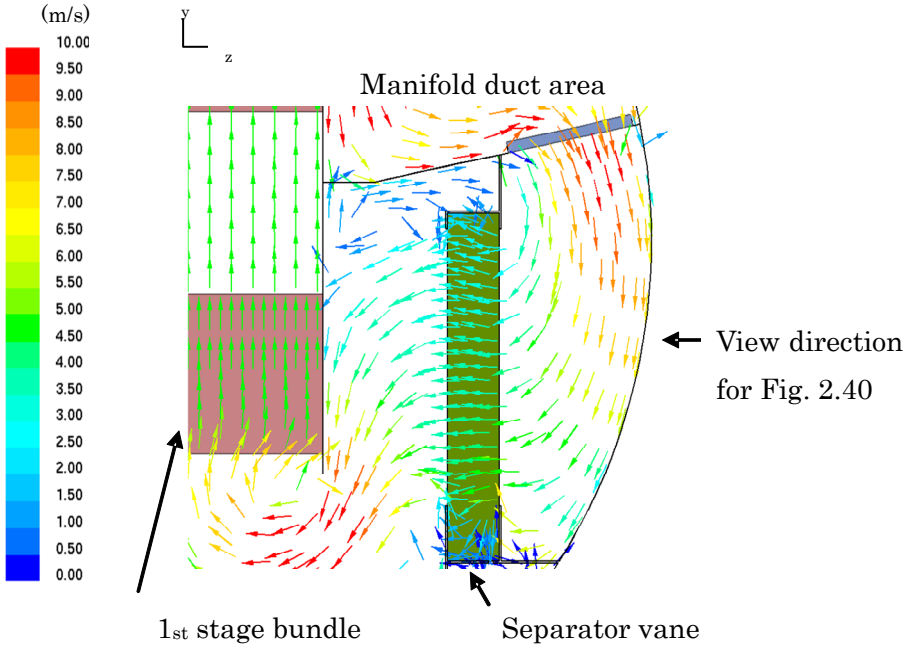

Fig. 2.39 Velocity vector around the separator vane

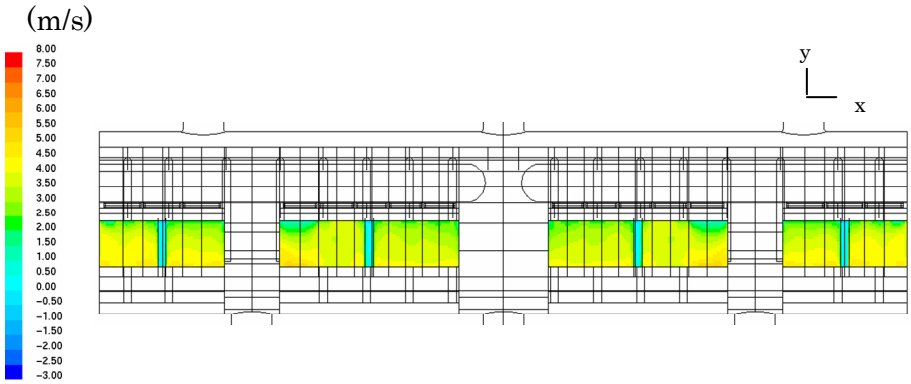

Fig. 2.40 Separator vane velocity contour (Average)

2.4.2 Mass velocity and optimum economy

The optimum design of MSR was implemented evaluating cost dominant items of tube surface and pressure vessel. The optimum mass velocity of the heat transfer tube outer side steam velocity, due to the dominating heat transfer resistance where the steam condition is superheated, was studied figuring out the specification of both MSR pressure vessel diameter and pressure loss of cycle steam on the conditions of reheat pressure of 1.2 MPa, effective heat transfer tube length of 10.0m and TTDs of both reheat stages of 13.9˚C. The tube bundle dimension of both height and width, associated with the pressure drop, was calculated by heat transfer coefficient through the tube bundle with the given condition of tube effective length and tube pitch with parameter of the mass velocity.

The pressure vessel diameter was figured out by which ever the larger one; *the diameter required in horizontal direction* which was the summation of tube bundle width (W_2) and the required one (W_1) from separator vane arrangement associated by its approach velocity, or *the diameter required in vertical direction* which was the summation of tube bundle height (H_2) and others (H_1, H_3) for cycle steam path shown in Fig. 2.41. The figured diameter, expressed in dimensionless, for the mass velocities are shown in Fig. 2.42 implementing that the case of mass velocity 2.9×10^5 kg/m^{2}h (60×10^3 lb/Ft^{2}h) requires the smallest one without wasted space in both height and width directions, despite the other cases require larger ones with a wasted space in direction of either height (shown as α) or width (shown as β).

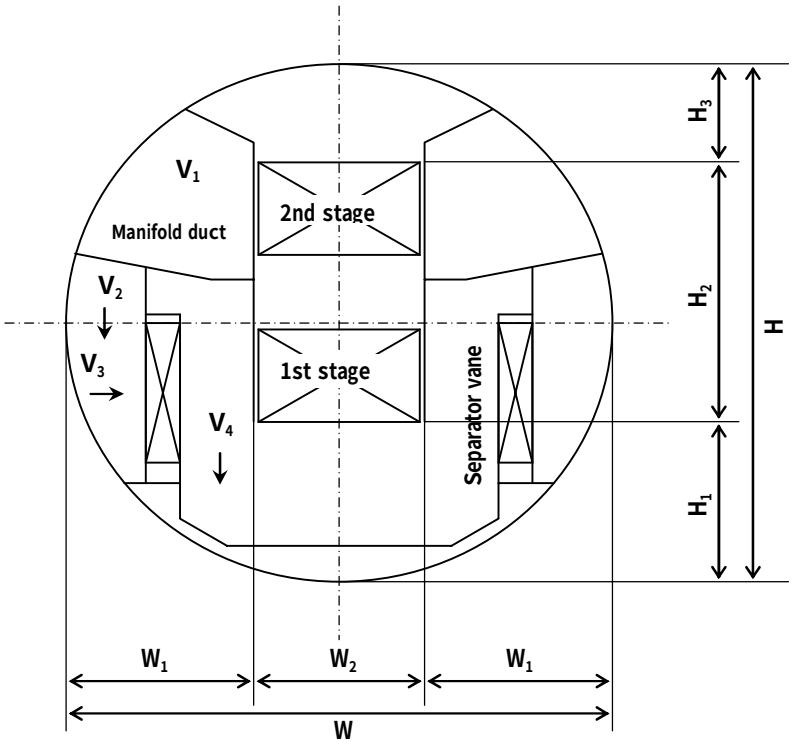

Fig. 2.41 Elements of dimension ruling MSR pressure vessel diameter

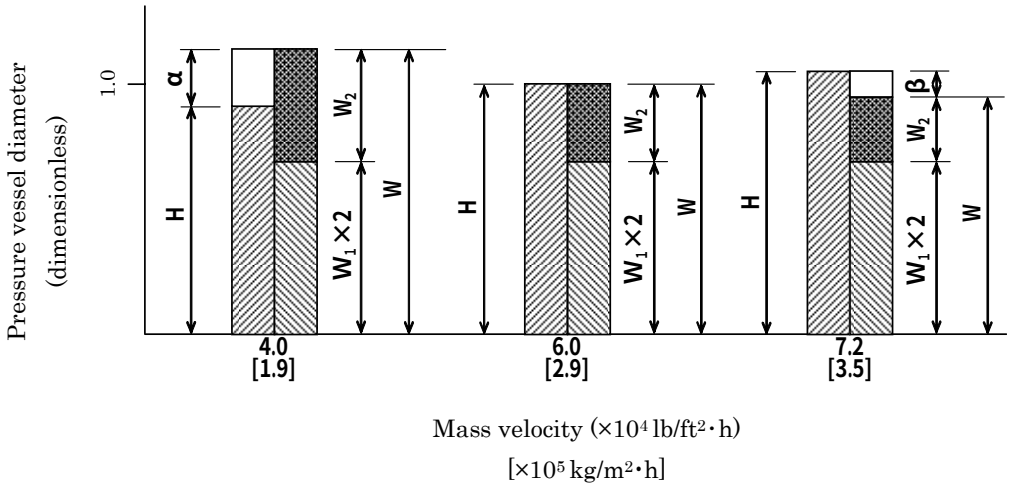

Fig. 2.42 Dimensions for height and width of the pressure vessel

The result of economic evaluation is shown in Fig. 2.43.

Manufacturing cost evaluation resulted that the mass velocity point of 2.9 × 10^5 kg/m^2h (60 × 10^3 lb/Ft^2h) gives the minimum due to the cost correlation of pressure vessel and heat transfer tubes. The manufacturing costs increases both in higher and lower ones, because the vessel diameter and tube surface increase in lower mass velocity, while vessel diameter increases despite the decrease of tube surface in higher mass velocity.

The economic evaluation for heat cycle performance (cycle steam pressure drop) and manufacturing cost of MSR resulted that the mass velocity of 2.9 × 10^5 kg/m^2h (60 × 10^3 lb/Ft^2h) also brings in the optimum point, with the evaluation factor of present value of 70,000 yen/ KW.

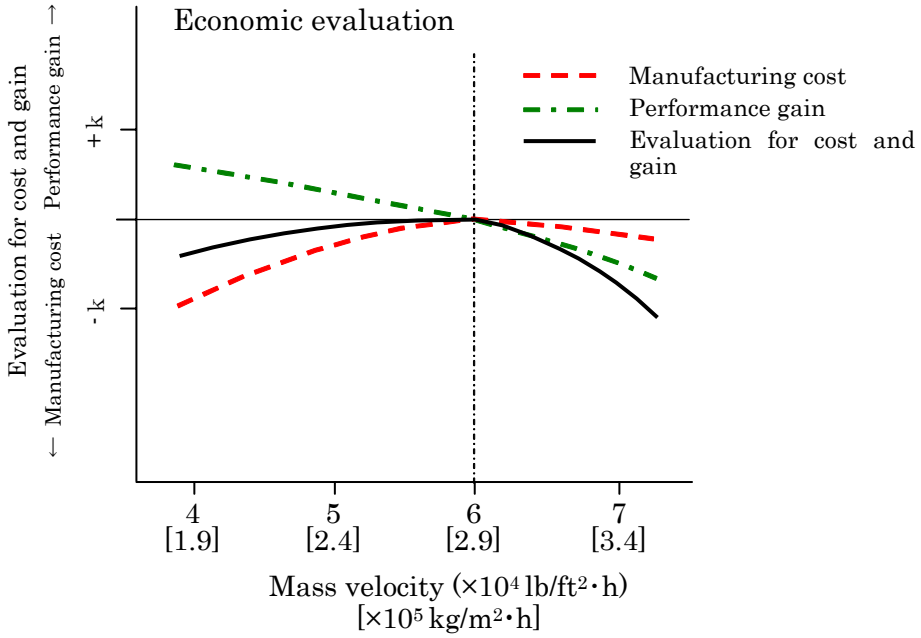

Fig. 2.43 Evaluation for optimum mass velocity

The rough estimation brings the optimum TTD of 12 to 14˚C for the mass velocity point of 2.9 $\times 10^5$ kg/m^{2}h (60 $\times$ 10^3 lb/Ft^{2}h) shown in Fig. 2.44

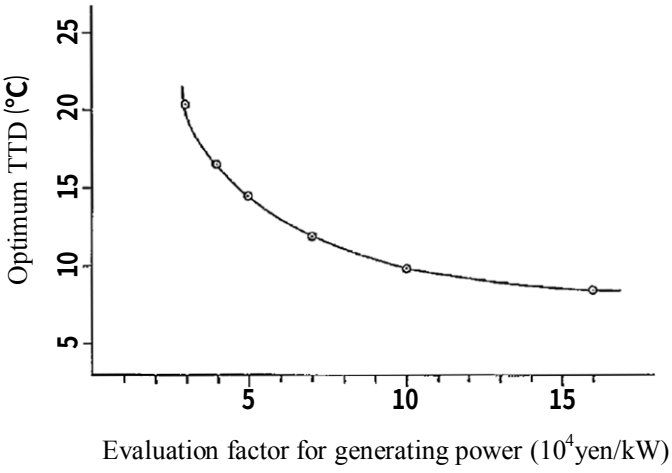

Fig. 2.44 Optimum TTD

2.5 Conclusion

Core issues for the MSR in both methods of predicting mist separator performance and suppressing tube drainage instability were developed, and their effectiveness was demonstrated on actual units. The carryover starting velocity of the mist separator under the actual steam condition is predicted using a configuration in which the mechanism is identical to that of the air-water condition. The instability of drainage from the heat transfer tube is suppressed by increasing the excess ventilation steam rate in partial turbine loads. The methods have been applied to units placed in service since the 1980s and will be applied to units planned in the future as well.

References

(Ex. 1) Spencer, R.C., Booth, J.A., Heat Rate Performance of Nuclear Steam Turbine-Generators, proceedings of the 30th annual meeting of the American Power Conference, April 23-25, 1968, Chicago, Illinois

(Ex. 2) Nakagami, Y., Manabe, J., Urabe, T., Nakahara, T., Kawaguchi, S., Design And Operation of Moisture Separator Reheater for Nuclear Steam Turbine System (in Japanese), The journal "The Thermal And Nuclear Power", 1982, Vol. 34, No. 2, pp. 185-198,

(Ex. 3) Mitsubishi Juko Giho, Recent Technology on PWR Secondary Systems (Turbine Generator Plant) (in Japanese), Araki, R., Kokubo, T., Nakagami, Y., Kawada, Y., Obara, I., Hayami, K., Vol. 19, No. 6

(Ex. 4) Mitsubishi Juko Giho, Design and Field Operation of Advanced 900 MW class PWR Turbine Plant (in Japanese), Nakagami, Y., Yoshioka, T., Sasaki, T., Manabe, J., Matsukuma, M., Taniguchi, M., Miyawaki, T. , 1985, Vol. 22, No. 3

(Ex. 5) Spalthoff, F.J., Hass, H., Heinrichs, F., First YEAR of Operation of the World's Largest Tandem- Cmpound Turbine-Generator, Proceedings of American Power Conference, Chicago, Illinois, April 21,1976

(Ex. 6) Yarden, A, Clement, T, kori gains 30 MWe from MSR reconstruction, Nuclear Engineering International, June 1997

(Ex. 7) M. Yamaguchi, H. Urushidani, Design Features and Operating Experiences of Moisture Separator Heater for Hamaoka Nuclear Power Station No. 4 unit (in Japanese), Sept. 1994, Journal of Thermal and Nuclear Power, Vol. 45, No. 9.

(Ex. 8) Manabe, J., Kasahara, J., Moisture Separator Reheater for NPP Turbines, JSME Journal of Power and Energy Systems, Vol. 3, No. 2, 2009

(Ex. 9) Jun Manabe, Jiro Kasahara, Toshiki Kojima, Issaku Fujita, Recent Moisture Separator Reheater Design Technologies, ASME Journal of Engineering for Gas Turbine and Power, April 2010, Vol. 132.

(Ex. 10) JSME,Corona Co, "Revised, Gas-Liquid two-phase flow handbook (in Japanese)", 2006.

Chapter 3 High All Volatile Water Treatment

Chapter 3 High All Volatile Water Treatment

3.1 Introduction

Wet steam distribution and FAC associated with scale adhesion

Despite the reheat system there remains wet steam condition in a range both from high pressure turbine to MSR and from lower half stream of low pressure turbine to condenser, associated with their extraction line equipments of high pressure FWH, first stage reheater, deaerater and low pressure FWHs.

The remained wet steam condition causes FAC and consequent scale adhesion as follows:

Flow accelerated corrosion arises especially in condensing process in the two phase region because the ammonia distribution factor for gas to water is 30 times larger which causes reduction of pH of water on the surface of the equipments. Consequent scale adhesion arises on surface of equipments in high temperature region of FWP impeller, high pressure FWH heat transfer tube inner surface and SG tube outer surface. Scale adhesion to the surface of FWP impeller causes increase of steam consumption of its driving turbine and electric currency of driving motor. Scale adhesion on inner surface of high pressure FWH causes increases of pressure difference through the FWH over the design value. Furthermore scale adhesion to the surface of SG tubes cause gradual decrease of main steam pressure, which not only affects turbine heat consumption rate but also causes possible rapid reduction of generating power due to limitation by turbine inlet nozzle capacity.

Conventional countermeasures for FAC and scale adhesion

Countermeasures for FAC were adoption of erosion endurable materials, decrease of local velocity and alkalization by water treatment.

Erosion endurable material of stainless steel or low alloy steel was adopted, due to its high cost, only to the area of both two-phase flow in relatively higher temperature and irregular shaped part where velocity is higher. Decrease of local velocity is also difficult because it causes scale up of the equipments and piping. Countermeasures of the materials and the local velocity could not be the final best method. Current water treatment could not raise pH in the system to the expected value described in followings.

Current all volatile water treatment (AVT)

Current water treatment is all volatile water treatment (AVT) using ammonia for alkalization and hydrazine for deaeration and reducing atmosphere, respectively. The purification process is demineralizing the full flow of condensate, which is the outlet flow of condensate pumps, with condensate demineralizer which catches ionic impurities both by resins of cation-exchage and anion-exchange. The maximum pH is 9.2 due to the prohibition from copper carry-on to SG on condition of copper material is adopted for auxiliary heat exchangers. This treatment resulted in insufficient pH value for preventing FAC due to the reduction of pH value in the condensed drain water on the surface of equipment in the liquid-vapor two-phase flow region, derived from large distribution factor for gas to water of ammonia. The minimum pH through the system is 8.9 at separated drain line of MSR, which is not able to suppress FAC.

New concept water treatment

It was reported that raising pH numerical value was effective for suppressing erosion developing rate. The sample of the effect is shown in Fig. 3.1[(3)], which is data in room temperature for carbon steal and low alloy materials.

Raising pH is selected as a counter measure for FAC and consequent scale adhesion.

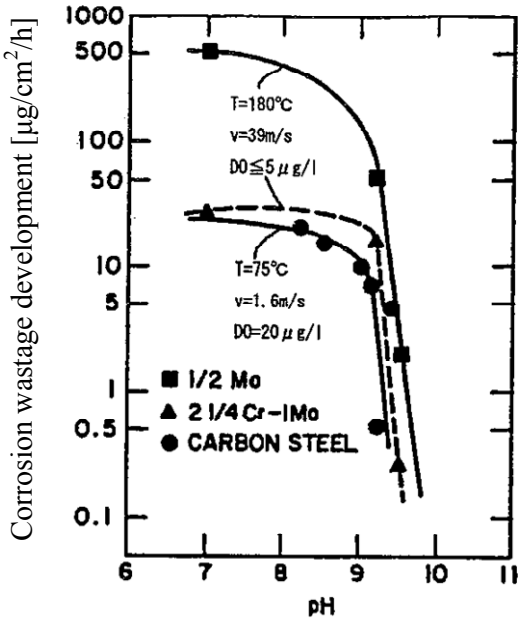

Fig. 3.1 Flow accelerated corrosion developing rate depending on pH for various kinds of materials

3.2 Requirement for water treatment

3.2.1 Requirement from FAC and scale adhesion

Requirement from FAC

Minimum pH value in the system is to be elevated to the value where the FAC progress rate reduces enough.

Scale adhesion

Requirement from scale adhesion was quantitatively determined as a target numerical value of iron concentration of feedwater. It was decided to keep the allowable minimum main steam pressure to confirm the rated generating power through the residual life time of plant of 30 years as described in Section 1.2.3. The iron concentration was calculated as followings.

(a) The allowable minimum main steam pressure was calculated on condition both of lowest vacuum in summer season and of the GV widely open.

(b) The fouling factor of SG tube was calculated which correspond to the above allowable pressure.

(c) The increase of fouling factor of SG tube was assumed to be relative to feedwater iron concentration.

(d) The required feedwater iron concentration was calculated which would reach the fouling factor in the residual 30 years by the fouling increasing rate converted from actual one in relation to the iron concentration.

The targeted value was decided to be 1.0 ppb which would be achievable with pH of 10 and without additional erosion endurable materials.

3.2.2 Reliability for steam generator

Alteration of water treatment is restricted by the requirement from the reliability for steam generator.

Fundamental requirement from seam generator

The requirement for water treatment is for preventing the corrosion of SG heat transfer tube and others. Fundamental design concept for preventing corrosion is as followings;

- Preventing impurities in the cycle adopting leak tight condenser, condensate demineraliser and others.
- Suppression of corrosion in the system by dosing ammonia for pH control and hydrazine for deaeration and reducing atmosphere.

Other than corrosion, water level oscillation and concentration of impurities, both derived from deposit of iron particle to the gap space between tube and tube-plate, are to be prevented by reducing iron concentration in feedwater which is the same way for scale adhesion.

Inter granular attack

The adoption of titanium tube for condenser had completely eliminated the possibility of pitting and denting because they were corrosions caused by chlorine ion from seawater in-leakage with oxide atmosphere. Residual possible corrosion in SG tube is *inter-granular attack* (*IGA*) after eliminating sea-water in-leakage.

IGA occurs on condition of high or low pH value with high electric potential referring from the SG tube corrosion susceptibility diagram which is investigated in the "Investigation of Improving Future Reliability on Secondary water Chemistry Environment" sponsored by JPEIC (Japan Power Engineering and Inspection Corporation) shown in Fig. 3.2 [(4)]. Design practice to prevent IGA is following two items simultaneously because pH may alter according to the impurities.

- To keep $pH_{300\,^{\circ}C}$ in the range between 5 and 10 accompanied by restriction of sodium (Na), kalium (K) for preventing increase of pH, chloride (Cl) and sulfur-oxide (SO_4) for preventing reduction of pH, respectively.
- To prevent ingress of oxidizing agents such as copper.

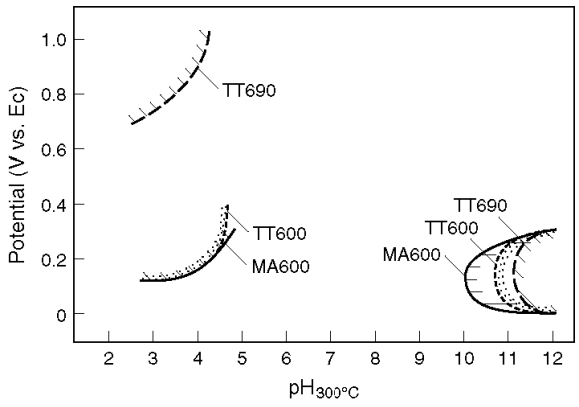

Fig. 3.2 IGA susceptibility for Alloy 600MA, 600TT and 690TT

Possible increase of impurities

Purification flow area of the new concept water treatment would be reduced, as described in following section, due to alteration of purification process from the full flow condensate-demineralizing to the SGBD - demineralizing preventing from over loading of ion exchange resin. This may cause increase of impurities.

3.3 Concept of high all volatile water treatment

The concept flow diagram of high all volatile water treatment (HAVT) is shown in Fig. 3.3, where the additional system for HAVT to the current AVT is colored in blue as SGBD cooling and heat recovery system.

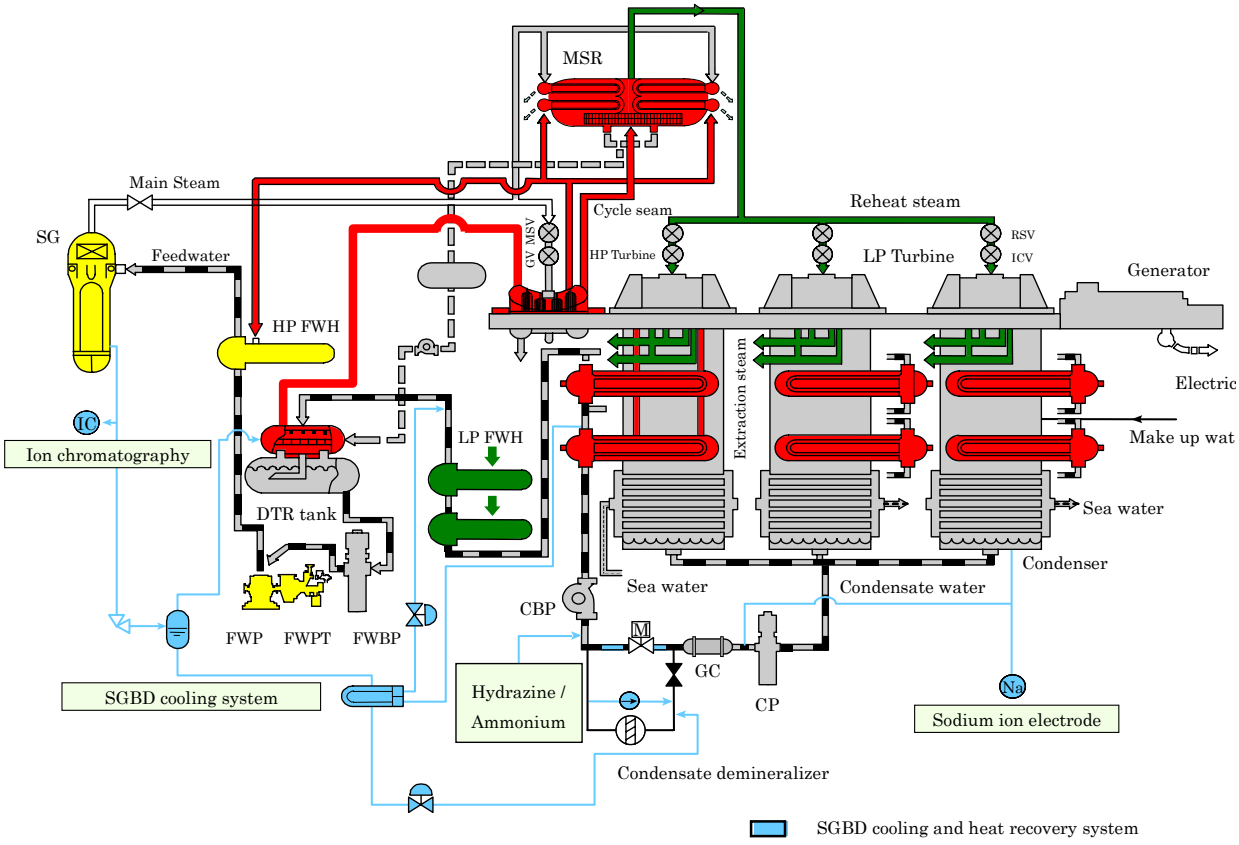

Fig. 3.3 Concept flow diagram of HAVT

3.3.1 Alkalizing agent

There are several kinds of agent for preventing FAC and scale adhesion, the features of which are as followings;

Ammonia

Increase of pH by ammonia from current 9.2 to 10.0, ammonia concentration of which corresponds to 0.5 ppm and more than 12 ppm, respectively. This method is expected to increase the pH to the requested numerical value in the water in two phase region despite the large distribution factor for gas to water along with the advantage of currently used agent and its lower cost.

Ethanol ammine and Morphorin

Distribution factor of Ethanol ammine is 1/10 to 1/100 to that of ammonia which brings the suppression effect for FAC in the two-phase region but insufficient for FAC in single-phase region. Distribution factor of Morphorin is 1.0 which is effective for FAC, but the final resolved organic acid affects the detection of sea-water in-leakage using increase of acid electric conductivity.

High pH by ammonia called High All Volatile Treatment (HAVT) is adopted for its advantages.

3.3.2 Purification method

Purification concept of HAVT is requested to treat high concentration ammonia, which would be about 20 times of that of AVT, in the ordinary condition. Furthermore the system is designed to operate condensate demineraliser which purifies the full flow of condensate (corresponds to 60% of feedwater flow rate) at sea-water in-leakage despite the leak tight condenser with titanium tubes. The design is as follows.

The interval of re-generation of resin

The interval of re-generation of resin of full flow-condensate-demineralizer in AVT operation is about 3 days. The higher ammonia concentration in HAVT would cause too higher load for resin in case of full-flow-condensate deminaralizer, resulting in the interval of re-generation of several hours.

SGBD demineralizing

Purification method of SGBD-demineralizing was devised aiming to reduce the resin load and succeeding prolongation of the interval, which purifies the most contaminated process of SGBD in the system by the isolated condensate demineralizer. The isolated condensate demineralizer is isolated from condensate flow and used only to purify SGBD, the flow rate of which is 1% of feedwater. The load for ion exchange resin is product of flow rate and its concentration which follows that the load of the SGBD demineralizing would be 1/10 to that of AVT due to the flow rate ratio of 1/60 despite the ammonia concentration rate of up to 20.

3.3.3 System Design

SGBD cooling system

The SGBD was about 270˚C and required to be of 1% of feedwater rate for purification of SG. The blow down was first led to flush tank, where the SGBD reduced its pressure to about 1.4 MPa reducing its temperature to about 194˚C, feeding its separated steam to deaerator recovering heat energy. The separated drain is cooled by condensate cooler to the acceptable temperature for ion exchange resin of 40-50˚C.

Condensate deminearizer

Condensate deminerarizer purifies the SGBD in HAVT operation with completely by-passed by condensate water, but is designed to be operated with full flow deminerarizing at sea water in-leakage.

Material

Materials of piping and equipment are shown in Table 3.1 Wet condition piping and others were all ready altered to stainless steel.

Table 3.1 Material list of turbine system piping and equipment

	Area and name	Materials
Piping	(1) Turbine extraction piping with wet steam	(1) Stainless steel
	(2) Cross under piping	(2) Stainless steel partially
	(3) HP-FWH drain line down stream of control valve	(3) Stainless steel
	(4) Condensate water piping	(4) Stainless steel partially
	(5) Others	(5) Carbon steel
Equipment	(1) Tubes of heat exchangers	(1) Stainless steel and titan
	(2) Inner component of LP- FWH	(2) Low alloy steel
	(3) Others	(3) Carbon steel

3.4 Numerical value of pH for HAVT

Numerical value of pH at feedwater is studied here to satisfy the requirement both for iron concentration in feedwater of 1.0 ppb and for minimum numerical value of pH in the system for suppressing the FAC.

3.4.1 Distribution of ammonia and numerical value of pH in the system

Distribution of ammonia concentration and numerical pH value in the system was estimated using the distribution factor of ammonia (5). The estimated pH values were in water phase both for water-gas two phase condition and water single phase condition. The estimate ammonia concentration and numerical value of pH is shown in Fig. 3.4, which verifies that feedwater ammonia concentration of about 12 ppm (pH 10.0) will bring the minimum pH in the system, where is moisture separator drain line, to keep about 9.5.

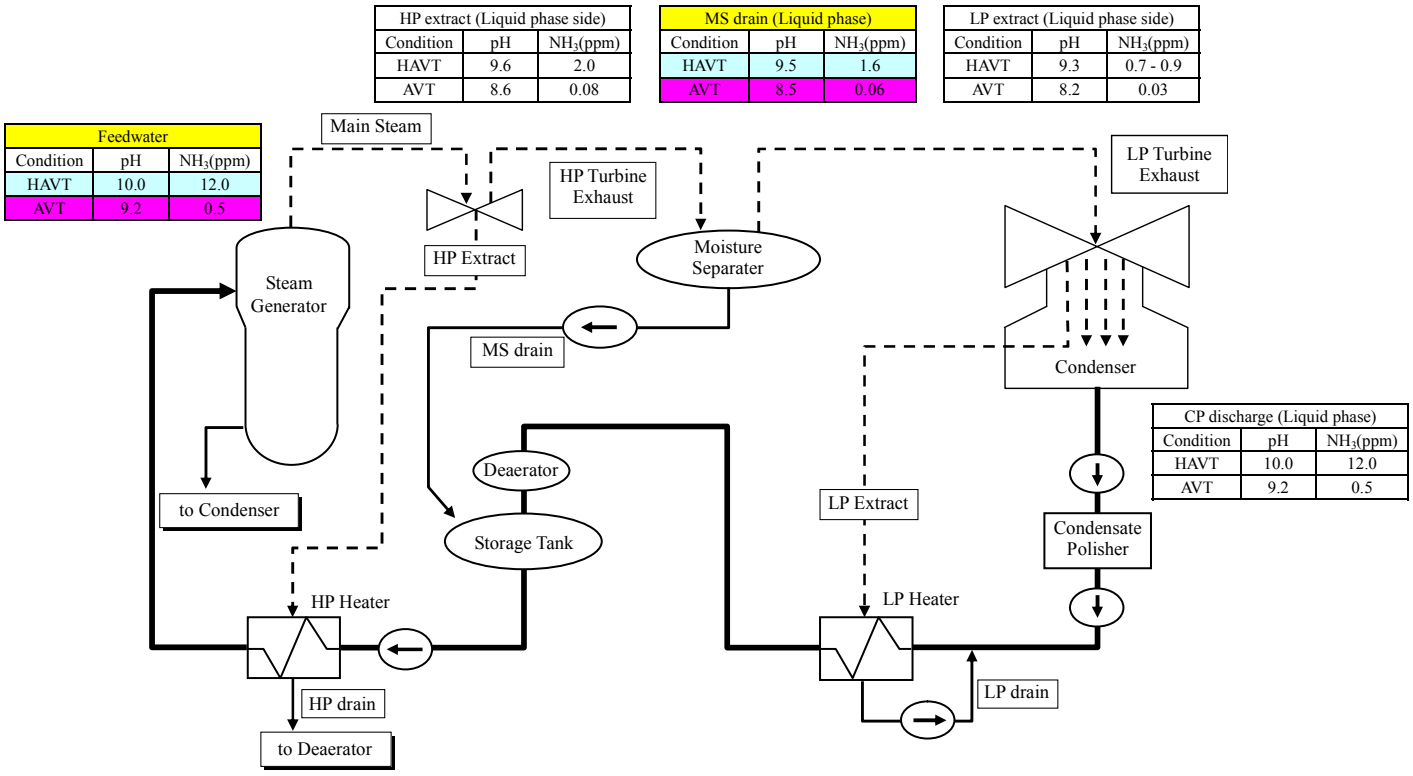

Fig. 3.4 The estimate ammonia concentration and numerical value of pH

3.4.2 Estimated iron concentration in feedwater

Reduction ratio of flow accelerate developing rate due to raising pH in the system was estimated using the relation of FAC developing rate to pH value (3) as shown in Fig. 3.1. The ratio was estimated on condition that the pH value was raised from 9.2 to 10.0 which correspond to 0.5 ppm and 12 ppm of ammonia concentration, respectively. The ratios were estimated to be less than 0.1 both for liquid side in two-phase flow region where the pH value was estimated to be raised from 8.5 to 9.5, and for liquid single phase flow region where the pH value was estimated to be raised from 9.2 to 10.0. The estimated ratio of less than 0.1 is applicable both for carbon steel and for low alloy which is indicated as 2 1/4 Cr-1Mo in Fig. 3.1.

Design numerical value of pH in feedwater for HAVT operation was determined to be 10.0 (ammonia concentration of 12 ppm) which would make feedwater iron concentration less than 0.5 ppb by estimation of reduction ratio of o.1 for usual maximum iron concentration of less than 5 ppb by feedwater pH of 9.2 in conventional AVT. The designed pH value was selected with safety margin due to inexperienced technology.

3.5 HAVT application results and evaluation of the effect

3.5.1 Ammonia and pH distribution in the system

Ammonia distribution and system pH under HAVT and AVT conditions of secondary system are shown in Fig. 3.5. The minimum value of pH in the system was raised from 8.9 to 9.6; the alteration of the value was estimated to reduce the FAC development rate by ratio of 1/10.

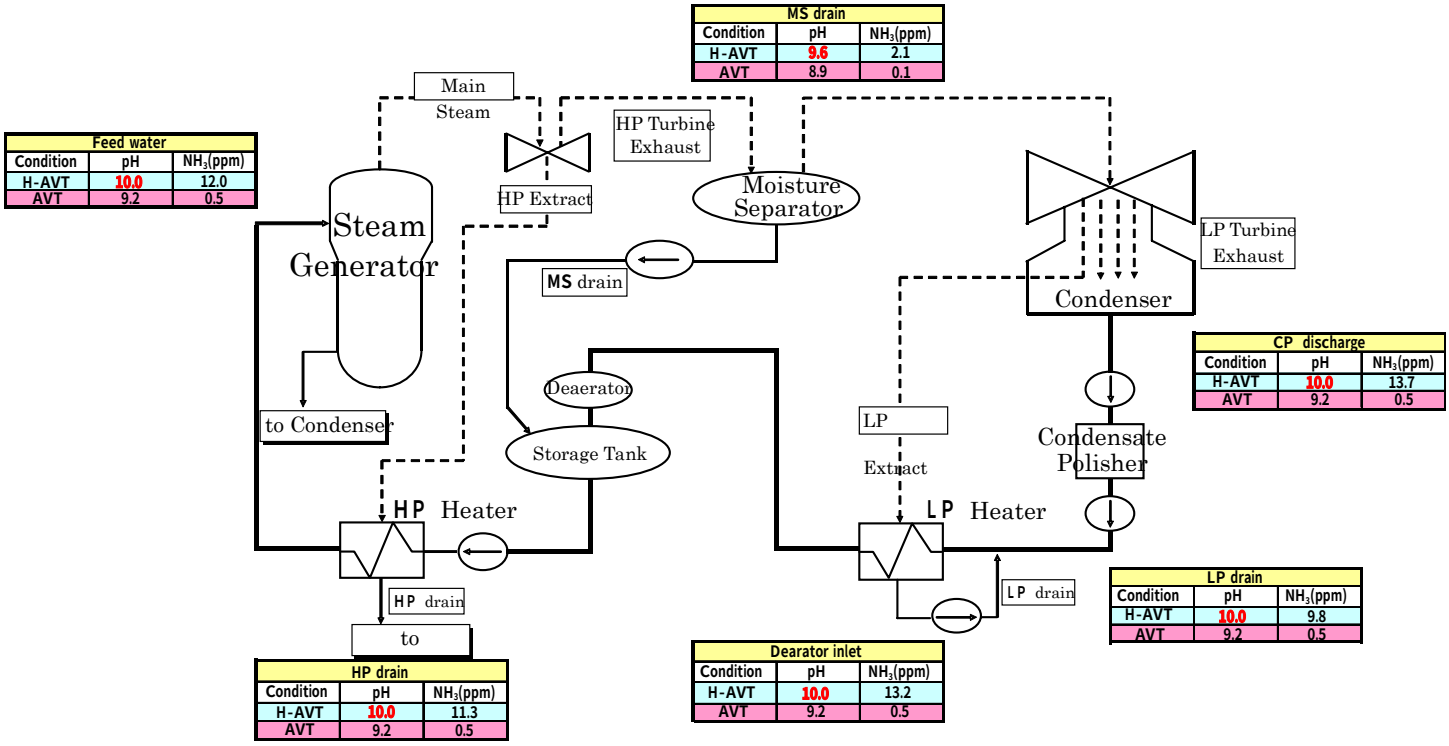

Fig. 3.5 Ammonia distribution and system pH

3.5.2 Iron concentration in feedwater and in the system

Total iron concentrations in the system under HAVT and AVT conditions are shown in Fig.3.6.

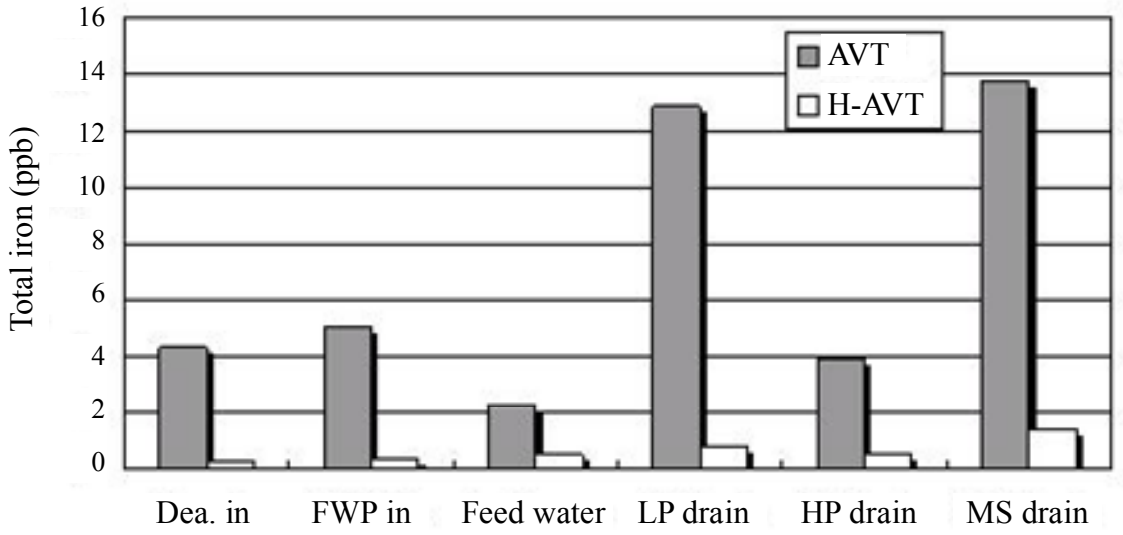

Fig. 3.6 Total iron concentration under HAVT and AVT condition

Under HAVT condition, total iron concentrations through the system are reduced drastically. Especially, feedwater iron concentration is reduced around to 1 ppb which is promising value for reducing scale adhesion sufficiently.

3.5.3 Scale adhesion

Addition to the result of feedwater iron concentration reduction to about 1 ppb by HAVT operation, effects for scale adhesion reduction were confirmed as alteration of several indications after one cycle operation show in Tables 3.2 and 3.3.

Driving motor current electricity increment of FWPs along with their two months operating intervals, which was the typical phenomena of scale adhesion to impeller for all the PWR units, ceased completely.

Table 3.2 FWP motor current electricity (Unit #2)

Operation cycle	Water treatment condition		Motor currency (A)		Increment (A)
	Treatment	Feedwater conductivity (μS / cm)	Operating interval initial	Operating interval end	
One cycle before	AVT	4.5	390	430	40
Corresponding cycle	HAVT	27 to 32	380	382	2

Pressure drop of a segment containing HP-FWHs stopped to increase. The pressure drop increase in AVT operation was 0.1 MPa, which means the scale adhesion increased the drop twice of the design value.

Table 3.3 Pressure drop of a segment containing HP-FWHs (Unit #1)

Operation cycle	Water treatment condition		Pressure drop (MPa)		Increment (MPa)
	treatment	Feedwater conductivity (μS / cm)	Cycle initial	Maximum	
One cycle before	AVT	7.0	0.4	0.5	0.1
Corresponding cycle	HAVT	15 to 18	0.4	0.4	0

3.5.4 Evaluation for reliability for steam generator

The reliability for steam generator was confirmed as followings;

- Numerical value of actual temperature pH300 ˚C in SG was in the range from 5.8 to 7.0 which was in the allowable range
- Oxidizing agent of copper was eliminated and was not detected.
- Impurities concentration level was maintained still low enough.

3.6 Conclusion

The first generation PWR power stations operating more than 20 years were replaced their copper alloy tube heat exchangers and altered there water treatment from AVT to HAVT aiming to suppress erosion in piping and equipment based on the life cycle management program resulting in both feedwater iron concentration reduction to around 1 ppb as indication of the effect and scale adhesion reduction of FWPs and HP-FWHs

.

References

(Ex. 1) Jun Manabe, Yasuhiko Shoda, Tatsushi Yamamura, Yuuichiro Kusumoto, Refurbishment of Secondary System and High AVT Water Treatment of GENKAI #1 and # 2, JSME Journal of Power and Energy Systems, Vol. 3, No. 1, 2009

(Ex. 2) Jun Manabe, Yasuhiko Shoda, Tatsushi Yamamura, Yuuichiro Kusumoto, Refurbishment of Secondary System and High AVT Water Treatment of GENKAI #1 and # 2, 16th International Conference of Nuclear Engineering, Orland, Florida, USA, May, 2008

(Ex. 3) Codes for Power Generation Facilities, - Rules on Pipe Wall Thinning Management- (in Japanese), JSME, SCA1-2005, 2005-3, JSME

(Ex. 4) Y. Shoda, M. Sato, H. Fujiwara, R. Kamio, T. Hattori, Improvement of SG Crevice Environment Estimation, 1998 JAIF International Conference of Water Chemistry in NPP at Kashiwazaki Japan

(Ex. 5) ASME handbook on water technology for thermal power systems, Paul Cohen, 1958, ASME 100284

Chapter 4 High Temperature NPSH and Its Application to A Feedwater System

4.1 Introduction

Nomenclature

H: Static head from DTR-tank water level to FWBP impeller (m)

$NPSH_{av}$: Available NPSH (m)

$NPSH_{req}$: Required NPSH (m)

$NPSH_{NC}$: NPSH causing no head down on condition of room temperature and saturation air (m)

P_d: DTR-tank pressure (MPa)

ΔP: Total pressure drop from DTR-tank to FWBP impeller inlet (MPa)

P_{sat}: Saturation pressure corresponding to impeller inlet feedwater temperature (MPa)

g: Acceleration of gravity (m/s^2)

ρ: Density (kg / m^3)

4.1.1 System behavior at load rejection

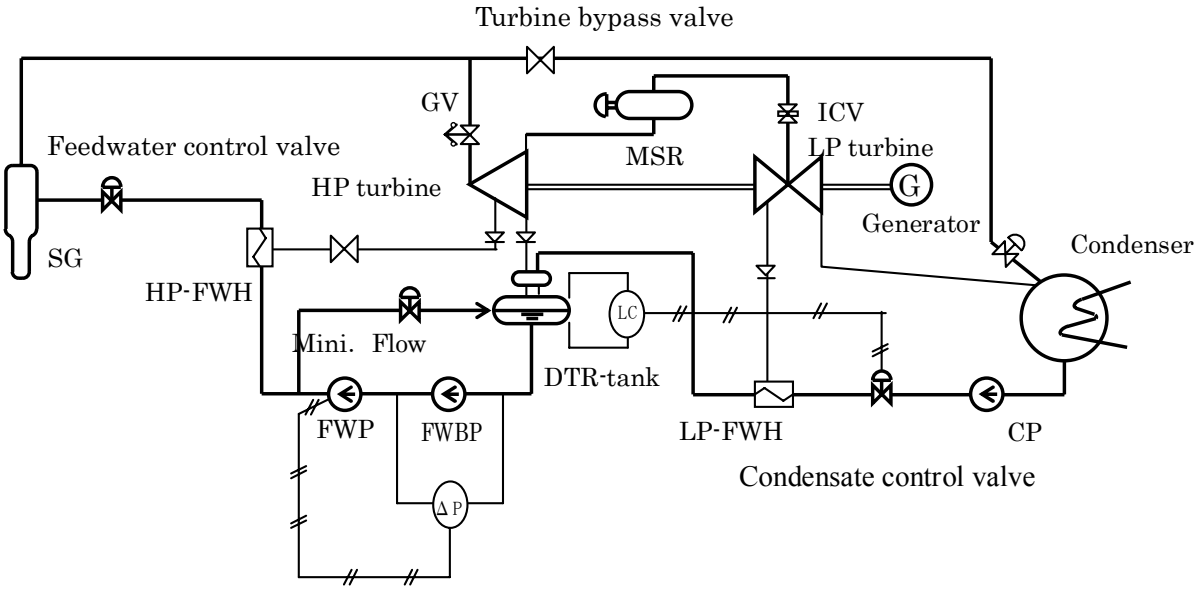

Fig. 4.1 Construction of PWR Turbine Unit System

Feedwater system construction

The feedwater system of the PWR turbine unit, shown in Fig. 4.1, consists of high and LP-FWHs, a DTR-tank, all of which are heated by turbine extraction steam, FWBPs and FWPs. The DTR-tank feedwater level is controlled by the condensate control valve. The DTR-tank is designed to have a capacity corresponding to the range of 3 to 4 minutes of feedwater flow rate and to have static head of 12 to 25 m for the FWBP impeller.

Feedwater pump system is constructed with FWP (Main feedwater pump) and FWBP (its booster pump), the head of which is selected to satisfy the required NPSH ($NASH_{req}$) of main FWP. The head distribution for each pump is 700 m for the main FWP and 100 m for the FWBP to the requisition from steam generator of total 800 m.

Turbine plant system behavior

More than half of the rated feedwater is continuously requested for about 3 to 4 minutes after turbine-generator load rejection for reactor cooling. DTR-tank pressure and its saturation condition temperature, about 1 MPa and 180°C, respectively, at full load or initial transition value, begin to reduce both by loss of its heating steam from turbine extraction, derived from a turbine casing pressure decrease, and by the continuation of colder condensate flow-in from the condenser to maintain the DTR-tank level via LP-FWHs, for which the heating extraction steam has also failed [(1)].

NPSH of FWBP

Available NPSH ($NPSH_{av}$) of FWBP shown in Eq. (4.1) begins to reduce at load rejection according to the reduction of both pressure and associated saturated temperature of the DTR-tank because the feedwater temperature at the FWBP impeller inlet becomes higher than that of the DTR-tank due to the retention time of the feedwater through piping and pump casing from the tank to pump impeller, which means the Pd-P_{sat} becomes a negative value, as shown in Fig. 4.2. $NPSH_{av}$ is designed to maintain larger than $NPSH_{req}$ through transition. (Eq. (4.2))

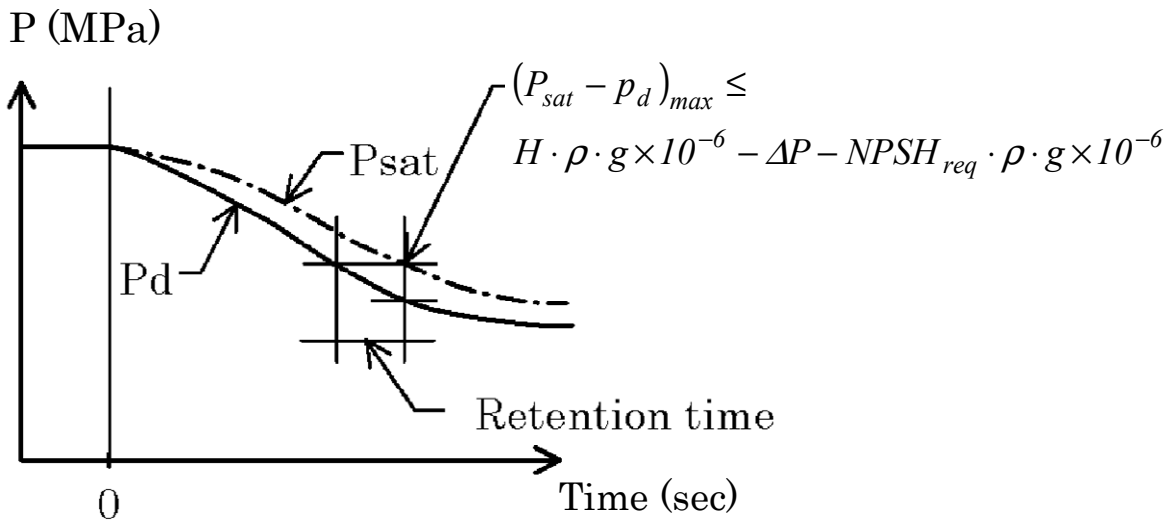

Fig. 4.2 $NPSH_{av}$ of FWBP at load rejection

$$(P_{sat} - p_d)_{max} \leq H \cdot \rho \cdot g \times 10^{-6} - \Delta P - NPSH_{req} \cdot \rho \cdot g \times 10^{-6} \quad (4.1)$$

$$NPSH_{av} \geq NPSH_{req} \quad (4.2)$$

Protection interlock and definition of NPSH

FWP are inter-locked to trip them for preventing cavitation by complete head loss of the corresponding FWBP. The NPSH studied here is, not suction head which causes 3% head reduction popularly used, but complete head

loss. In this study nevertheless, a suction head causing reduction to 50% of head is used because of the difficulty of the testing conditions causing zero head. The difference between NPSHs giving zero head and a half head is negligible small.

4.1.2 Experience in actual unit

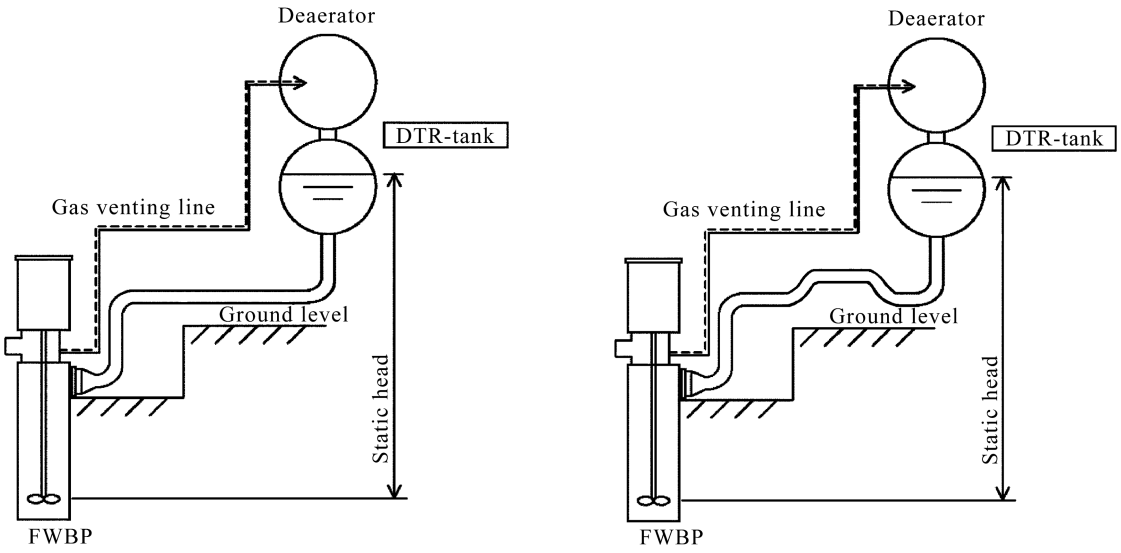

(a) Arrangement of unit A (b) Arrangement of unit B

Fig. 4.3 Arrangement of DTR-tank and FWBP

Two similarly designed second generation 800MWe class units A-1 and A-2, having a DTR-tank situated at ground level with a static head of 11.7 m for the impeller of vertical type FWBP, with no control other than DTR-tank level control and FWP minimum flow control, maintained smooth operation during a load rejection test in trial operations in 1970s, with neither loss of the FWBP head nor tripping of the FWP by the interlock. This datum suggests that the NPSH of FWBPs was maintained through the transitions.

In contrast, another similarly designed unit B, which differs slightly from units A-1 and A-2 in the piping arrangement between the DTR-tank and FWBP, where the pipe is arranged upwards and then downwards forming a possible gas pocket and which is considerably longer, lost its 2 × 50% capacity FWPs' function caused by FWBP head loss and consequent tipping of FWPs by interlock, succeeded by the additional start-up of another 1*50% stand-by FWP maintaining the feedwater requirement. The arrangement of the DTR-tank, FWBP, and piping for units A and B is shown in Fig. 4.3.

4.1.3 History

PWR NPP (nuclear power plant) turbine systems are generally furnished with deaerator and feedwater storage tank (DTR-tank) for feedwater system, derived from their design concept of fossil power units. The main contributing factors for maintaining the $NPSH_{av}$ for FWBP are the static head for FWBP and the requisition of feedwater continuity from steam generator at the load rejection.

Specification of the feedwater system of PWR units is shown in Table 4.1.

Fossil unit

DTR-tank is situated at the turbine building top, one floor over the main turbine situated floor, maintaining the static head of over 20 m for the FWBP suction corresponding to three times of the generally selected $NPSH_{req}$ of 10 m of high speed vertical type pump. The capacity of the tank is designed for a range of 100 to 150 m3 corresponding to 2-3 minutes of the feedwater flow rate in case of 1000 MW class unit.

The required feedwater continuity from oil or gas fired boiler to continue operation is negligibly small, substantially zero, attributing to the FCB of the fuels. Coal fired boiler unit is not generally required to continue operation at the load rejection due to the difficulty of fuel cutoff.

PWR NPP in Japan

The required feedwater continuity of NPP is, as shown in the preceding section, more than half of the rated flow for about 3 to 4 minutes on the condition of reducing $NPSH_{av}$.

In 1970s there was not requirement for the unit to continue operation at load rejection; the system design configuration was follows. Vertical type FWBP was selected for PWR NPP for its built-in advantage of static head from its suction pipe connection to impeller coupled with small $NPSH_{req}$ by low rotation speed. The DTR-tank was designed in a range of 350 to 400 m3 capacity corresponding to 4 minutes of the feedwater flow rate and situated ground level, maintaining static head of about 12 m corresponding to three times of the $NPSH_{req}$.

In 1980s there increased was the design requirement of the capability to continue operation at the load rejection especially the unit located Japan Sea or far from the electricity consumption area, where the electricity transmission grids were susceptible to sunder damage; the design concept was follows. The succeeding constructed units were designed in a similar way to fossil unit concept that the DTR-tank was situated at the turbine floor or higher maintaining static head of 20 m or higher with both the DTR-tank capacity of 4 to 5 minutes of the feedwater and NSPH controller which suppressed reduction of the $NPSH_{av}$ during the transient, due to the lack of the understanding for the experience of A and B units.

The arrangement of FWBP and DTR-tank is shown in Fig. 4.4 for both constructed in 1970s and 1980s.

Table 4.1 History of the system specification

Representative unit	JAPAN in 1970s	JAPAN in 1980s	JAPAN in 1990s	US	Germany
Generating power (MW)	800 class	900 class	1200 class	950 class	1300 class
DTR-tank pressure (MPa)	1.0 class	1.3 class	1.3 class	0.8 class	0.4 class
DTR-tank capacity (m3) Corresponding time for feedwater flow rate (minute)	350 4	500 5	600 5	300 3	560 4
Static head (m)	11.7	24.5	28.7	16.7	14.3
FWBP type and $NPSH_{req}$ (m)	Vertical 4.0	Horizontal 7.5	Vertical 4.8	Horizontal 8.2	Horizontal 7
Additional tool for increasing $NPSH_{av}$	None	NPSH controller	NPSH controller	Pegging steam	Pegging steam
Load rejection capability as a design condition	Not equipped	Equipped	Equipped	Equipped	Equipped

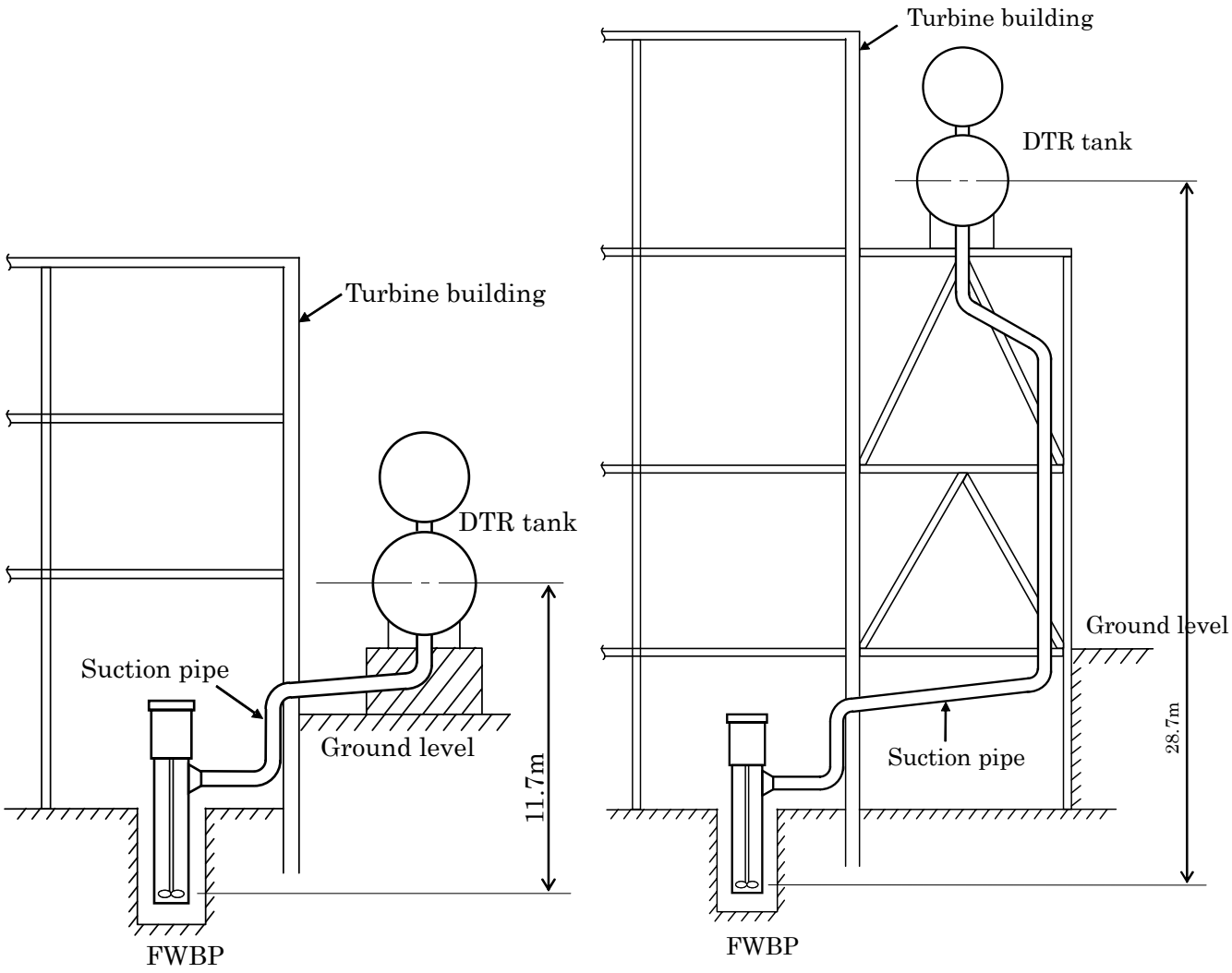

(a) Arrangement in 1970s (b) Arrangement in 1980s and after

Fig. 4.4 The arrangement of DTR-tank and FWBP

PWR NPP overseas

Germany PWR unit design is that deaerator rated operating pressure is selected for about 0.4 MPa, lower point compared to that of Japan, which brings gradual pressure reduction rate at the load rejection due to its initial lower enthalpy, though it brings the lower heat cycle efficiency for lower temperature point of FWP heat inlet. DTR-tank has the capacity corresponding to 4minutes of feedwater and is situated turbine floor maintaining static head of twice of $NPSH_{req}$.

In the US scarcely a little number of PWR units has DTR-tank. V. C. summer unit [(2)] is designed to situate DTR-tank at turbine building top floor for maintaining enough static head of 16.7m with the capacity of tree minutes of the feedwater.

4.2 Available NPSH ($NPSH_{av}$)

4.2.1 Simulation method for $NPSH_{av}$

$NPSH_{av}$ for FWBP was evaluated by a simulation, modeling the system ranging from DTR-tank to FWBP via feedwater piping to the pump casing. The modeling is dividing the piping and the pump casing into several segments with volume and elevation.

The method was to calculate the enthalpy, pressure and temperature of each element (corresponding to the segment) by thermal and mass balance between the elements and finally to calculate $NPSH_{av}$ and quality of feedwater at each element. Simulation program is a node-link network of thermal-fluid elements named "PRANET" [3].

Model

Energy balance of the system, shown in Fig. 4.5 as model for $NPSH_{av}$, is calculated on the assumption shown below in the each segment which is a divided volume in several numbers of suction piping containing the FWBP suction casing volume upstream of the pump impeller.

(a) Mass flows are uniform.

(b) No velocity gap between liquid and gas

(c) Mass flow of inlet and outlet of each the segment is kept equal.

The piping and pump casing are divided in number of *n* starting from DTR-tank outlet.

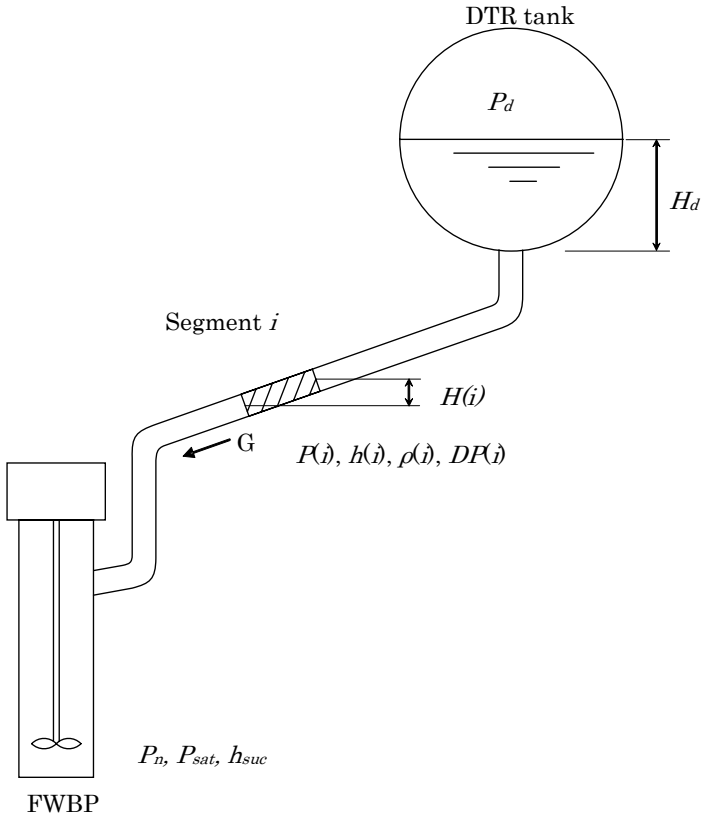

Fig. 4.5 Model of $NPSH_{av}$

Prediction method for $NPSH_{av}$

The pressure at segment number *k* is shown Eq. (4.3), where the first term P_{Dout} is DTR-tank outlet pressure, the second is static head and the third is pressure drop both from DTR-tank outlet. The enthalpy of the segment *k* is shown in Eq. (4.4). The enthalpy and temperature of feedwater at DTR-tank outlet or suction pipe inlet are those of saturation condition of the deaerator pressure P_d. DTR-tank outlet pressure P_{Dout} is expressed by Eq. (4.5).

The enthalpy at the pump impeller inlet h_{suc} is calculated as *h (n) (Eq.* (4.6)*)* by simultaneous differential Eqs. (4.3) and (4.4).

$NPSH_{av}$ is expressed in Eq. (4.7).

$$P(k) = P_{Dout} + \sum_{i=1}^{k} H(i) \cdot \rho\left(p(i), h(i)\right) \cdot g \cdot 10^{-6} - \sum_{i=1}^{k} DP_0(i) \cdot \frac{\rho_0(i) \cdot G^2}{\rho\left(p(i), h(i)\right) \cdot G_0^{\ 2}} \tag{4.3}$$

$$\frac{dh(k)}{dt} = \frac{1}{V(k) \cdot \rho\left(p(k), h(k)\right)} \cdot \{h(k-1) - h(k)\} \cdot G \tag{4.4}$$

$$P_{Dout} = P_D + H_d \cdot \rho \cdot g \cdot 10^{-6} \tag{4.5}$$

$$h_{suc} = h(n) \tag{4.6}$$

$$NPSH_{av} = \frac{1}{\rho \cdot g} \cdot \left(P_n - P_{sat}\right) \cdot 10^6 \tag{4.7}$$

Nomenclature

DP(i) : Pressure drop of the segment *i* (MPa)

G: Suction pipe flow rate (kg/s)

g: Acceleration of gravity (m/s^2)

H(i): Elevation difference between inlet and outlet of the segment number *i* (m)

h(i): Enthalpy of the segment *i* (kJ/kg)

H_d: DTR-tank water level (m)

h_{suc}: Enthalpy at the pump impeller inlet (kJ/kg)

n: Total segment number; the n^{th} segment corresponds to the segment of pump impeller inlet

P(i) : Pressure of the segment *i*（MPa)

P_{Dou}: DTR-tank outlet pressure (MPa)

P_{sat}: Saturation pressure to the pump impeller inlet enthalpy of h_{suc} (MPa)

$\rho(i)$: Density (kg / m^3)

Subscript

0; Initial time

Verification

The accuracy of the program had been verified in case of another actual unit [4], which was designed to maintain sufficient $NPSH_{av}$ through transition, using actually measured data of feedwater flow, minimum flow of FWP, pressure and water level of DTR-tank, by demonstrating equivalency of the simulated $NPSH_{av}$ to the actual one derived from the measured feedwater pressure and temperature at the impeller inlet. The simulated and actual ones of the difference of $(NPSH_{av} - NPSH_{req})$ is shown in Fig. 4.6, using for both cases a same value of the $NPSH_{req}$ measured in room temperature and saturation air.

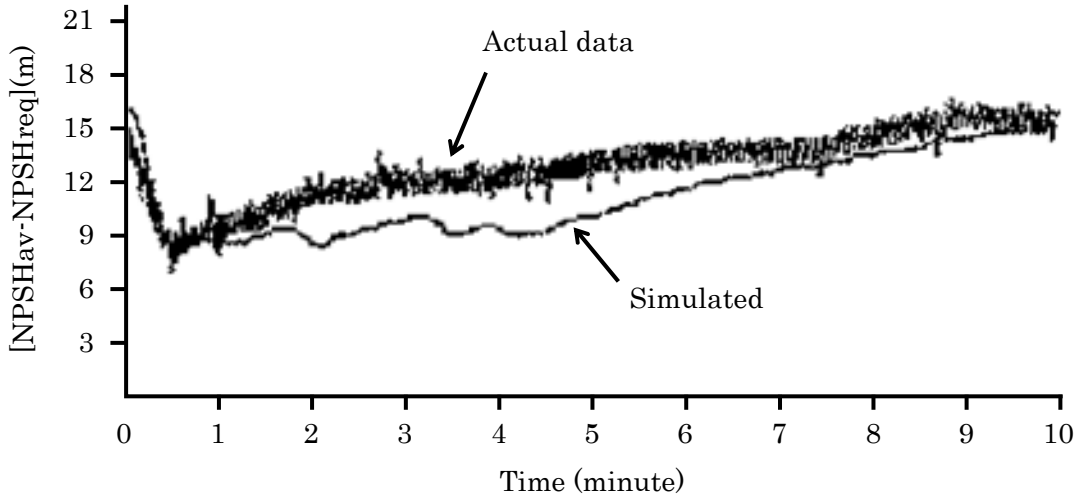

Fig. 4.6 Verification of the simulation

4.2.2 $NPSH_{av}$ in actual unit

Simulation of $NPSH_{av}$ in unit A and B were also conducted.

Construction of FWBP

System construction of feedwater pump is 2 trains of FWP and FWBP of each 50% capacity, and the same construction one train for stand-by. Construction of FWBP shown in Fig.4.7 (a), applied to both A and B unit, is two stage impellers and with double flow suction for the first stage to reduce $NPSH_{req}$. The concept of the double flow suction is shown in Fig. 4.7 (b), where two 25% capacity first stage impellers feed the water to second stage impeller. Feedwater for lower-side-suction impeller of the first stage is suctioned via the minimum area between pump casing and the volute casing. Feedwater for upper-side-suction impeller of the first stage is suctioned freely via wide space between the connection pipes of feeding for the second stage.

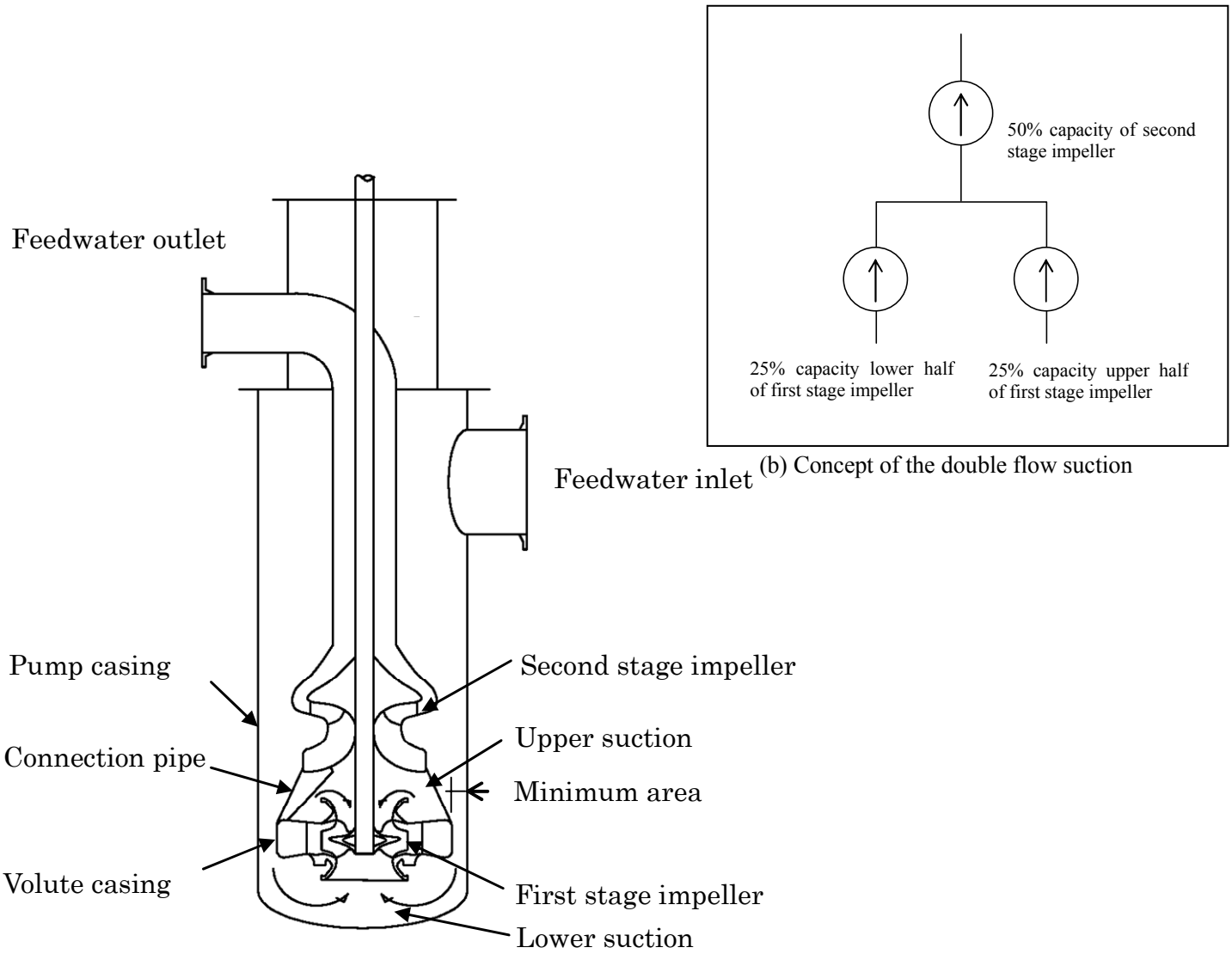

(a) Construction of 50% capacity FWBP

(b) Concept of the double flow suction

Fig. 4.7 Construction of FWBP

Simulation for unit A

Model of unit A is shown in Fig. 4.8, where the piping and inner volume of FWBP are divided into 12 segments.

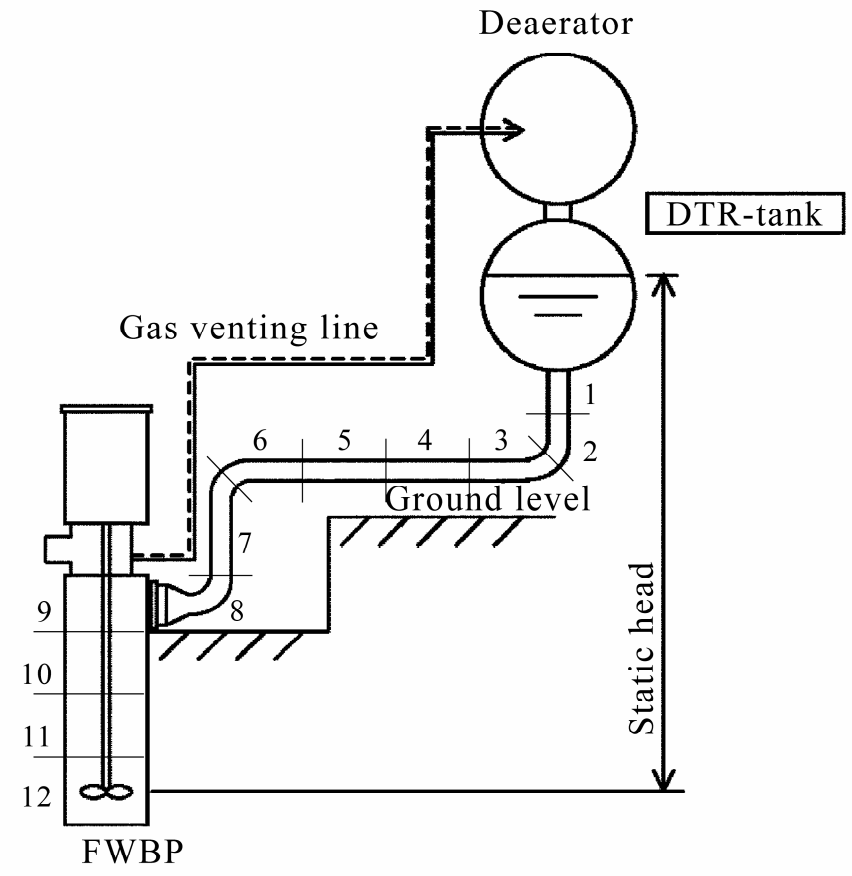

Fig. 4.8 Model of unit A for simulation of $NPSH_{av}$

Simulation of unit A, presented in Figs. 4.9 (a)"Prior conditions" (Measured data of feedwater flow, DTR-tank water level and DTR-tank pressure), 4.9 (b) (Calculated available $NPSH_{av}$ and quality of each segment) showed that $NPSH_{av}$ rapidly reduced soon after the load rejection to a minimum value of -1.4 m at 240 sec, then recovered, attributable to interlocked opening of the FWP minimum flow line resulting in a shorter retention time. The steam quality distribution of the suction line showed depressed boiling gas generated at 240 sec only in the FWBP casing, segments 10, 11, 12, which were calculated to be about 2.8 t/h and were small compared to an allowable gas amount of more than 3.0 t/h (Corresponding to generating gas of -1.5 m of $NPSH_{av}$) by pressure difference in the drive, which was vented by 80 A diameter piping from the FWBP casing top to the DTR-tank gas area, resulting in saturation of the feedwater at the impeller and perhaps slightly in a gas phase.

(a) NPSH simulation of unit A-Prior conditions

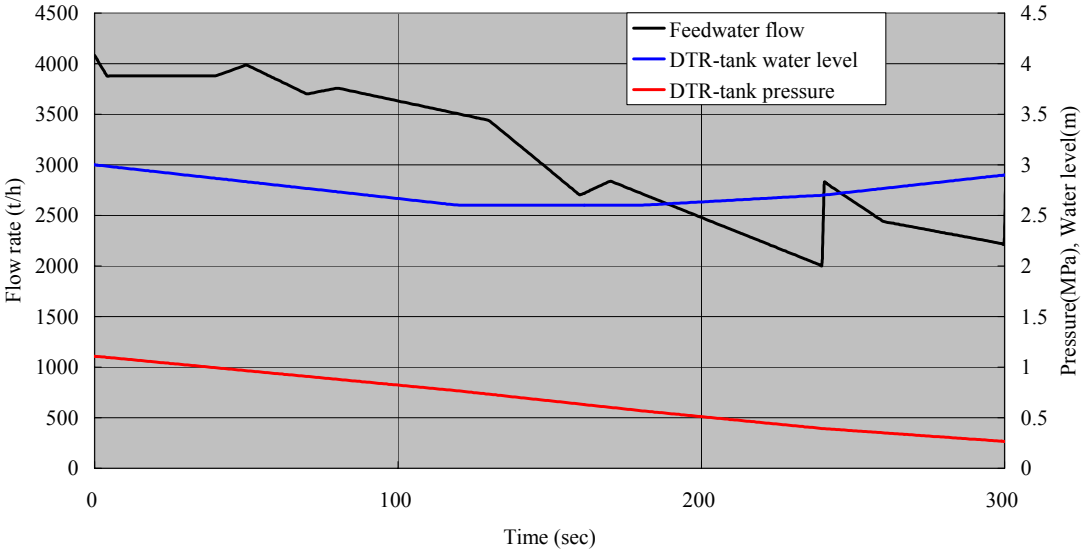

(b) NPSH Simulation of unit A-Caluculated available NPSH and quality of each segment

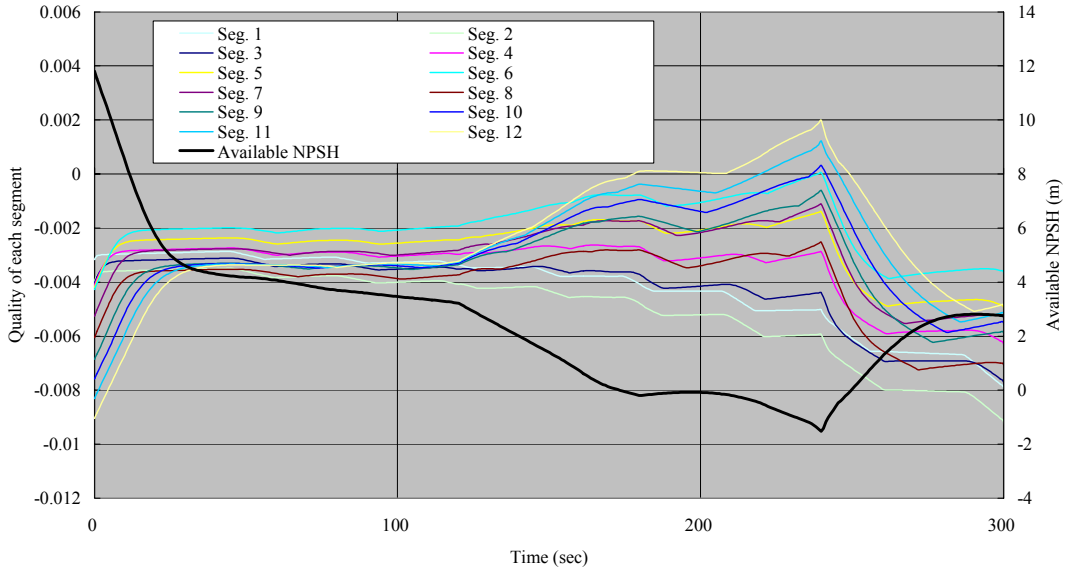

Fig. 4.9 Simulation of unit A

Simulation for unit B

Model of unit B is shown in Fig. 4.10, where the piping and inner volume of FWBP are divided into 11 segments.

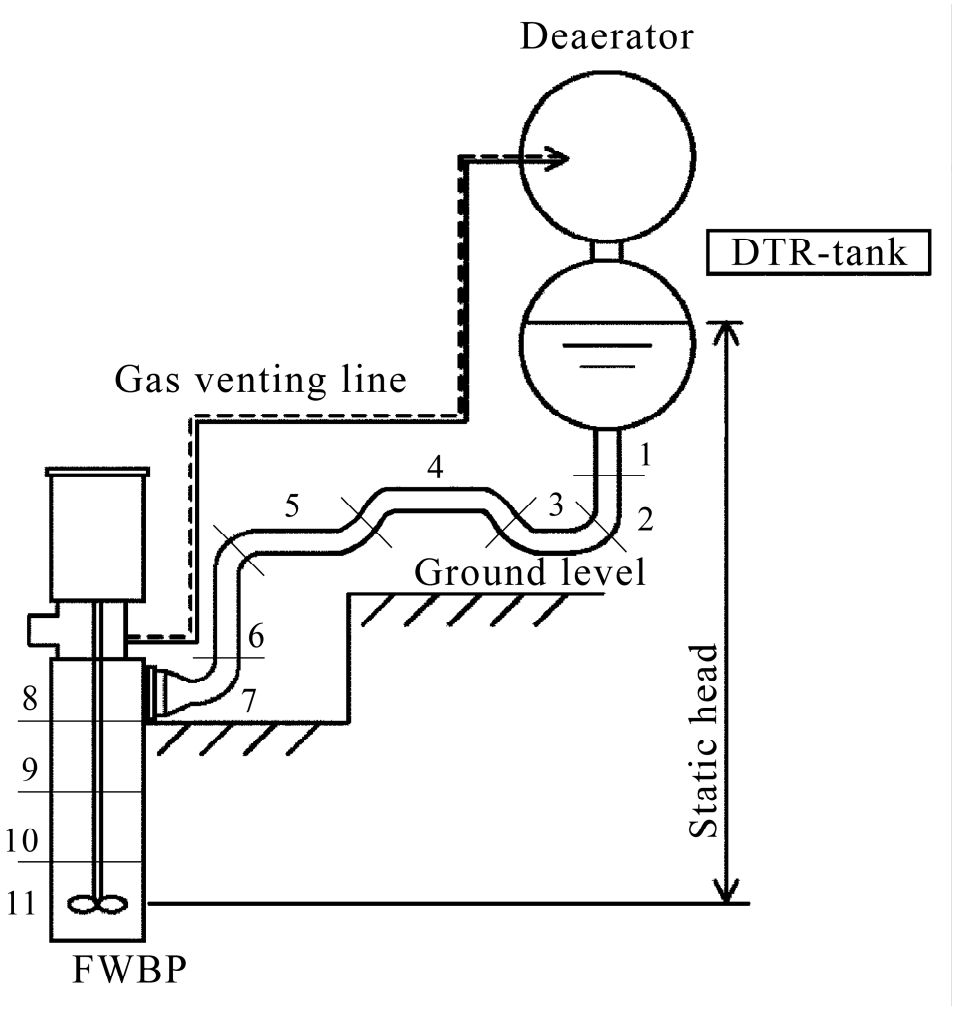

Fig. 4.10 Model of unit B for simulation of $NPSH_{av}$

However, simulation for unit B, presented in Figs. 4.11 (a) ”Prior conditions” (Measured data of feedwater flow, DTR-tank water level and DTR-tank pressure), 4.11 (b) (Calculated available $NPSH_{av}$ and quality of each segment) showed that $NPSH_{av}$ rapidly reduced to about -6 m, indicating the gas quality was positive, generating depressed boiling, throughout the suction line from the FWBP casing to the horizontal piping containing the pocket shaped area (Segment 4), except for the descending line below the DTR-tank (Segment 1,2 and 3). The generated gas rate in the FWBP casing of about 7.0t/h was larger than the venting capacity. Furthermore, the generated gas in the pocket shaped piping, which was not equipped with a venting line, stagnated to plug the piping. Both resulted in FWBP head loss.

(a) NPSH simulation of unit B-Prior conditions

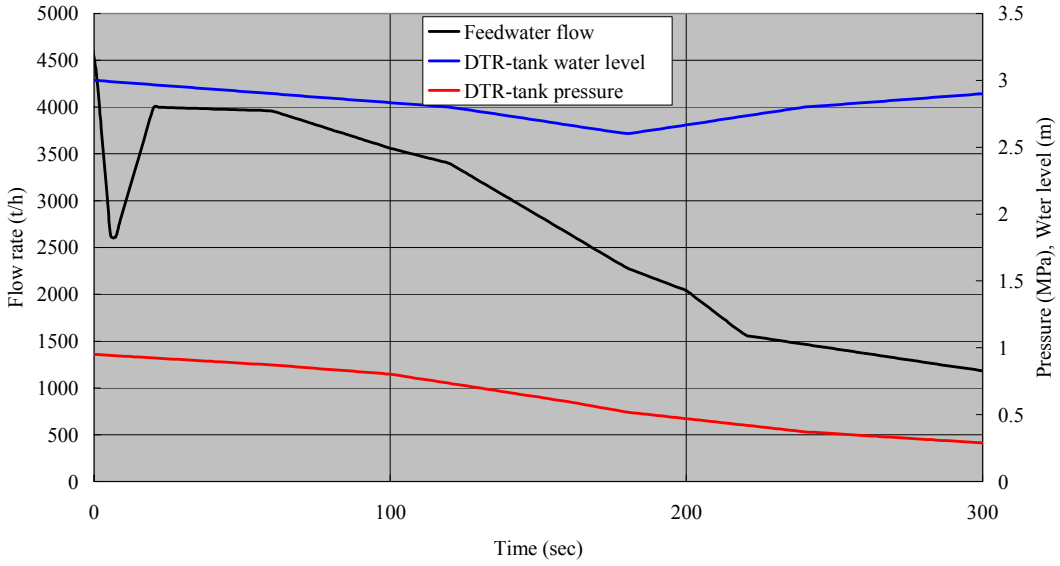

(b) NPSH Simulation of unit B-Caluculated available NPSH and quality of each segment

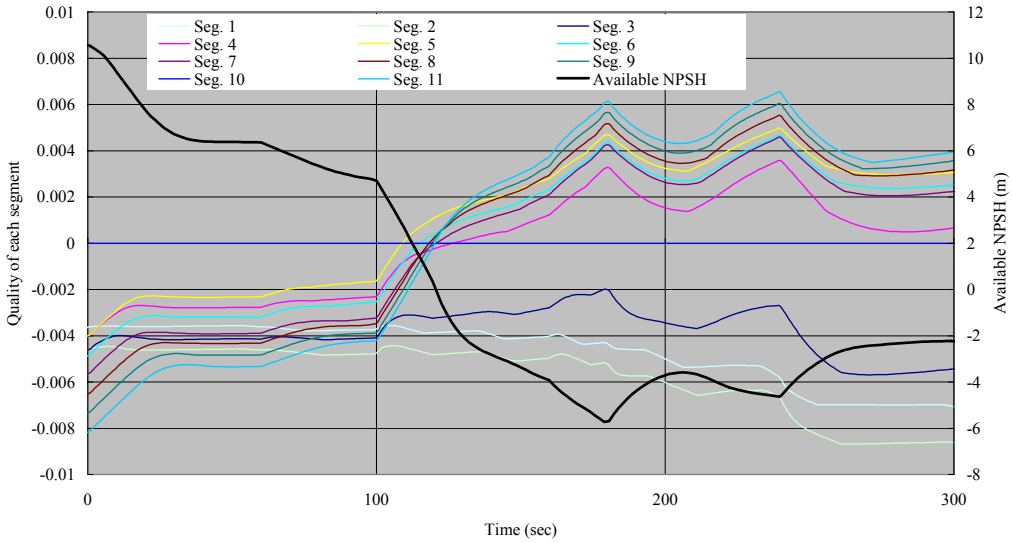

Fig. 4.11 Simulation of unit B

4.2.3 Problem to be solved

Analyses mentioned above demonstrated that unit A-1 and A-2 could only maintain zero $NPSH_{av}$ or saturated water with a small volume of gas, but unit B could neither maintain sufficient $NPSH_{av}$ nor transport feedwater because of plugged gas in the piping.

Therefore, the problem remains as to why zero $NPSH_{av}$ or a saturated condition is sufficient for FWBPs to maintain their head in units A-1 and A-2.

4.3 Required NPSH ($NPSH_{req}$)

Nomenclature

H: Head

η: Efficiency

q: *Flow rate*

$NPSH_{NC}$: NPSH which does not cause head down on condition at room temperature and air saturated.

H_{NC}: Head which is confirmed by available NPSH of $NPSH_{NC.}$

Subscript

0: Numerical value of the rated point

4.3.1 Planning of the study procedure

Dependency of $NPSH_{req}$ on temperature

Dependency of $NPSH_{req}$ on temperature was presented by Stepanoff [5], [6], Ruggeri-Moore [7] and others.

Ruggeri also stated that pump might keep a range of 0.85 to 0.97 head coefficient with $NPSH_{req}$ of nearly zero, may it be a foretelling of negative $NPSH_{req}$.

Inlet gas presence

According to Minemura and others, increase of the ratio up to range of 6 to 7 % reduces head gradually to several percentages and then reduces the head rapidly to zero head within the ratio nearly 10% in case of a centrifugal pump[8].

Planning of the Study Procedure

- The Ruggeri-Moore method taking advantage of the thermal effect of cavitation was utilized here to predict head in higher temperature, using experimental data of the modeled impeller at room temperature and 95˚C.
- The NPSH was defined to be suction head giving 50% of the rated head
- Deaeration was to be evaluated
- Assessment of the data
- The predicted pump head in higher temperature in negative $NPSH_{req}$ region was assessed to be valid on condition of complete gas elimination which means that water at the inlet of impeller was saturation condition.

4.3.2 Experiment of high temperature $NPSH_{req}$

Experiment facility

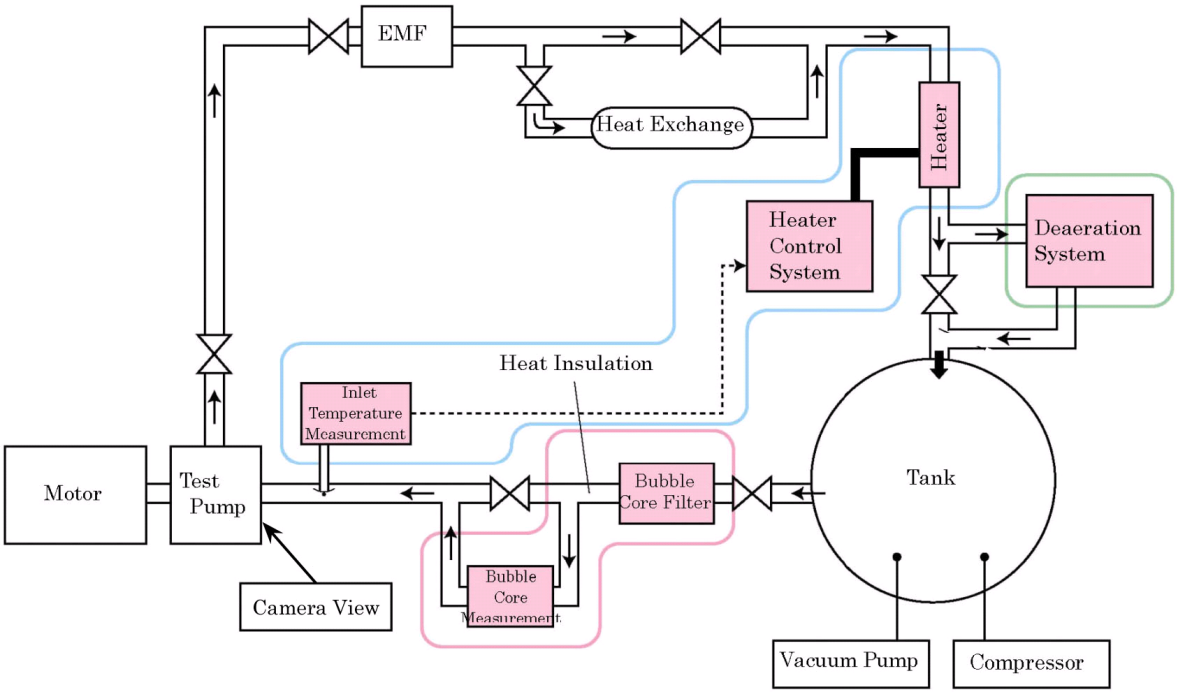

Fig. 4.12 Pump Test Facility

The test facility was equipped with a heating deaerator, feedwater reserve tank pressure controlled by vacuum pump and nitrogen injection, process temperature control system with heat exchangers, electro-magnetic flow element, core bubble filter of 3 micron pore diameter, thermo-couples for measuring the process temperature at the outlet of the model impeller, pressure gage both at the inlet and outlet of the impeller and flow observation window as shown in Fig. 4.12. Process water was used de-ionized water.

Solution air

Dissolved oxygen in actual feedwater is about 2 ppb which occupies less than 10^{-4}% on condition of completely solved out bringing no influence to NPSH. Process water was to be deaerated to about 100 ppb for eliminating influence of solution air to NPSH. Solved air effect for each test case is shown in Table 4.2.

Table 4.2 Solved air effect for each test case

Test case	Actual condition 180˚C	95˚C with deaeration	Room temperature deaeration	Room temperature without deaeration
dissolved gas	2 ppb (oxygen)	100 ppb (air)	100 ppb (air)	8 ppm (air)
Gas to water volume ratio	0.0001%	0.01 %	0.15 %	12 %
Influence to NPSH	Not influenced	Not influenced	Not influenced	Influenced

Model impeller

Fig. 4.13 Model pump impeller

Table 4.3 Specification of model impeller

	Model impeller	Actual impeller
Impeller outer diameter	0.245 m	0.623 m
Rotation speed	41 s^{-1} (2460 rpm)	14.75 s^{-1} (885 rpm)
Flow rate(l/s)	0.0206 (74.13 l/h)	0.122 (439.6 l/h)

Geometrically similar model pump of its scaling ratio of 0.39 is shown in Fig. 4.13 and the specification is described in Table 4.3.

Test condition

The water conditions of the test process were room temperature with saturated air, room temperature deaerated to nearly 100 ppb, high temperature of about 95˚C deaerated to nearly 30 ppb, each with varying flow rate from 40%, 60%, 80%, 100% and over the rated point of 130%, respectively. Test condition is shown in Table 4.4.

Table 4.4 Test condition

Test case	95˚C with deaeration	Room temperature with deaeration	Room temperature without deaeration
dissolved gas	30 ppb (air)	100 ppb (air)	8 ppm (air)
Flow rate (%)	40, 60, 80, 100, 130	40, 60, 80, 100, 130	40, 60, 80, 100, 130

4.3.3 Test results and error assessment

Performance

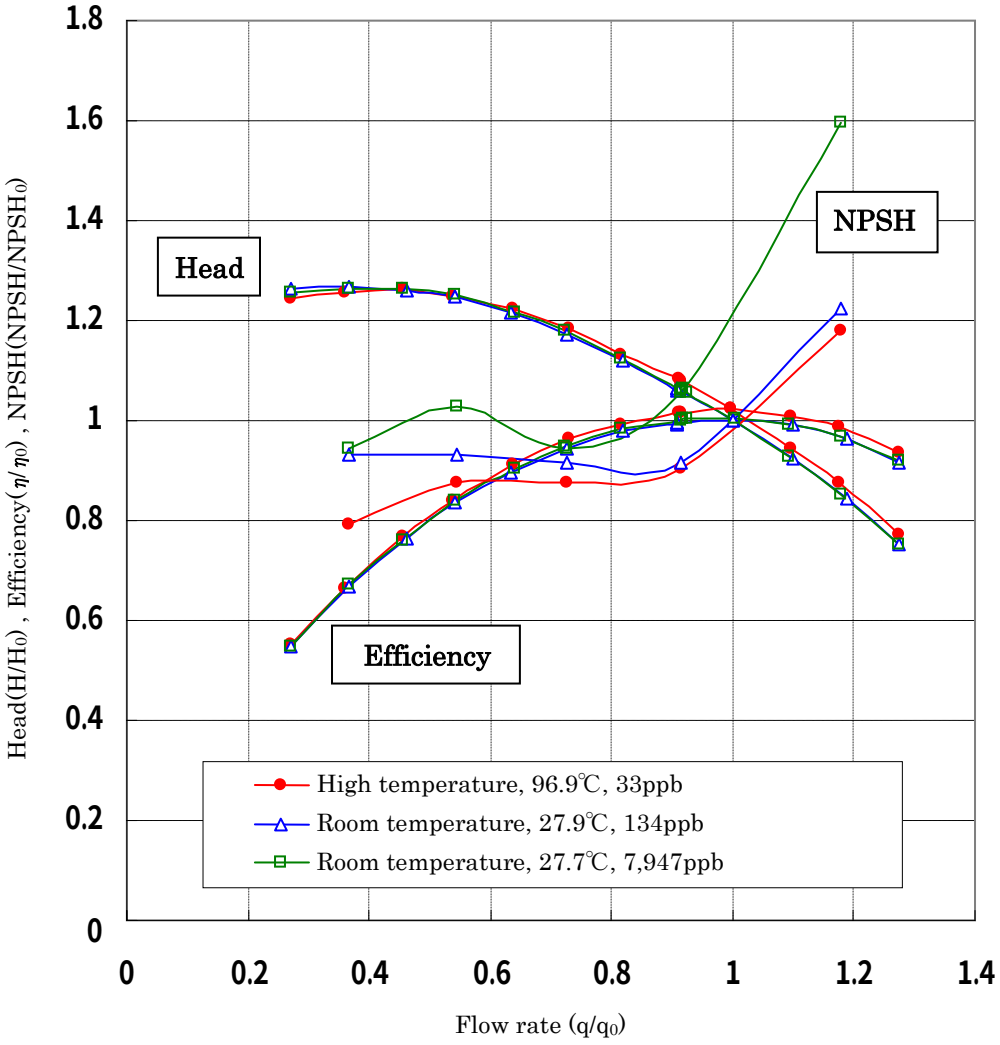

Fig. 4.14 Pump performance on various conditions

Pump performance of head alteration and others for each condition of room temperature with air saturation, room temperature and 96.9˚C both with deaeration is shown in Fig. 4.14. H_0, η_0 and $NPSH_0$ are those of the rated point on condition of room temperature with deaerated.

$NPSH_{req}$ of 100 and 40% flow at room temperature with and without deaeration, and 95˚C

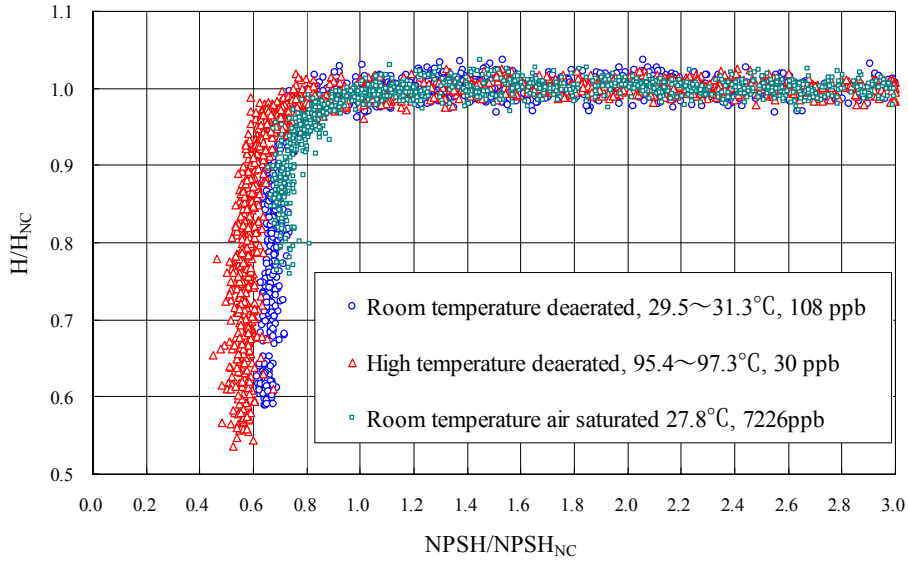

(a) NPSH at 100% flow

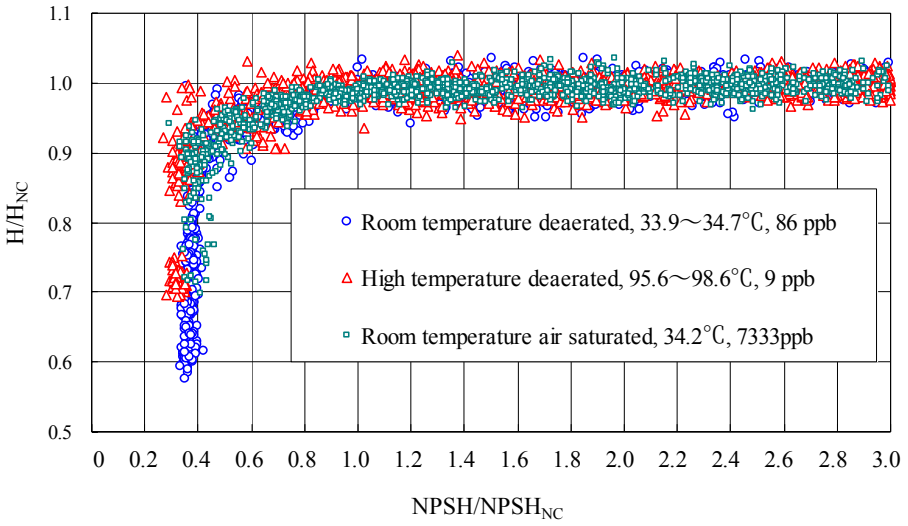

(b) $NPSH_{req}$ at 40% flow

Fig. 4.15 $NPSH_{req}$ of 100% and 40% flow at room temperature with and without deaeration, and 95˚C

Cavitation test data are shown in Fig. 4.15 on the test condition of air saturated room temperature, deaerated room temperature and deaerated 95˚C for the flow rate of 100 and 40% respectively. The NPSH and the head are indicated as NPSH/ $NPSH_{NC}$ and H/H_{NC} respectively.

Both deaeration and temperature increase contributed to reducing $NPSH_{req}$, which was defined as causing 3% head down, by 0.08 with deaeration and by 0.04 with temperature rise to 95˚C, respectively at rated flow, shown in Fig. 4.15(a) as the ratio to $NPSH_{NC}$.

Visual observation

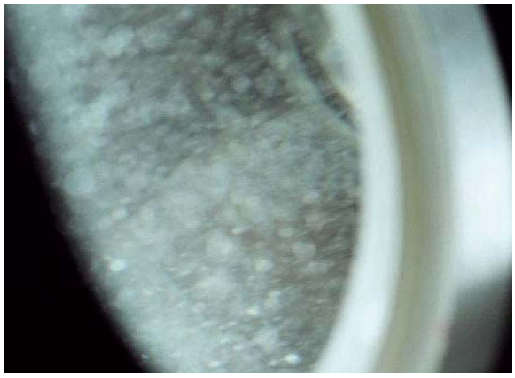

(a) Visualized data at room temperature with saturated air, $NPSH_{av}$ = 7.93 m, rated flow

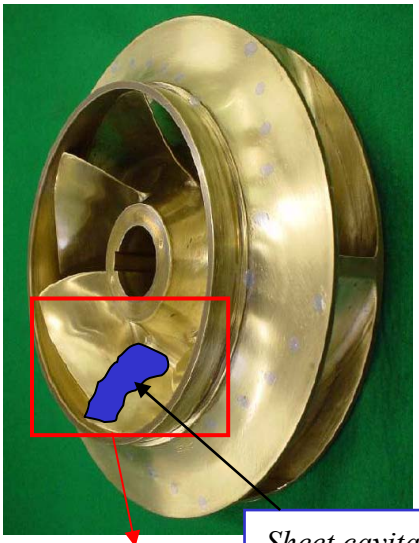

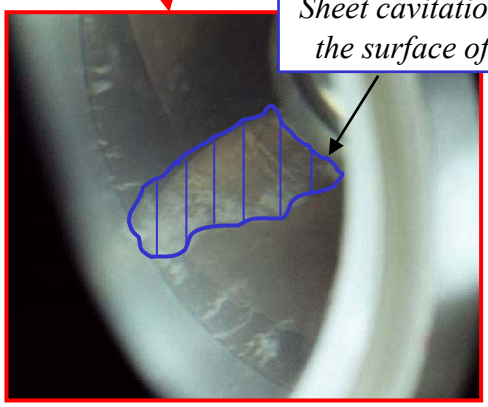

(b) Model impeller and cavitation on impeller at room temperature deaerated to 134 ppb, $NPSH_{av}$ = 7.93 m, rated flow

(c) Cavitation on impeller at 95℃ deaerated to 33 ppb, $NPSH_{av}$ = 8.06 m, rated flow

Fig. 4.16 Model impeller and visualized data for a moment in various conditions with nearly the same $NPSH_{av}$

Visualized data for a moment of each condition with nearly the same $NPSH_{av}$ exhibited cavity air from upper stream piping in the case of room temperature with saturated air, cavity gas of water generated on the surface of impeller in the case of both room temperature deaerated and 95˚C deaerated, shown in Figs. 4.16 (a), 4.16 (b) and 4.16 (c), respectively.

Confident interval and dependency on temperature

Each 99.5% confident interval for both deaerated room temperature and 95˚C of the 100% flow in the range of H/H_{NC} = 0.6 to 0.85, as shown in Fig. 4.17, does not interfere each other, explaining significant difference. This follows the temperature dependency of $NPSH_{req}$.

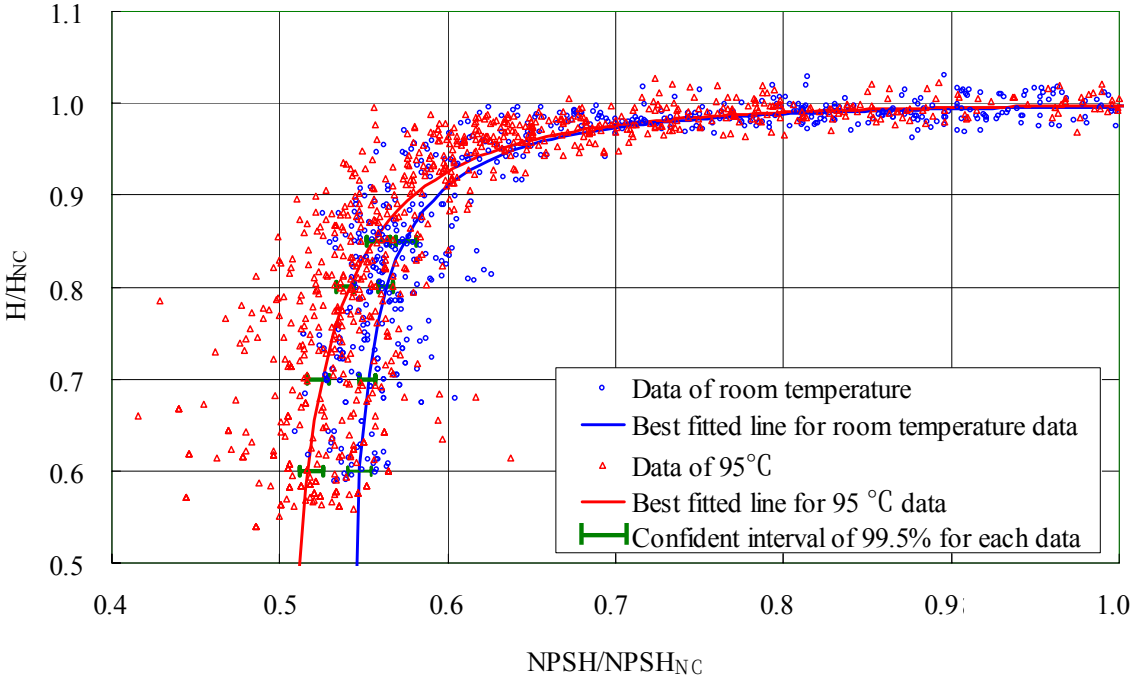

Fig. 4.17 Confident interval of 99.5 % reliability of the rated (100%) flow at room temperature with deaeration, and 95˚C

Error of the instruments

Total error derived from instrument accuracy is following.

The accuracy of thermocouple of JIS class B measuring the process temperature is 0.8 K at 100˚C, which corresponds to 0.29 m of saturation pressure. The accuracy of pressure gage of full scale 0.2 MP with error of 0.5% corresponds to the pressure of 1.0 m Aq.

The total error derived from instrument estimated by RMS is

$$\sqrt{(Thermcouple)^2 + (Pressure\ \ gage)^2} \tag{4.8}$$

$$= \sqrt{0.29^2 + 1.0^2}$$

= 1.04 m

4.3.4 Prediction for high temperature $NPSH_{req}$

Ruggeri prediction

Nomenclature

D: Representative length (m)

L: Latent heat] (kJ/kg)

T: Temperature of free-stream liquid (K)

V_l: Liquid volume concerning evaporation (m^3)

V_v: Gas volume concerning evaporation (m^3)

U: Representative velocity (m/s)

Δx: Cavity length (m)

α: Thermal diffusivity (m^2/s)

ρ: Density (kg/m^3)

cp: Specific heat (kJ/(kg·K))

g: Acceleration of gravity, 9.8 (m/s^2)

h_v: Vapor pressure (m)

Subscript

l: Liquid

v: Vapor

ref: Reference

pred: Prediction

$$\Delta h_v = \frac{1}{g} \cdot \left(\frac{\rho_v}{\rho_l} \right)^2 \cdot \left(\frac{L^2}{c_{pl} T} \right) \cdot \left(\frac{V_v}{V_l} \right) \tag{4.9}$$

$$\left(\frac{V_v}{V_l} \right)_{pred} = \left(\frac{V_v}{V_l} \right)_{ref} \cdot \left(\frac{\alpha_{ref}}{\alpha} \right)^{1.0} \cdot \left(\frac{U_0}{U_{0,ref}} \right)^{0.8} \cdot \left(\frac{D}{D_{ref}} \right)^{0.2} \cdot \left(\frac{\Delta x / D}{(\Delta x / D)_{ref}} \right)^{0.3} \tag{4.10}$$

$$\Delta h_v = \frac{\rho_v}{\rho_l} \cdot \frac{V_v}{V_l} \cdot \frac{L}{c_{pl}} \cdot \left(\frac{dh_v}{dT} \right) \tag{4.11}$$

Higher temperature $NPSH_{req}$ derived from gas occupation and plugging in the passage between blades by ingenerated gas on the blade surface was evaluated by applying the Ruggeri-Moore method using data of the above test, and summarized as follows. A certain amount of bulk water adjacent to the cavity is deprived of its heat by latent heat for the ingenerating cavity. Reduction of vapor pressure Δh_v of the bulk water corresponding to temperature reduction is shown in Eq. (4.9). Gas to liquid volume ratio of V_v/V_l, which concerns evaporation, is evaluated from experimental Eq. (4.10), showing the relation between the two conditions, because the ratio could not be measured directly. $(\Delta h_v)_{ref}$ and $(\Delta h_v)_{pred}$ are calculated for room temperature and 95˚C respectively, by the heat relation in Eq. (4.11) for an assumed $(V_v/V_l)_{ref}$ and corresponding $(V_v/V_l)_{pred}$ derived from Eq. (4.10). The $(V_v/V_l)_{ref}$ which gives good agreement between the calculated and experimented results of $(\Delta h_v)_{ref} - (\Delta h_v)_{pred}$ leads, by Eq. (4.10), to $(V_v/V_l)_{pred}$ for any temperature and rotative speed, as long as both flow coefficient and head coefficient are equivalent in the scaled pump. The $(V_v/V_l)_{pred}$ ingenerates the delta saturation pressure Δh_v or reduction of $NPSH_{req}$ using Eq.(4.9).

Cavity length

Cavity length in the Eq. (4.10) was regarded as constant in the prediction for higher temperature NPSH because the prediction manner was to calculate the $NPSH_{req}$ which gave both the same head coefficient and the same flow coefficient as of the referenced two temperature conditions, where the flow pattern between the impellers was identical implying the cavity length was constant through the temperature conditions from the referenced ones to the predicted.

Prediction for high temperature $NPSH_{req}$ of 180˚C at rated flow

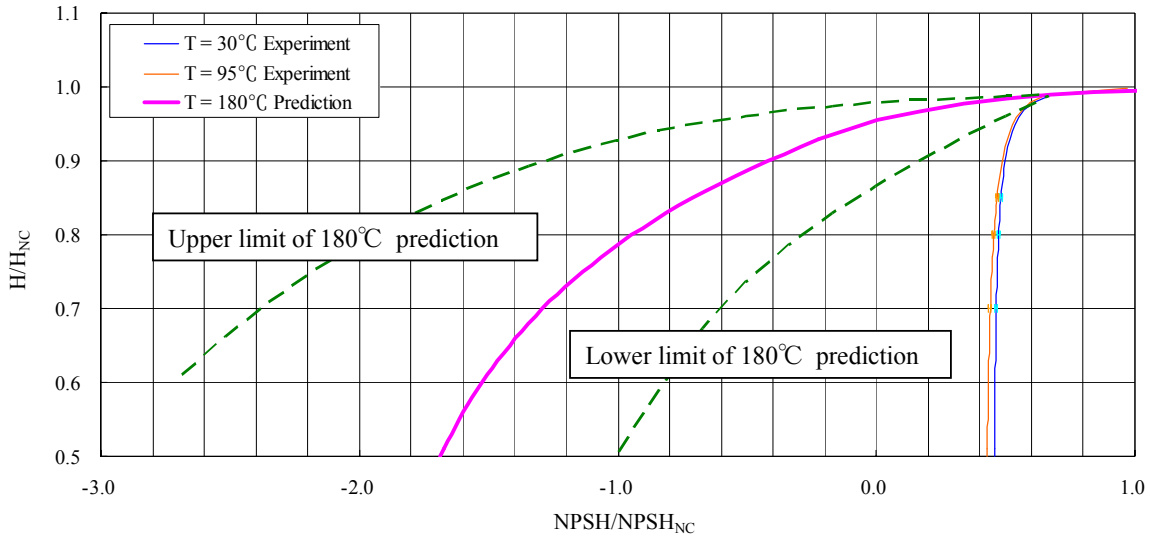

Fig. 4.18 Prediction of 180˚C and confident interval at rated flow (100%)

$NPSH_{req}$ in the highest temperature in actual unit of 180˚C, which is the steady condition of turbine rated power, was predicted by Ruggeri method shown in Fig. 4.18, using each H/H_{NC} of 0.6, 0.7, 0.8 and 0.85 of deaerated room temperature and 95˚C data of Fig. 4.17.

Confident interval of the predicted $NPSH_{req}$ is calculated using the upper and lower limit of the 99.5% confident interval of the room temperature and 95˚C in a following manner resulting in 99.0% interval.

The upper limit is the predicted one using the largest difference between the lower limit of the room temperature and upper limit of the 95˚C. The lower limit is the predicted one using the smallest difference between upper limit of the room temperature and the lower limit of the 95˚C. The predicted 180˚C NPSH are -0.7 for H/H_{NC} of 0.85 with the confident interval between -1.7 and -0.1, -1.3 for H/H_{NC} of 0.7 with the confident interval between -2.4 to -0.6.

The instrument error does not affect the prediction because the prediction is based on the difference of the measured values by same instrument stated Section 4.3.3.

Prediction for high temperature $NPSH_{req}$ of 151.3˚ at 40% flow

The prediction of high temperature $NPSH_{req}$ at 151.3˚C of 40% flow, with confident interval of 99.0% and experimental data of room temperature and 95˚C are shown in Fig. 4.19.

This figure explains that the predicted $NPSH_{req}$ is negative figure contributing to the integrated configuration as shown in Fig. 4.20.

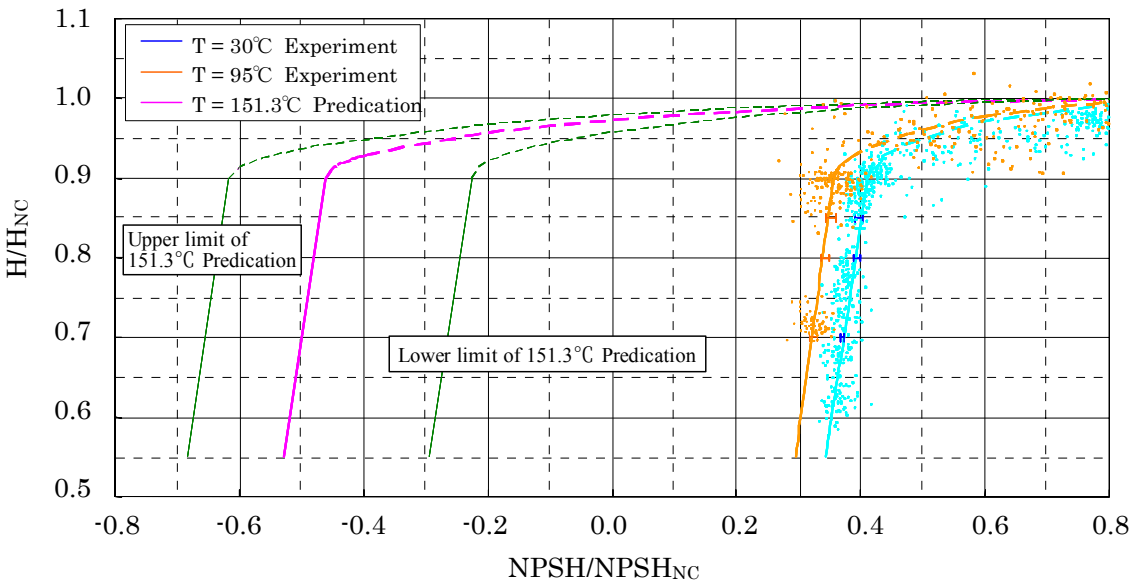

Fig. 4.19 Prediction of 151.3˚C at 40% flow and confident interval

4.4 Configuration of high temperature NPSH

4.4.1 Extension of Ruggeri-Moore method to negative area

Ruggeri method

High temperature NPSH predicted by the Ruggeri-Moore method is the $NPSH_{req}$ derived from gas occupation and plugging in the passage between blades by ingenerated gas on the blade surface, using the experimental data of two different conditions of positive pressure at the impeller inlet. The method is applicable in the area where positive pressure at the impeller inlet is assured to maintain the same flow pattern as that of the reference experiments.

Extension of Ruggeri method

The Ruggeri-Moore method may be applicable even in the area where $NPSH_{req}$ is a negative figure on condition that boiling gas at impeller inlet is vented out of the system because the residual feedwater is maintained in the saturation condition and gives the same flow pattern as that requested from the method.

Boiling gas venting capability depends on feedwater velocity and arrangement of the suction piping, as well as the pressure difference in driving.

Influence of gas presence at impeller inlet

In contrast, according to $NPSH_{av}$ reduction to a negative value, the gas volume ratio to gas-water mixture at the impeller inlet increases sufficiently to affect the pump head. According to Minemura and others, increase of the ratio up to 6 to 7% reduces head gradually to several percent and then reduces the head rapidly to zero head within the ratio nearly 10% in case of a centrifugal pump[(6)]. The gas to gas-water mixture volume ratio of 5% corresponds to that in condition of -0.125 m of the $NPSH_{av}$ at 151.3˚C, resulting in another $NPSH_{req}$.

4.4.2 Integrated configuration of high temperature NPSH

Integrated configuration of high temperature NPSH presented here is the combined one with the prediction of the Ruggeri-Moore method extended to the negative area on condition of gas venting and the restriction from the impeller inlet gas presence.

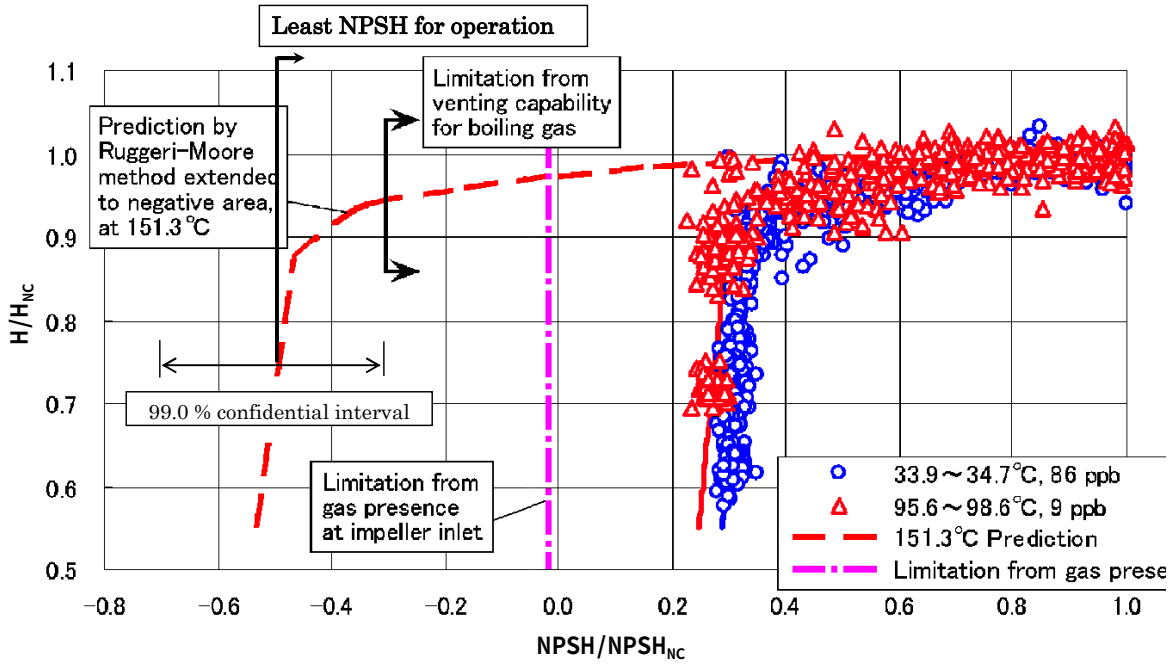

Fig. 4.20 Integrated high temperature NPSH configuration, 151.3˚C, 40 % rated flow of unit A

High temperature NPSH of 151.3˚C at 40% flow rate in unit A

Figure 4.20 is the illustration of required NPSH on the condition of 151.3˚C at 40% flow rate of units A-1 and A-2 where $NPSH_{av}$ of FWBP became minimal through the transition after 240 sec from load rejection described in Section 4.2.2, Fig.4.9. X-axis is NPSH normalized by $NPSH_{NC}$ which does not affect the head on condition of room temperature and saturation air. Y-axis is pump head normalized by H_{NC} which is pump head with sufficient $NPSH_{av}$. The High temperature NPSH of 151.3˚C at 40% flow rate, as shown in red dashed line, was predicted by Ruggeri method using the attained data of experiments on condition of room temperature with deaeration and 95˚C, shown in blue circles and in red tri-angles, respectively. Confidential interval of the prediction is from -0.7 $NPSH/NPSH_{NC}$ to -0.3 $NPSH/NPSH_{NC}$.

Integrated configuration

The figure shows that minimum $NPSH_{req}$ which maintains nearly half of the rated head on condition of gas venting is -0.5 $NPSH/NPSH_{NC}$, illustrated as "Least NPSH for operation ". 0n condition without gas venting, the allowable minimum NPSH is -0.025 $NPSH/NPSH_{NC}$ which corresponds to 5% volumetric ratio at the inlet of the impeller, illustrated in red dot dashed line as "Limitation from gas presence at impeller inlet". The venting capability of more than 3.0 t/h, described in Section 4.2.2, is -0.3 $NPSH/NPSH_{NC}$ for units A-1 and A-2, illustrated in the figure as "Limitation from venting capability for boiling gas".

Verification of operability of unit A

Simulation resulted in the minimum value of available NPSH for unit A through the transient is -1.4 m described

in Section 4.2.2, corresponding to -0.2 8 NPSH/$NPSH_{NC}$ which is in a rage of gas venting of the unit. Thus the operability of unit A is verified on the assumption of gas exhaust at the impeller inlet.

Application of the configuration

The configuration enables the operation in higher temperature with insufficient $NPSH_{av}$ by exhausting the generating gas, and contributes to the simplicity and reliability of the feedwater system by distribution of DTR-tank to ground level, higher rotation speed smaller pump and others.

4.4.3 Overview of the system on the condition of insufficient NPSH for FWBP

Feedwater system behavior is overviewed here on the condition of insufficient NPSH for FWBP at load rejection. System loss curve and head of FWP is shown in Fig. 4.21.

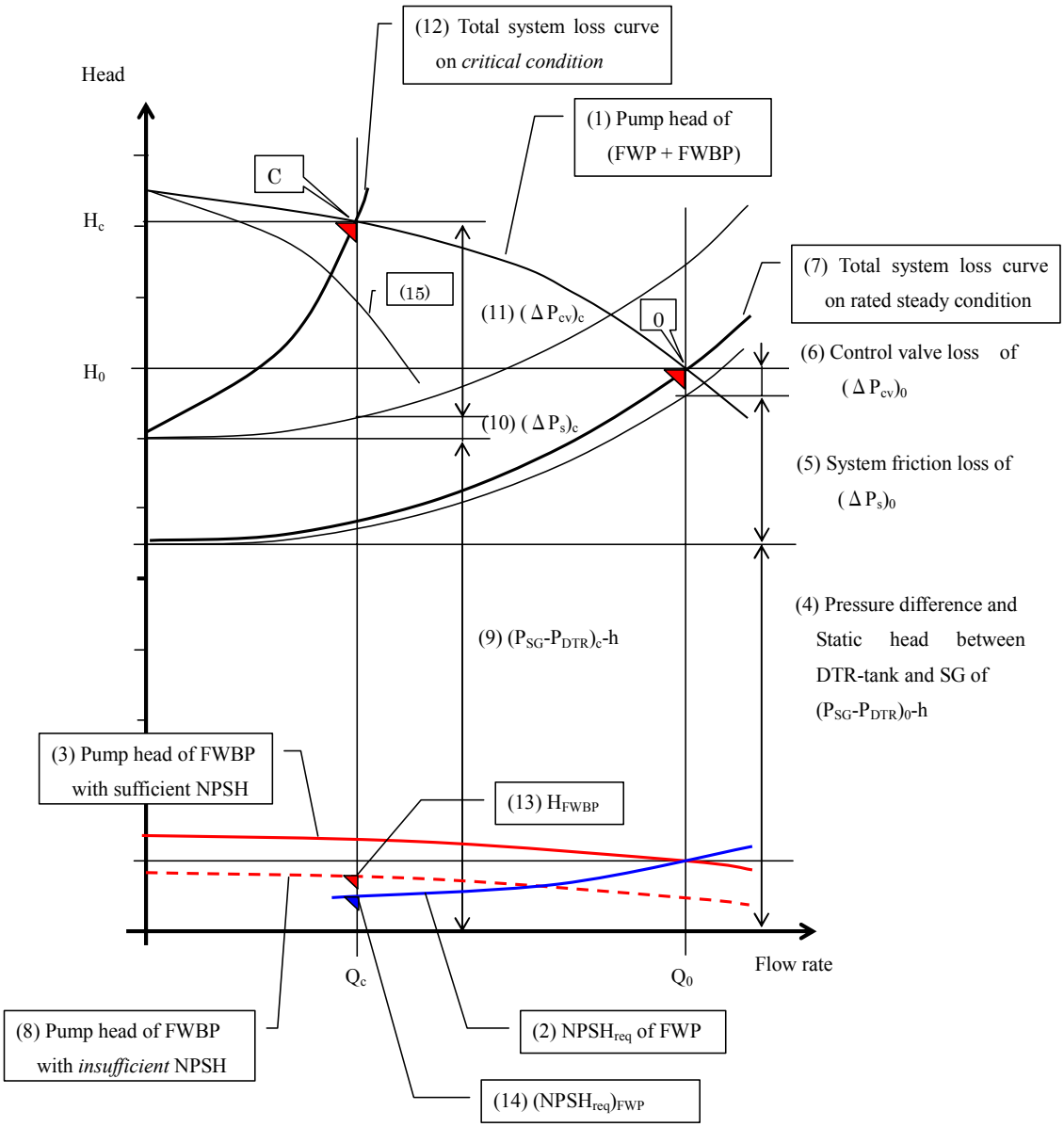

Fig. 4.21 System loss curve and head of FWP

Nomenclature

P_{SG}: Pressure of SG

P_{DTR}: Pressure of DTR-tank

h: Static head between DTR-tank water level to SG water level

ΔP_s: System (friction) loss of feedwater containing HP-FWH, piping and feedwater control valve.

ΔP_{cv}: Control valve loss

Q: Flow rate

H: Head of pump

Subscript

0: Rated steady condition

C: Critical condition where available NPSH for FWBP is least through the transient

Turbine system (Refer to Section 4.1.1)

Turbine load reduces suddenly from full power to house load of about 5 % at load rejection. In turbine system, both GV and ICV close rapidly to suppress the over speed of turbine.

DTR-tank pressure and its saturation condition temperature, about 1 MPa and 180°C, respectively, at full load or initial transition value, begin to reduce both by loss of its heating steam from turbine extraction, derived from a turbine casing pressure decrease, and by the continuation of colder condensate flow-in from the condenser to maintain the DTR-tank level via LP-FWHs, for which the heating extraction steam has also failed. More than a half of the rated feedwater is continuously requested for about 3 to 4 minutes after the load rejection for reactor cooling.

Feedwater system

Feedwater system operating condition at the load reduction is as followings.

Total feedwater pump head, which is the summation of FWP and FWBP, is shown as " (1) Pump head of (FWP + FWBP). Required NPSH of FWP and head of FWBP is shown "(2) $NPSH_{req}$ of FWP" and "(3) Pump head of FWBP with sufficient NPSH", respectively. Head of FWBP is selected to satisfy the required NPSH of FWP at the rated flow.

Feedwater pump operation point at turbine rated steady condition is "0" where the feedwater flow rate is 100% and the pump head is the summation of "(4) Pressure difference and static head between DTR-tank and SG of $(P_{SG} - P_{DTR})_o$-h", "(5) System friction loss of $(\Delta P_s)_0$" and "(6) Control valve loss of $(\Delta P_{cv})_0$".

The critical condition for NPSH of FWBP ingenerates in a few minutes after beginning of the load rejection, where the pressure of DTR-tank is reduced to nearly half of the rated and the pressure of SG is raised due to the close of GV and succeeding steam dump to condenser of 40% rated flow. The operation point of FWP at the critical condition is "C", where the flow rate is 40% in case of unit A and the pump head is the summation of increased pressure difference and static head between DTR-tank and SG of "(9) $(P_{SG} - P_{DTR})_c$-h", decreased system friction loss of "(10) $(\Delta P_s)_c$" and increased control valve loss of " $(\Delta P_{cv})_c$".

Pump head of FWBP at 151.3 ˚C for unit A, is predicted as "(8) Pump head of FWBP with insufficient NPSH", which is higher than half that with sufficient NPSH.

Feedwater pump is operated at point "C" with available NPSH by FWBP of point "H_{FWBP}" which is higher than the required NPSH "$(NPSH_{req})_{FWP}$" of FWP. The required NPSH of FWP here is not modified with temperature dependency and may it be lower than the plotted giving more margin.

NPSH both of FWBP and FWP

Pressure drop caused by turning and velocity increase at impeller inlet reduces static pressure. Cavitation begins to arise caused by the reduction of static pressure along with the reduction of $NPSH_{av}$, but does not affects the pump head. Numerical value of $NPSH_{av}$ which causes the head down by 3%, in a manner occupying the passage between impellers with ingenerated cavitation gas, is NPSH generally used in industries. The required NPSH here is defined as numerical value of $NPSH_{av}$ which causes head down to 50% of the rated. The reason is that the required NPSH of FWP, which is the required head for FWBP, is less than half that of the rated flow at the discussion condition of 40 % flow rate.

FWBP

The minimum numerical value of $NPSH_{av}$ is estimated to be negative of -0.28 $NPSH/NPSH_{NC,}$ where the generated gas could be exhausted out of the system by venting line but a part of the gas would be pulled into the pump. The head of FWBP was kept at least 50% of the rated on condition that the gas presence at the impeller inlet was less than 5% volume ratio, despite association with cavitation in the passage between impellers.

Behavior considering the generated gas in the lower half suction is described later.

FWP

FWP head was kept with sufficient suction head by FWBP because the required NPSH of FWP was half that of the FWBP rated head in the discussed condition flow rate 40%.

Steam generator

The generating steam in SG was dumped to condenser, for cooling of the primary system, with turbine bypass line due to the closure of GV. The water level of SG declines by the clash of bubble caused by the pressure rise. Feedwater is required for 10 to 15 minute until the stationary of the reactor, but the condition with insufficient $NPSH_{av}$ for FWBP dose not continue more than a few minutes because of opening the minimum flow line which functions when the suction flow reduces less than 40%.

Reliability for possible damage by the cavitation

Continuation of insufficient NPSH operation is in several minutes which would be small enough to cavitation damage which arises in several hundred hour operation.

Gas exhaust at the impeller considering the lower half suction

Nomenclature

U_c: Feeding flow rate by upper half impeller of the first stage of the FWBP during the lack of $NPSH_{av}$ transient

L_c: Feeding flow rate by upper half impeller of the first stage of the FWBP during the lack of $NPSH_{av}$ transient

The construction of the FWBP is double suction type impeller of first stage and single suction of second stage, as shown in Fig. 4.7. The minimum area for the lower side impeller is 0.57 m^2, apparent liquid velocity of where is slightly smaller than 0.3 m/s at the time of minimum $NPSH_{av}$. It is difficult for gas, except for single-gas, to rise against the down stream velocity.

Ingenerating gas around the upper suction can easily be exhausted because feedwater for upper-side-suction

impeller of the first stage is suctioned freely via wide space between the connection pipes of feeding for the second stage.

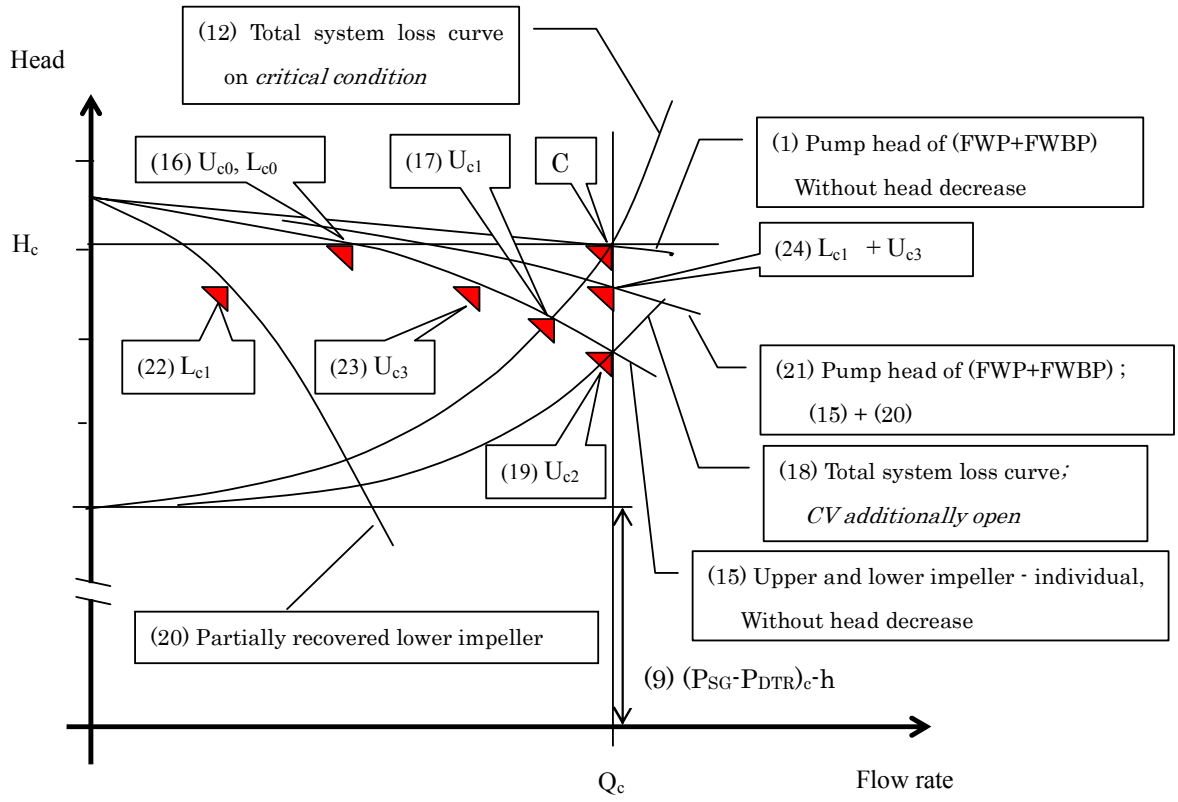

Fig. 4.22 Feedwater operating point and system loss curve at the time of minimum $NPSH_{av}$

Feedwater operating point and system loss curve at the time of minimum $NPSH_{av}$ is shown in Fig. 4.22, which is the enlarged drawing of Fig. 4.21 for the area of the critical operating point.

Pump head curve of upper half impeller and lower half impeller, assuming that the double flow impeller is divided into 2 individual impellers, is indicated as "(15) Upper and lower impeller-individual, Without head decrease". The divided each pump is operated at the point of "(16) U_{c0}, L_{c0}" feeding a half of the feedwater, respectively.

The lower impeller pump looses its head when depressed boiling gas ingenerating at the inlet of lower impeller is not exhausted. The remained upper half impeller moves to the operating point of "(17) U_{c1}", attributing to the pump head curve and system loss curve, soon after the loss of lower half impeller head. Then it moves to "(19) U_{c2}" because the system loss curve descend gradually to "(18) Total system loss curve; *CV additionally open*" according to short of feedwater by opening the feedwater-control valve which controls the water level of SG.

The flow rate at the point of (19) is 80% of the rated because the rate is 40% at the point of (16) for the upper and lower impeller, respectively. High temperature NPSH prediction of 151.3˚C at 80% flow is shown in Fig.

4.23, which explains that the $NPSH_{req}$ is -0.28 NPSH/$NPSH_{NC}$. The $NPSH_{av}$ is also -0.28 NPSH/$NPSH_{NC}$ as described in Section 4.4.2. The impeller is able to operate because $NPSH_{av}$ is equal to $NPSH_{req}$ at this (19) point.

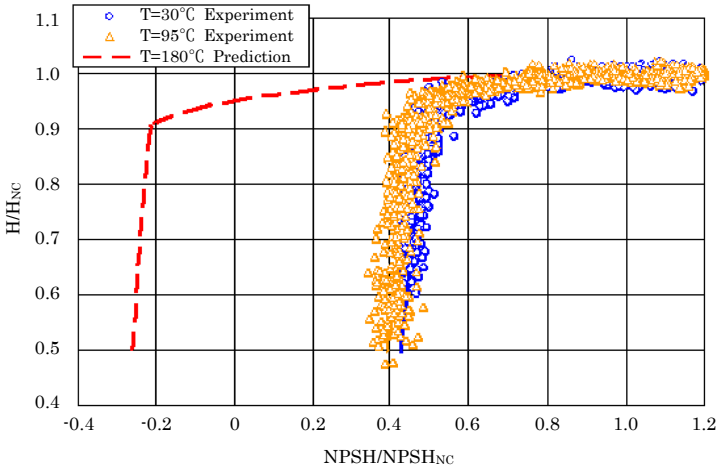

Fig. 4.23 High temperature NPSH prediction of 151.3˚C at 80% flow

The depressed boiling gas would begin to rise through the minimum area and be exhausted when the lower impeller pump ceases feeding water, due to loss of down comer velocity. Then the lower impeller pump recovers the head for example to the curve (20), which synthesizes the head curve of "(21) Pump head of (FWP +FWBP); (15) + (20)" with remained upper impeller head of (15). Lower and upper impeller operates at "(22) L_{c1}" and "(23) U_{c3}", respectively, keeping the operating point of "(24) L_{c1} + U_{c3}".

Upper impeller operates between "(16) U_{c0}" and "(19) U_{c2} ", lower impeller operates between zero flow to "(22) L_{c1}". The flow rate of L_{c1} could not be defined, but the combined upper and lower impeller sustains nearly the designed head and keeps the feedwater with support of feedwater control valve opening.

The behavior of the pump is estimated to repeat above for about 1 minute when the $NPSH_{av}$ is negative value.

4.5 A design theory of high temperature NSPH

A design theory of high temperature NPSH in the case of PWR turbine unit FWBP is stated followings. This theory could be applied for other pump systems operating on condition of high temperature.

4.5.1 NPSH

$NPSH_{req}$

Pump required NPSH of high temperature is to be estimated by Ruggeri-Moore method using experimented data of cavitation test, the sample of which is shown in Fig. 4.15, conducted at room and practicable higher temperatures by proper test facility with enough deaeration to about 100ppb. The data on condition of air saturation at room temperature could not be used for the prediction because *the prediction* contains not only the effect of temperature but also the effect of dissolved air.

The integrated high temperature NPSH configuration, the sample of which is shown in Fig. 4.20, is to be constructed. Because the predicted high temperature $NPSH_{req}$ in negative area is a hypothetical field to put the whole picture together throughout the alternation of $NPSH_{av}$ from positive to negative, it could be available on condition exhaust of gas corresponding the negative figure of NPSH, at the impeller inlet except for the allowable residual gas of about 5 % volume ratio to water.

From the designer's point of view, it is advantageous that there is no need to have the precise $NPSH_{req}$ value in negative area but only to have a conviction that the value is negative, because the system is popularly furnished venting system which would satisfy the gas venting requirement. This means that there is no need of design margin.

DTR-tank capacity and suction pipe

DTR-tank capacity is generally selected as that corresponding to 4 to 5 minutes of feedwater for the rated operating pressure of 1.0 to 1.3 MPa, based on not only $NPSH_{av}$ but also stability of feedwater. Lower rated pressure would cause the smaller tank capacity, despite the adverse effect for turbine heat rate due to lower heat injection point by FWP.

Suction pipe line is designed both as short and strait as possible in allowable range from thermal stress, and to have a small decline of 5/100 to the pump to transport saturation water, which also is effective for the possible generated gas to break away upward from the very small vertical component speed of feedwater. The velocity of the feedwater is selected as up to 3.0 m/s in current design.

Gas venting line is necessary for the top of pump casing and preferable for the equipment installed midstream of the piping for example of strainer casing.

$NPSH_{av}$

$NPSH_{av}$ is calculated by time-history analysis throughout the transient based on the pump impeller inlet physical value of enthalpy, pressure, void fraction as the case may be and temperature by the algorithm described in Section 4.2.1.

$NPSH_{av}$ is to be kept larger than the $NPSH_{req}$ through out the transient which is stated in Section 4.4.2 by furnishing enough capacity of venting to exhaust the possible gas. Adoption of so called NPSH-controller stated later would contribute to increase $NPSH_{av}$ without excessively high static head.

4.5.2 NPSH controller

Concept of NPSH controller

DTR pressure reduction is caused both by loss of its heating steam from turbine extraction and the continuation of colder condensate flow-in from the condenser to maintain the DTR-tank level during the transient of load rejection. NPSH controller is the system to increase $NPSH_{av}$ through out the transient as stated followings.

(1) Mitigating the DTR-tank pressure reduction rate by *suppressing the cold condensate flow* rate into the tank by reducing the condensate flow rate nearly to half of the rated initial one through the transient until the reduction of $NPSH_{av}$ ceases. The tank level control is changed to the program control, by the initiation of the transient, to reduce the condensate flow to the minimum rate to keep the low water level of the tank through the transient. This method is expected for the improvement of $NPSH_{av}$ up to 3 to 4m.

(2) Mitigating the DTR-tank pressure reduction rate by supplying available steam to the DTR-tank with pressure control for prohibiting from the over pressure. The available steam is inevitably the main steam due to loss of all the available extraction steam of the turbine. The main steam is to be supplied to the turbine extraction line for confirm the condensing by mixing with condensate flow to prohibit from the over pressure despite the pressure control. This method is expected for the improvement of $NPSH_{av}$ up to 1m.

Supplying available steam to the LP-FWHs to prohibit the flow-in condensate from temperature reduction is a preferable alternative though it was not proven in actual unit.

(3) Opening the minimum flow line to shorten the retention time of the feedwater for reducing the temperature difference between the DTR-tank and FWBP impeller. The retention is the time for the feedwater of DTR-tank to reach the FWBP impeller. This method is expected for the improvement of $NPSH_{av}$ up to 1m because its applicable time period is rather small prohibiting the over flow rate of pump suction.

Prevailing NPSH controller

Prevailing method is applying only the *suppressing the cold condensate flow* rate for its advantage of both improvement value and simplicity comparing to the others as shown its concept flow diagram in Fig. 4.24 and behavior of process parameters in Fig. 4.25.

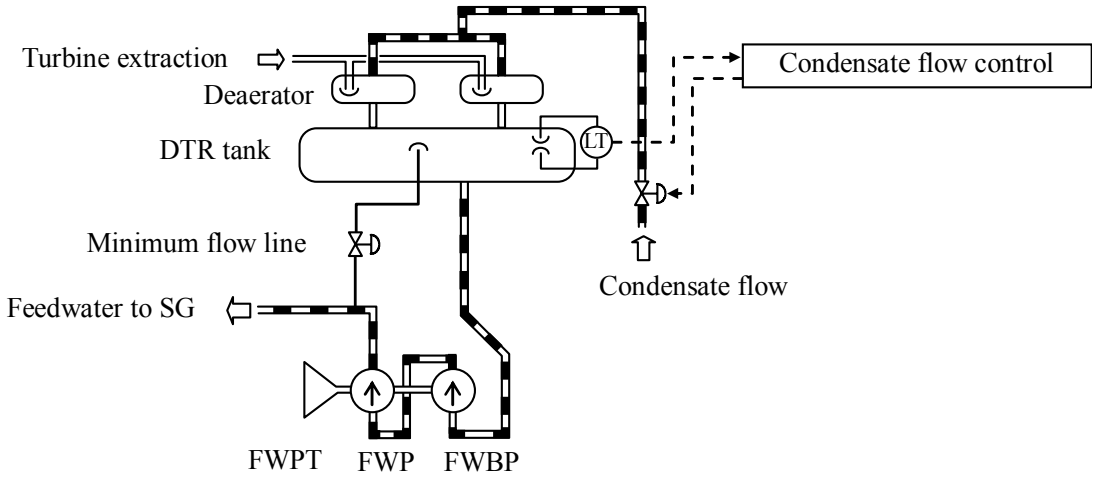

Fig. 4.24 Prevailing NPSH controller concept flow diagram (*Suppressing the cold condensate flow rate*)

Behavior of process parameters is following.

(1) The generating power is reduced suddenly to the house load of 5% from the rated at the load rejection, but the feedwater requirement continues for several minutes keeping the flow rate corresponding not to the generating power but to cooling the primary cycle. The load rejection is detected by the high pressure turbine first stage blade pressure reduction.

(2) The condensate flow is controlled to reduce to nearly a half of the rated contributing to the mitigation of DTR pressure reduction rate associated with the water level reduction of the tank. $NPSH_{av}$ reduces for the first time then recovers gradually by the mitigation of the tank pressure reduction rate. The alteration of $NPSH_{av}$ through the transition, on the condition of program controlled condensate flow rate, is to be calculated by time historical simulation program for the selected DTR-tank capacity, static head and $NPSH_{req}$ to both maintain the enough $NPSH_{av}$ and to meet other limitations from the tank low water level.

(3) The system is serviced out which ever the tank level reach the tank low water level or the end of the transient recovering the tank water level to the normal water level gradually.

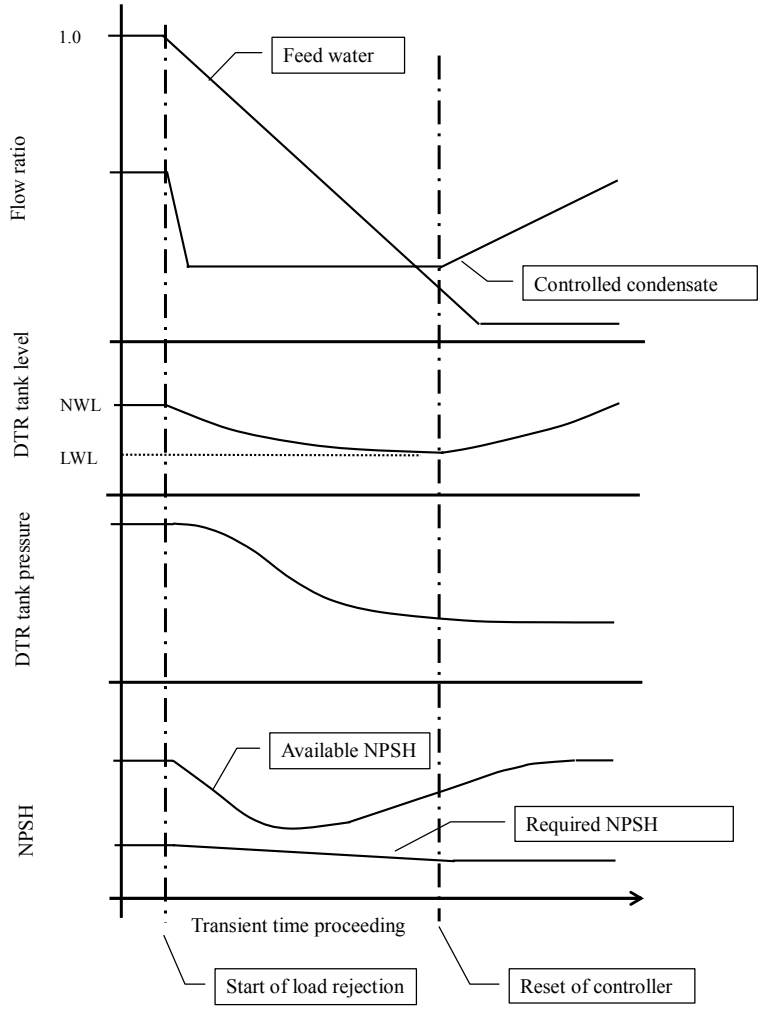

Fig. 4.25 Transient behavior with NPSH controller

4.5.3 Effect of high temperature NPSH design

Effect of high temperature NPSH design is verified by evaluating the unit A-1 and 2, NPSH of which was secured in actual operation and the mechanism was cleared, in the current design as followings.

The minimum $NPSH_{av}$ of Unit A is -1.4 m with static head of 11.7 m. Current design method is that $NPSH_{req}$ is the measured value on condition of room temperature with air saturated industrial water, applying value of the rated flow whatever the actual flow rate is, and additional design margin prohibiting from sharp decline of head by deficiency of $NPSH_{av}$. Thus the conventional design method is to give additional static head corresponding to (1.4 m + $NPSH_{NC}$) accompanied by design margin. This follows the current design requires the increase of static head by 7 to 8 m which corresponds to one floor height of turbine building.

The advantage of high temperature NPSH is not only able to reduce the $NPSH_{req}$ but also to eliminate the design margin whatever the accuracy of $NPSH_{av}$ by keeping the actual $NPSH_{av}$ at impeller inlet to be zero or slightly a negative by venting system. The $NPSH_{req}$ is only to be confirmed negative but not required high degree of accuracy in negative region in this method.

4.6 Conclusion

High temperature NPSH

High temperature NPSH was evaluated and presented as an integrated configuration, using both the Ruggeri-Moore method extended to the negative area on condition of gas venting out of the system and accepting small gas presence at the impeller inlet without gas venting.

The presented high temperature $NPSH_{req}$ with a slightly minus value at the temperature demonstrated the successful operation of units A-1 and A-2 maintaining zero $NPSH_{av}$ at load rejection with sufficient venting capacity.

Application to design

The integrated high temperature NPSH configuration has altered the design criteria of the feedwater system to adopt a zero value of the $NPSH_{req}$ by facilitating both sufficient venting capacity and once-through descending piping arrangement as short as possible, thereby contributing to possible cost reduction by allowing a ground level smaller capacity DTR-tank, and smaller horizontal type higher rotative speed pump. Additionally the ground level location of DTR-tank would increase the reliability for seismic design.

References

(Ex. 1) Araki, R., Kokubo, R., Nakagami, Y., Kawada, Y., Obara, I., Hayami, K., Recent Technology on PWR Secondary System (Turbine Generator Plant) (in Japanese), Mitsubishi Heavy Industries Technical Journal, (in Japanese) Vol.19 No.6 (1982 -11), pp 80-95

(Ex. 2) Final Safety Analysis Report of South Carolina Electric and Gas CO. VIRGIL C. SUMMER Nuclear Station

(Ex. 3) Kuwabara, K., Murata, R., simulation program using node-link network of fluid plants, Mitsubish heavy industries technical journal, (in Japanese) Vol.22 No.6 (1985-11), pp 55-58

(Ex. 4) Nakagami, Y., Yoshioka, T., Sasaki, T., Manabe, J., Matsukuma, M., Taniguchi, M., Miyawaki, T., Design and Field Operation of Advanced 900 MW Class PWR Turbine Plant, Mitsubishi Heavy Industries Technical Journal, (in Japanese) Vol.22 No.3 (1985-5), pp 38-45

(Ex. 5) Stepanoff, A.J., Cavitation Properties of Liquids, Journal of Engineering for Power, April, 1964 / 195

(Ex. 6) Stahl, H.A., Stepanoff, A.J., Thermodynamic Aspects of Cavitation in Centrifugal Pumps

(Ex. 7) Ruggeri, R., Moore, R., Method for Prediction of Pump Cavitation Performance for Various Liquids, Liquid Temperatures, and Rotative Speeds, NASA TN D-5292, 1969, Lewis Research Center Cleveland Ohio NASA

(Ex. 8) Minemura, K., Uchiyama, T., Shoda, S., Egashira., K., Prediction of Air-Water Two-Phase Flow Performance of a Centrifugal Pump Based on One-Dimensional Two-Fluid Model, Journal of Fluids Engineering, ASME, JUNE 1998, Vol. 120, pp 327-334

(Ex. 9) Manabe, J., Miyagawa, k., High Temperature NPSH and Its Application for a Feedwater Sytem, Proceedings for 13th International Conference on Nuclear Engineering, Beijing, China, May 16-20, 2005 (ICONE13-50163)

(Ex. 10) Manabe, J., Miyagawa, k., High Temperature NPSH and Its Application for a Feedwater System, Japan Society of Mechanical Engineering International Journal, series B, vol. 49, No.2, 2006

Chapter 5 Conclusions of the Study

Reheat system

The core issues for the MSR of both methods of the mist separator performance prediction and tube drainage instability suppression were developed and demonstrated of their effectiveness in actual units.

The mist separator carryover start velocity in actual steam condition is predicted using the configuration that the condition is identical to that of air-water

Heat transfer tube drain instability is suppressed by increasing the excess steam in partial turbine load. The methods have been adopted for the units placed in service ever since in 1980s and so will be to the planning units.

High all volatile water treatment

High all volatile water treatment (HAVT), raising pH value in the feedwater to 10, was developed resulting both the reduction of iron concentration in feedwater to less than 1ppb and cease the scale adhesion in equipment. HAVT is the most economical and reliable counter measure for flow accelerated corrosion and succeeding scale adhesion which was inherent defect for saturation condition nuclear steam turbine system.

High temperature NPSH

High temperature NPSH was evaluated and presented as an integrated configuration, using both the Ruggeri-Moore method extended to the negative area on condition of gas venting out of the system and accepting small gas presence at the impeller inlet without gas venting.

The integrated high temperature NPSH configuration has altered the design criteria of the feedwater system to adopt a zero value of the NPSHreq by facilitating both sufficient venting capacity and once-through descending piping arrangement as short as possible, thereby contributing to possible cost reduction by allowing a ground level smaller capacity DTR-tank, and smaller horizontal type higher rotative speed pump. Additionally the ground level location of DTR-tank would increase the reliability for seismic design.

Acknowledgment

The author would like to acknowledge professor Yoshio Yoshizawa of jury president for thesis committee, and jury professors of Masanori Aritomi, Minoru Takahashi, Yukitaka Kato, Shigenari Kikura in Tokyo Institute of Technology, and the advice and assistance provided by author's associates of Nobuo Nakamori, Jiro Kasahara for *the reheat system*, Yasuhiko Shoda for the *water treatment*, project team members of Kazuyoshi Miyagawa, Toshiki Kojima and Shinji Fukao for the *high temperature NPSH*, and Yukiko Naruo for preparation of drawings.